THE RELATIONSHIP BETWEEN THE BENDING AMPLITUDE AND BENDING STRESS/STRAIN AT THE MOUTH OF A SO-CALLED SQUARE-FACED CLAMP FOR DIFFERENT CONDUCTOR SIZES AND DIFFERENT TENSILE LOADS: EXPERIMENTAL APPROACH

by

Yatshamba Daniel Kubelwa
(Student Number: 211559874)

Submitted in fulfilment of the academic requirements for the degree of Master of Science in Mechanical Engineering

School of Engineering,
Discipline of Mechanical Engineering,
Supervisor: **Dr Richard Loubser**
Co-supervisor: **Dr Konstantin O. Papailiou**
University of KwaZulu-Natal Durban

February 2013

As the candidate's supervisor I have~~/have not~~ approved this thesis/dissertation for submission.

Signed: RC Loubser Name Date: 16 February 2013
Dr Richard Loubser (Supervisor)

"For my father ***Leonard Kubelwa Musaya*** and in memories of my lovely mother ***Audrey Kakenge Bushindi***"

Abstract

In this research, realistic models were developed using experimental approach and statistical or deterministic analysis in the relationship between bending amplitudes and bending stress (strain) of the overhead line conductor. This was rigidity clamped and subjected to Aeolian vibration (1Hz-150 Hz). The experiments were performed at the Vibration Research and Testing Centre (VRTC) laboratory of the University of KwaZulu-Natal. A shaker connected to the conductor was used to simulate the Aeolian vibration and transducers (accelerometers, thermocouples and strain-gauges) to control the shaker and collect data. For almost half a century, in transmission lines, bending stress which is a key factor in determining the life expectancy prediction of overhead conductor is assessed by using an idealized model the so-called Poffenberger-Swart formula based on cantilever beam theory and many assumptions [2].

Four overhead line ACSR (Aluminum conductor steel-reinforced) conductors i.e. Rabbit (6 Al. /1St.), Pelican (18 Al. /1St.), Tern (45 Al./7St.) and Bersfort(48 Al./7St.) were investigated at three different ranges of tensile load i.e. 20 %, 25%, and 30% Ultimate Tensile Strength (UTS). Bending amplitudes (0.0 1mm -1.2mm) and bending stresses measurements were collected and plotted as bending stress σ_b versus bending amplitude Y_b, curve-fitting with polynomial function of the third order in terms of four parameters (where curve fitting coefficients B_0, B_1, B_2, and B_3) provided excellent simulations (predictions) of the experimental data for the conductors. However, it was found that the accuracy of the fit is not improved by the inclusion of higher order terms. Therefore, only four-parameters (for all cases high order than 3 are ambiguous, in spite of the Regression parameter or predictor were $R^2 \geq 0.998$ but Standard errors were large). It was noticed that the precedent model is the simplest polynomial to be employed for the characterization of all conductors investigated (for all three wires). Other ways to obtain the best curve fittings were explored and discussed such as power model. The experimental results were compared to the Poffenberger-Swart model. In all cases, it was observed that the deviation from the results to the above model is significant for small bending amplitudes and is small for high bending amplitudes and good correlations were observed when associated this with the bending stiffness model developed by Papailiou [17].

Preface

The experimental work described in this dissertation was carried out at The Vibration Research and Testing Centre (VRTC) in the School of Engineering, University of KwaZulu-Natal, Durban, from April 2011 to January 2013, under the supervision of Dr Richard Loubser and Dr Konstantin O. Papailiou.

These studies represent original work by the author and have not otherwise been submitted in any form for any degree or diploma to any tertiary institution. Where use has been made of the work of others it is duly acknowledged in the text.

YD. Kubelwa

DECLARATION 1 - PLAGIARISM

I, **Yatshamba Daniel Kubelwa** declare that

1. The research reported in this thesis, except where otherwise indicated, is my original research.

2. This thesis has not been submitted for any degree or examination at any other university.

3. This thesis does not contain other persons' data, pictures, graphs or other information, unless specifically acknowledged as being sourced from other persons.

4. This thesis does not contain other persons' writing, unless specifically acknowledged as being sourced from other researchers. Where other written sources have been quoted, then:
   a. Their words have been re-written but the general information attributed to them has been referenced
   b. Where their exact words have been used, then their writing has been placed in italics and inside quotation marks, and referenced.

5. This thesis does not contain text, graphics or tables copied and pasted from the Internet, unless specifically acknowledged, and the source being detailed in the thesis and in the References sections.

Signed: ……

DECLARATION 2 - PUBLICATIONS

DETAILS OF CONTRIBUTION TO PUBLICATIONS that form part and/or include research presented in this thesis (include publications in preparation, submitted, *in press* and published and give details of the contributions of each author to the experimental work and writing of each publication)

Publication 1

YD. Kubelwa, KO Papailiou, R. Loubser and P. Moodley, How Well Does the Poffenberger-Swart Formula Apply to Homogeneous Compact Overhead Line Conductors? Experimental Analysis on the Aero-Z® 455-2z Conductor, 18th WCNDT, ISBN: 978-0-620-52872-6, Durban, 4000, April 2012.

Publication 2

YD. Kubelwa, KO. Papailiou, R. Loubser and P. Moodley, Assessment of Bending Amplitude-Bending Stress Relation of Single Steel Core Overhead Line ACSR Conductor: Statistical or Determinist Approach, Cigre Auckland 2013 (in preparation)

Publication 3

YD. Kubelwa, R. Loubser, KO. Papailiou, and P Moodley, Probabilistic modeling of Bending Stress for Single overhead transmission line rigidly clamped. (In preparation)

Signed: ……...……..

Acknowledgements

May the Almighty God be glorified in Jesus-Christ's name my King and Saviour!

I gratefully acknowledge my supervisor Dr Richard Loubser, The Vibration Research and Testing Centre (VRTC) grant holder. I am grateful to my co-supervisor, my mentor and the promoter of this research Dr Konstantin O. Papailiou, Cigre B2 (Overhead Lines) chairman. Big thanks to Mr Pravesh Moodley for the technical assistance and his passion for the VRTC lab. During this thesis, I also received advice from Mr Umberto Cosmai, Mr Charles B. Rawlins, Dr David G. Havard, Professor Glen Bright, Dr Frederic Levesque (University of Laval), Dr Freddie Inambao, Mr Bharat Haridass, Mr Joseph Kapuku, Mr Remy Badibanga and Mr Evans Ojo. I am grateful to Professor Alex Arujo and Professor Aida A. Fadel, the Lab move and their team at the University of Brasilia where I learnt a lot during my training.

I am grateful to the VRTC, Eskom, Pfisterer and Aberdare Cable for their sponsorship and donations. Special thanks to Mr Logan Pillay, Eskom Academy of Learning, Mr Henni Scholtz, Aberdare Cables and Mr Thabani Nene, Pfisterer (South Africa) "the power connection".

Many thanks to my Cigre family and especially to the B2 study committee for the extraordinary works.

The unconditional support of my lovely family "les ***Kubelwas***" is gratefully acknowledged.

YD. Kubelwa

Table of Contents

Abbreviations

ACSR	Aluminium conductor steel reinforced
ALCOA	Aluminium Company of America
ANOVA	Analyse of Variance
ASD	Allowable Stress Design
CIGRE	International Council on Large electric Systems
DAQ	Data Acquisition
DOF	Degree-of-freedom
EDS	Every Day Stress
EHV	Extra High Voltage
EPRI	Electrical Power Research Institute
ESKOM	Electricity Supply Commission (South Africa)
FEA	Finite Element Analysis
HBM	Hettinger Baldwin Messtechnik
HV	High Voltage
IEC	International Electrotechnical Commission
IEEE	Institute Of Electric and Electronic Engineer
LPC	Last Point of Contact
MSE	Mean Standard Error
PS	Poffenberger-Swart
SC	Study Committee
SSE	Standard Error
UKZN	University of KwaZulu-Natal
UTS	Ultimate Tensile Strength
VIP	Vibration Interactive Programme
VRTC	Vibration Research and Testing Centre

List of Figures

List of Tables

List of Symbols

Symbol	Description	S.I. Unit
a	function parameter	
A	Area of the cross-section	[m^2]
A_a	Total area of aluminium wires	[m^2]
A_s	Total area of Steel wires	[m^2]
α	Exponent of the power law	
B	coefficient	
β	Angle between wire in the conductor	
C	parameter related to the Catenary equation H/W	[m]
C_i	Integration constants	
δ_a	Diameter of the outer layer wire	[m]
δ_s	Diameter of the steel wire	[m]
d	Overall diameter of the conductor	[m]
d_s	Bending diameter	[m]
E	Young's modulus	[N/m^2]
ε	Strain	
ε_b	Bending strain or dynamic strain	
ε_t	Longitudinal static strain	
ε_s	Static Strain	
$\in_i$	random error on the bending stress	[MPa]
F	Shear force	[N]
f	Force of the wind acting on each finite element	[N]
f	Frequency	[Hz]
G_f	Gauge factor	
H	Horizontal component of conductor tension	[N]
I	moment of inertia	[m^4]
k	degree of freedom	
k_c	Critical curvature of the conductor	[1/m]
k_f	Amplification Factor	
k_{p-s}	Poffenberger-Swart factor	[MPa/m]
k_s	Slippage coefficient	
L	Span length	[m]
M	Bending moment	[N.m]
m_L	Mass per unit length	[kg/m]
μ	coefficient of friction	
n	number of wires	
N	Number of samples	
ω	Circular frequency	[Hz]
φ	Lay angle of wire in the conductor	
ρ	density	

Symbol	Description	S.I. Unit
ρ_0	bending curvature function amplitude	[1/m]
R^2	estimator or predictor factor	
σ_a,σ_b	Bending Stress	[MPa]
σ_t	Tensile stress in the wire prior to bend	[MPa]
T	Tension	[N]
θ	Angle through which conductor is bent , and exponent of the power law	
V	Voltage	[V]
V_{exc}	Voltage of excitation	[V]
V_{out}	voltage drop at the bridge sensor	[V]
y_0	Free span amplitude	[m]
$y_{(x)}$	Transversal displacement	[m]
Y_b	Bending amplitude	[m]
Y_{max}	Antinode single-peak amplitude of vibration	[m]
Y_s	amplitude of the Shaker	[m]

CHAPTER 1

INTRODUCTION

1.1 Problem definition

This project examines the relationship between bending amplitude and bending stress or strain at the conductor clamp system for various conductor sizes, at different tensioned levels for each conductor, as illustrated in figure 1-1. The primary aim is to examine the relationship between the real stress at the outer layer of a conductor supported by the rigid suspension clamp and subjected to vibrations with the so-called bending amplitude.

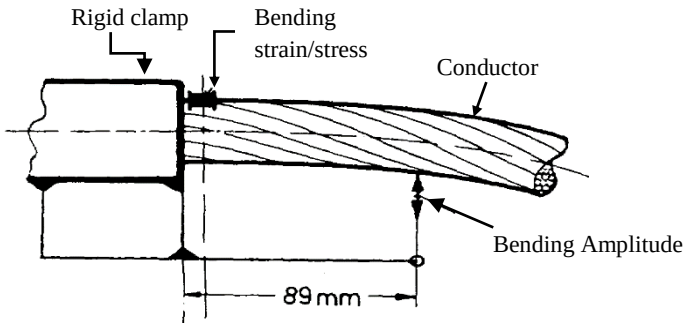

Figure 1-1 System of conductor-rigid clamp

The bending amplitude method is widely used to roughly estimate by field measurements the fatigue performance of conductors for a range of conductor sizes and by comparison with experimental fatigue tests for various conductor/clamp combinations, which provide the amount of cycles it is going to endure for a given bending amplitude. It is also useful to assess the effect of clamp geometry and/or of the sag angle of the clamp on the fatigue performance for a specific conductor. Associated to the above the remaining life expectancy of the conductor in the field could be estimated from the collected data obtained using a vibration recorder (figure 1-2) for outdoor measurements.

Figure 1-2 Vibration Recorders (Vibrec 400)

1.2 Background

The conductors installed on most of the overhead power lines represent a large financial investment, referring to more than 40 % of the total lines cost [1]. Due to the complexity of the network, the transmission line conductors could cover thousands of kilometers from the power plant sites to the consumer centers and they require several procedures [2]. To maintain all the equipment in service and evaluate its life expectancy could save time and money for a power supplier company like ESKOM which currently uses voltage that ranges from 22 kV to 765 kV in order to transport power over long distances. The spans between conductor towers could be between 80 m and 450m for 22 kV and 765 kV respectively [1].

Figure 1-3: Example of Eskom Transmission lines 765kV Majuba-Umfolozi (South Africa)

ESKOM transmissions lines, as well as transmission lines in most parts of the world are exposed to severe weather conditions such as varying temperature, snow, rain and wind, which can age conductors and their hardware (amour rods, dampers, ties) as in extreme cases insulators and towers, causing conductor failure. The most commonly known cause for conductor damage is the wind-induced vibration known as Aeolian vibration.

Cyclic bending fatigue is one of the most common causes of component failure in overhead transmission lines subjected to wind induced vibration. Depending on the conductor properties, wind velocity or when combined with the presence of ice on the conductor surface, the vibratory motion may take the form of: (i) Aeolian vibration, (ii) conductor galloping, (iii)

or wake-induced oscillations [1]. Although Stockbridge damper designs have been proposed to be attached on the conductor lines to reduce the problems caused by vibrations, cyclic bending fatigue is still one of the main concerns in overhead transmission lines in which damage often happens at the end fittings (clamps) [3] , especially when conductors are subjected to Aeolian vibration.

Previous research indicates that the fatigue failure of overhead transmission lines happens when conductors are exposed to wind induced vibrations because of fretting [9]. Strand failures occur mainly at the suspension clamps where stiffness discontinuities are noticed. In order to evaluate the life expectancy of a conductor exposed to Aeolian vibration, it is necessary to quantify the stress combinations favouring strand failures. These stresses are not easily accessible to direct measurements.

Furthermore, because of the helical structure of the conductor, the stress regime on the individual wires of a conductor is too complicated to be expressed by a simple formula. For this reason, it would be extremely helpful to find out for a series of conductor sizes and for at least three different tension levels concerning each conductor size, the "real" relationship between bending amplitude and outer layer wire stress/strain. The range of bending amplitudes examined should also cover small amplitudes as for this amplitude strong non-linearity in the relationship bending stress/bending amplitude is expected.

Various measurement methods are performed at the system conductor-clamp in order to assess these stresses. The most significant and practical method is the bending amplitude method. This is based on the relationship between the bending amplitude and bending stress / strain. In the laboratory strain-gauges and accelerometers / displacement sensors are used to measure this relationship whilst in the field vibration recorders are often used to collect the necessary data.

1.3 Research Question

As mentioned earlier, this study focuses on the relationship between bending amplitude and bending stress/strain at the conductor/clamp system. Various analyses and measurements must be completed in the laboratory regarding the choice of conductor sizes. A question is raised in this study: How well can these measurements correlate with the Poffenberger-Swart formula for different conductor sizes and different tensile loads? An answer to this important question will be found using the necessary techniques and methodology during the course of the experimental work.

In terms of useful prerequisites, experimental skills and a good understanding of mechanics of solids are needed to build up a comprehensive outcome (or answer) that can meet the expectations of the study.

For this project to be successfully achieved, conductor types and related tensile loads that are most commonly used in South Africa are considered. The results of the study will therefore be beneficial to ESKOM and the transmission line industry in this country and abroad.

1.4 Project Aims and Objectives

A good understanding of the stress mechanism from the dynamic behaviour concerning the conductor-clamp system is essential to determine a suitable design methodology and also to quantify the nominal stress at the outer layer of the conductor. Quantifying the real stress is useful in evaluating the life expectancy of the transmission line. This approach is not only important for ESKOM, but also for the conductors and fitting hardware manufacturing companies.

An important application of this project is to find out the reasons behind the anticipated lack of correlation between the measured and the predicted stresses by the Poffenberger-Swart formula.

Based on most considerations raised before, this study aims to:

- Establish an experimental procedure that allows to develop reliable results;
- Collect data from test measurements;
- Analyze the data results obtained applying statistical methods;
- Determine the relationship between bending stress/strain and bending amplitude for the various conductors and tensions;
- Verify if and how well the measurements obtained do correlate with the Poffenberger-Swart formula.

1.5 Applications of the outcomes of the study

Several blackouts happened around the world in the past due to many causes, one of them being conductor failures. For instance recently in India almost half of the country (300 million people) were in darkness for seventy two hours. Therefore in many countries, methods are sought in order to assess risk of fatigue of overhead line conductors, the main one being to measure amplitudes and cycles (frequencies) of the conductor.

The industry standard is to use a vibration recorder in order to collect the bending amplitude; such a modern recorder is shown in figure 1-2. The recorder is attached to the conductor clamp for a long period of up to 12 months (full season). The measured amplitudes can be converted to stress by the PS formula [2]. The measured number of cycles at various amplitudes can be used in the context of a cumulative damage theory, i.e. the Palmgren-Miner Rule [2] in order to roughly estimate the fatigue lifetime prediction, one of the main objectives of establishing suitable maintenance plans.

CIGRE study committee 22 (now B2) working group 04 has given beneficial recommendations for the evaluation of the lifetime of the transmission line conductors [37] These have been extended to guides for the use of vibration recorders, which are the devices.

Numerous vibration recorders are installed in the ESKOM transmission lines for the evaluation of the fatigue damage performance (life expectancy) of the conductors undergoing vibrations for safety and maintenance purposes. This assessment is of importance in overhead transmission line design, maintenance planning and operation management [2].

The outcome of this research will contribute to the following:

- Improvement of the methods for assessing the life expectancy of overhead conductors using simple and realistic stress expression when analyzing the data collected from the vibration recorder. This induces the possibility to improve line design i.e. suitable choice of conductors, clamps, tensions,
- Development of a calibration protocol of vibration recorders using the Vibration Research and Testing Centre (VRTC) laboratory which is designed according to international standard.
- To design a vibration recorder made in South Africa at an affordable prize.

1.6 Assumptions of this experimental approach

This experimental study is based on the measurement of three parameters: bending amplitude, bending strain (or stress) and bending stiffness.

For small displacements of the conductor, the temperature resultant from vibration will be neglected; however, compensation due to temperature on the strain measurements will be applied.

- In theory, the calculation of bending stiffness of stranded conductors is based on two assumptions: Firstly, there is no friction between the strands and each wire moves on their

own axis; this provides the minimum value of bending stiffness. Secondly, the conductor behaves as a solid body; this results to the maximum stiffness flexion.

1.7 Research Overview

The following is a brief description of the information and data to be presented:

Chapter 2 gives an overview on the existing models; all parameters related the Poffenberger and Swart formula, and other analytical models to assess the stress/strain at the end clamp of the conductor/clamp system.

Chapter 3 focuses on the laboratory portion of this research project. This chapter includes an overall description of the bench of testing vibrating conductors at the University of KwaZulu-Natal as well as the instrumentation used. Finally, diagrams of the load frame and test procedures are presented.

Chapter 4 presents and discusses laboratory data. Tables and plots are shown representing typical results. The experimental results are compared to the Poffenberger-Swart model and the model improved by Papailiou.

Chapter 5 gives the realistic models developed from the experimental results and the statistic regression models i.e. polynomial and logarithmic regression method.

CHAPTER 2

LITERATURE REVIEW

2.1 Introduction

Various aspects of the dynamic behavior of conductor-clamp systems with varying lengths and conductors (ACSR, ACCR…), in particular in overhead line conductors such as Aluminum Conductor or Aluminum Conductors Steel Reinforced (ACSR), have been studied in the past by engineers, companies and international institutions (IEEE, CIGRE…). Concerns for the reliability and safety were the main causes raised during these investigations. It was recorded that the evaluation of the stress mechanism on the fitting where damage on the conductor most often occurred posed the biggest challenge for its assessment and control.

Reuleaux [4] performed the first experiments about stress on the cables. Later on in 1907, Isaachsen provided an approach to evaluate the bending stress on the catenary of a cable [2]. In 1925 when the importance began to be appreciated, Aluminum Company of America (ALCOA) started an investigation for both indoor and outdoor tests. This work was presented by Theodore Varney in two papers [4, 5] in which a theory based on conductor failure was presented and received general acceptance. In 1932, Sickley completed the stress-strain studies of transmission line conductors [6]. Within the same year, Monroe and Templin presented both analytical and experimental approaches to assess vibrations in finding an idealized stress [7]. During their work in situ, specimens have been tested in the Massena vibrations laboratory using a span of 35.6 m with various tensions and frequencies.

The first measurement approach of quantifying the dynamic strain at the mouth of suspension clamp to the point where the bending of maximum bending was completed by both Steidel [8] in 1954 and later by Hard in 1958 [9]. Five years later, Edwards and Boyd [10] suggested the bending amplitude as the parameter directly related to the bending strain at the suspension clamp.

Before almost half a century, Poffenberger and Swart [11] presented for the first time an analytical solution. In their study, they showed how to quantify the stress at the fittings. However, it is important to affirm that Tebo [12] had initiated this work earlier. Poffenberger and Swart proposed a relationship between differential displacement and conductor strain, which could provide a realistic assessment of the bending stress in the conductor tested, if the conductor

tension and flexural rigidity were considered. A year later, the IEEE [13] adopted the method in showing how this method was independent of vibration frequency, loop length, conductor diameter, tension and vibration on adjacent spans. The work completed by Claren and Diana [14] showed the correlation which exists between the dynamic strains occurring on the spans and those occurring at the rigidly clamped ends were weak. Papailiou [16] has studied the factor affecting the above method, which is the bending stiffness. He developed a model assessing the mechanism of the bending stiffness; this model has been well accepted by many researchers and has been as well recognized by Poffenberger himself [17] as significant in order to highlight the "cloudy region" of the bending amplitude Method.

Many other researchers have carried out similar studies, such as Levesque et al [18], Goudreau et al [19] and Cloutier et al [20] who have recently presented experimental studies on the method comparing theory and strain measurements. Also, the work presented by Dalpe et al. [21], Lanteigne and Akhtar [22], Hardy et al. [23] and McGill et al.[24] have a substantial contribution to the bending amplitude method.

The Poffenberger-Swart (P-S) method is widely recommended by the Institute of Electrical and Electronic Engineers (IEEE) [8], and adopted by the International Council on the Large Electric Systems (CIGRE) [3] and by the Electrical Power Research Institute (EPRI) [1]. These three organizations since they have been created are still doing excellent research on how to express the bending stress as a function of the bending amplitude accurately and its practical application.

CIGRE has been created in 1921; in a specifically dedicated Study Committee (SC) scientific and technical discussions are undertaken on how to improve the quality of the transmission lines. From 1966 to 2002 this committee became SC 22 and since 2002 became SC B2. The CIGRE working group B2.11 has published guidelines on the investigation of the life expectancy through the bending stress measurement by using a vibration recorder [28].

The literature review will be mainly focused on three areas: bending amplitude, bending strains and bending stiffness which are the variables in the PS formula.

2.2 Bending amplitude method [2-14].

2.2.1 Equation of motion and boundary conditions

It is assumed that the conductor [5] is a prismatic beam. The mechanical structure is exposed to transverse vibration and is presented by figure 2-1

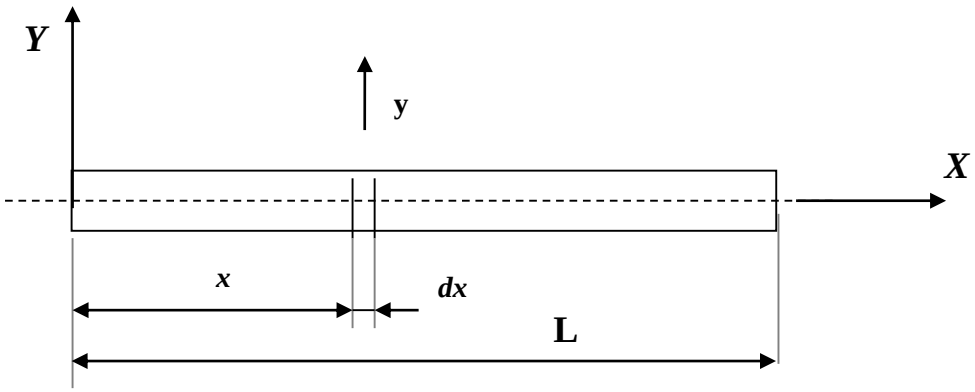

Figure 2-1 Structure of a prismatic b

All forces applied on the element dx are illustrated as follows:

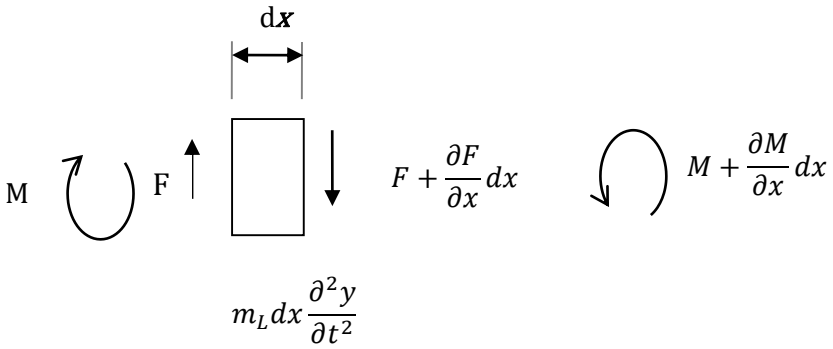

(2.1)

Where,

M is the bending moment

F is the shear force

m_L is the mass per unit length

When the beam is vibrating, the dynamic equilibrium force in the vertical direction y can be written as:

$$F - F - \frac{\partial F}{\partial x}dx - m_L dx \frac{\partial^2 y}{\partial t^2} = 0 \tag{2.2}$$

And the equation for the corresponding moment is given as follows

$$-Fdx + \frac{\partial M}{\partial x}dx \approx 0 \tag{2.3}$$

The complex structure of the conductor is modeled as a taut string with a mass per unit length m_l, tension T and the stiffness EI.

Consider a string attached under load-induced vibration as illustrated by figure 2-2:

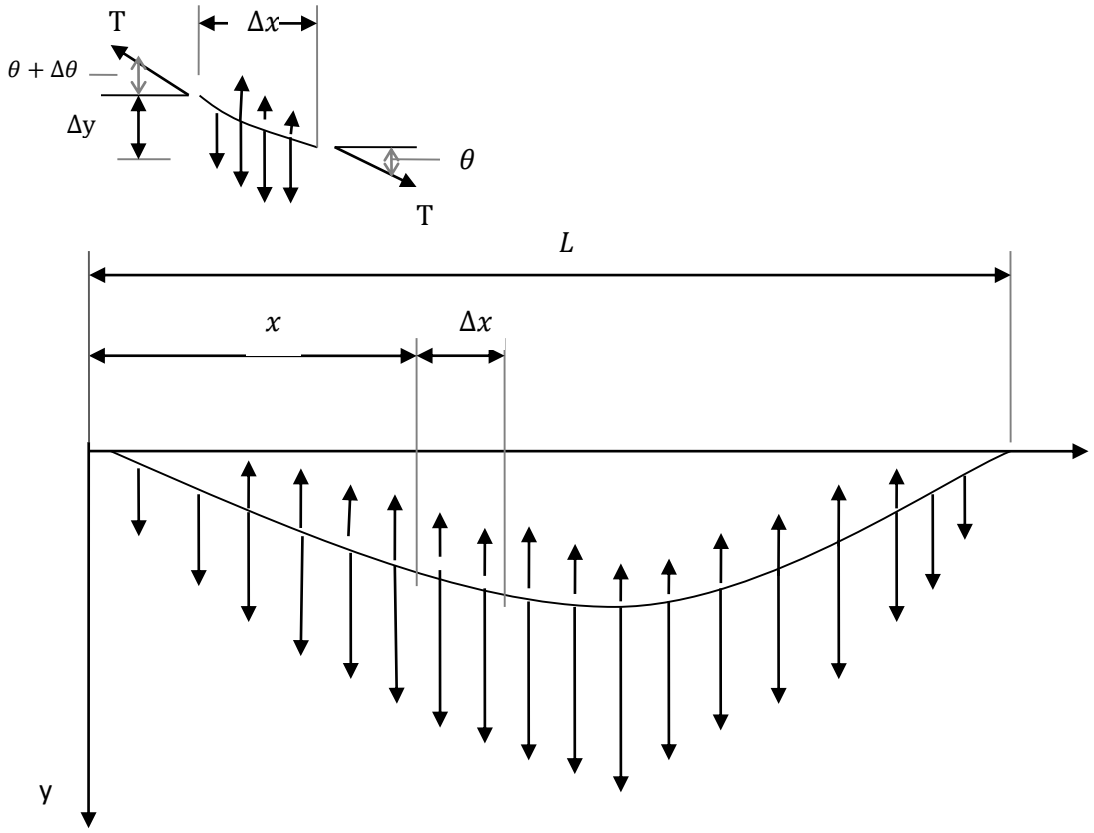

Figure 2-2 Schematic of taut string under alternate load

The development of the finite element using concepts from matrix analysis of structures could be performed in this case. A small deflection of a cable can be assimilated to an elasticity problem since the balance force is combined with a geometric constitutive equation that defines the slope

of the cable. The tension T is assumed to be constant for small deflections (in theory) and allows to get the analytical solution for a cable with fixed ends, the external load f that could quantify the force of the wind acting on each finite element, the damping factor k and the length L.

$$T\,sin\theta - T\sin(\theta + \Delta\theta) - f(x)\Delta x + k(x)y(x)\Delta x = 0 \tag{2.4}$$

In addition, the small deflection theory implies that $sin\theta \approx \theta$ and $\sin(\theta + \Delta\theta) \approx \theta + \Delta\theta$, thus the equation (2.3) gives the governing differential equation:

$$T\frac{d^2y(x)}{dx^2} - k(x)y(x) = -f(x) \tag{2.5}$$

Therefore, the structure is a cable with a tension T, the dynamic equilibrium force in the direction x is zero and the elementary theory of elastic beam shows that the bending moment can be written as:

$$M = EI\frac{\partial^2 y}{\partial x^2} \tag{2.6}$$

Where, E is the Young's modulus and I is the moment of inertia

Equations (2.3), (2.5) and (2.6) give:

$$\frac{\partial^2}{\partial x^2}\left[EI\frac{\partial^2 y}{\partial x^2}\right]dx = -m_L dx\frac{\partial^2 y}{\partial t^2} \tag{2.7}$$

At first approximation, the stiffness or flexural rigidity *EI* is constant, and the fundamental equation of the conductor subjected to the vibration of the free oscillation at constant bending stiffness can be written as:

$$EIy_x{}^{(IV)}(x,t) + m_L y_t{}''(x,t) - Ty''(x,t) = F(x,t,y,y_t) \tag{2.8}$$

The equation (2.8) represents the equation of conductor with constant bending stiffness, where $y(x,t)$ is the transverse deflection of the conductor at location x and at time t, $F(x,t,y,y_t)$ represents the external load and the damping due to the conductor hysteresis, y_x and y_t represent the derivatives with respect to space and time, respectively.

The mass per unit length is given by $m_L = \rho A$, where ρ is the average density of the conductor and A is the area of the cross-section. In case the conductor is undamped, the equation (2.8) can be written as follows:

$$EIy_x{}^{(IV)}(x,t) + \rho A y_t{}''(x,t) - Ty''(x,t) = 0 \tag{2.9}$$

It can be reasonably assumed that the equation of conductor rigidly clamped at one of the ends provides suitable boundary conditions. As a result, equation (2.6) can easily find solutions using the separation of variables method for this partial differential equation. In addition, when the beam is vibrating in its natural mode, the deflection at any point varies harmonically and can be written:

$$Y(t) = X(A\cos\omega\, t + \, Bsin\, \omega t) \tag{2.10}$$

With ω the circular frequency, the general solutions to (2.6) can be presented in the following form:

$$Y(x) = K\, e^{\alpha x} \tag{2.11}$$

Thus the roots of the characteristic equation are: two real roots

$$n_{1,2} = \pm\alpha \tag{2.12}$$

with $\alpha = \sqrt{\frac{T}{2EI} + \sqrt{\frac{m\omega^2}{EI} + (\frac{T}{2EI})^2}}$

And two imaginary roots:

$$n_{3,4} = \pm j\beta \tag{2.13}$$

with $\beta = \sqrt{-\frac{T}{2EI} + \sqrt{\frac{m\omega^2}{EI} + (\frac{T}{2EI})^2}}$

At the end, the general solution to equation (2.6) can be written using the hyperbolic functions:

$$Y(x) = C_1\cosh\alpha x + C_2\sinh\alpha x + C_3\cosh\beta x + C_4 sinh\beta x \tag{2.14}$$

where C_1, C_2 , C_3 and C_4 are the integration constants.

Considering the boundary conditions and with good approximation of C_4 which is equal to the free span amplitude y_o in the equation (2.14), the transversal displacement $y(x)$ of the conductor taking into accounts both the bending stiffness and its tension can be described as:

$$y(x) = y_0 \sin \beta x \tag{2.15}$$

Hence, the conductor is considered as an elastic structure assumed that one of its ends is free because the boundary conditions are simplified.

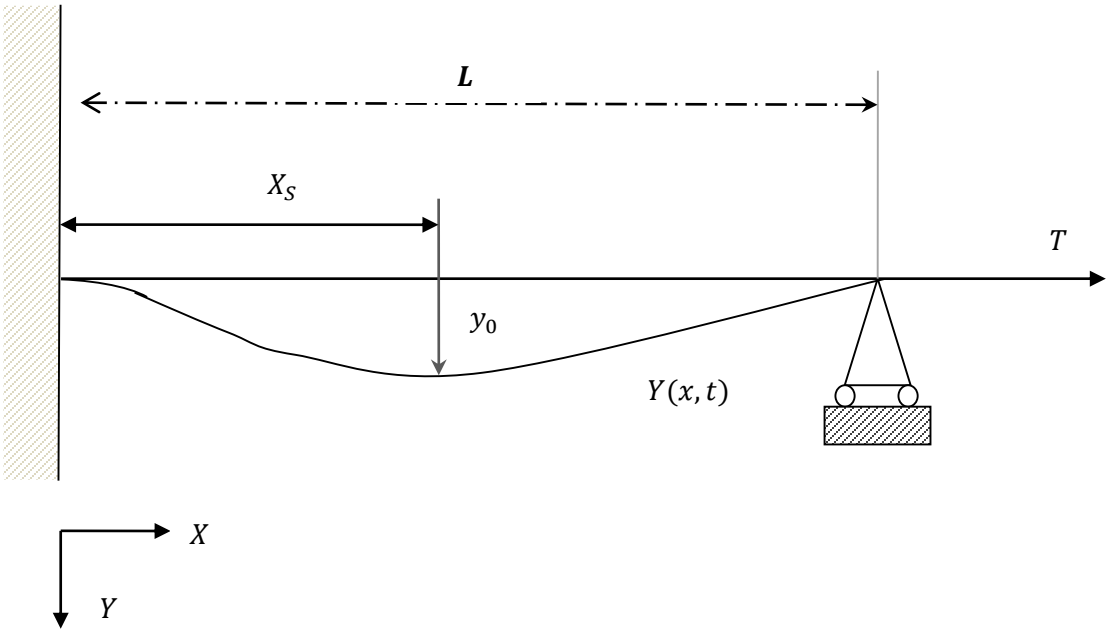

Figure 2-3: Schematic of conductor clamped structure.

2.2.2 Idealized stress model –Poffenberger and Swart [7]

Using equation (2.15) Poffenberger and Swart elaborated the bending amplitude method based on the relationship between bending amplitude and bending strain at the conductor-end clamp[2,7].This was achieved considering the conductor-clamp system as a cantilever beam according to the Bernoulli-Euler theory with one end horizontally rigidly fixed and a force acting to the other end. The deflection curve of the beam is often called the elastica [12]. This curve may be determined by the following equation

$$\frac{d^2y}{dx^2} = \frac{M(x)}{EI} \tag{2.16}$$

where $M(x)$is the bending moment at x and the quantity EI, where E is Young's modulus and I (for the conductor the moment of inertia tends at it minimum value I→ I_{min}) is the moment of inertia of a cross section for the beam around its central axis, is called the flexural rigidity.

Consequently,

$$M = H.Y_t \tag{2.17}$$

With H the tension due to the weight of conductor and $Y_t$is the deflection of the conductor. Equation (2.17) substituted into equation (2.16) provides the following expression:

$$\frac{d^2Y_t}{dx^2} = \frac{H.Y_t}{EI} \tag{2.18}$$

The solution of equation (2.16) leads after consideration of $Y_b = 2\,Y$, i.e. for measuring the peak-to-peak value of y at x = 89 mm (IEEE 1966), to the bending amplitudeY_b.

With the "bending amplitude", an ideal bending stress σ_a is calculated in the top-most outer-layer strand of the conductor in the plane of the last point of contact (LPC) [18] at the clamp edge, by the well-known PS formula:

$$\sigma_a = \frac{E_a\,\delta_a\,p^2}{4(e^{-px} - 1 + px)} Y_b \tag{2.19}$$

Where E_a is the modulus of elasticity of the outer wire material (N/mm^2) , δ_a is the diameter of the outer layer wire (mm), and $p = T/EI_{min}$. Moreover, the equation (2.19) can be written:

$$\sigma_a = k_{p-s}.Y_b \tag{2.20}$$

where k_{p-s} is a factor that connects bending amplitude to bending stress and replaced by:

$$k_{p-s} = \frac{E_a\,\delta_a\,p^2}{4(e^{-px} - 1 + px)} \tag{2.21}$$

The result in equation (2.19) provides a relatively simple relationship between the bending amplitude Y_b and the bending stress σ_a at the mouth of an idealized square faced clamp. It should be explicitly mentioned that this is an ideal stress. It can be estimated from the vibration amplitude and correlates well enough with conductor fatigue tests. As a result, it can be used in establishing a single endurance limit for a certain range of conductor sizes [2].

Initially the PS formula has come from the strain expression presented by equation (2.22), an analytical solution defining the relationship between differential displacement and flexural strain for the bare clamp case [11] reported in the session below.

2.2.3 Alternate Poffenberger-Swart model (strains)

Once vibrations are induced, the major longitudinal dynamic strain component results from bending at the conductor support points. Poffenberger and Swart developed an equation relating these strains at the edge of a square-faced clamp to the bending amplitude at a point close to the clamp [13]. Their expression for dynamic bending strain is:

$$\varepsilon_{db} = \frac{cp^2}{2(e^{-px} - 1 + px)} Y_b \tag{2.22}$$

with c = distance from the neutral axis to the point in question and other factors as defined above.

Equation (2.22) can be written in another commonly useful equation:

$$\varepsilon_{sb} = 2\pi c \sqrt{\frac{m_l}{EI}} f y_{max} \tag{2.23}$$

with m_l = mass per unit length of the conductor; f = frequency of the vibrating conductor and y_{max} = vibration bending amplitude at the antinode.

The static strains are based on the clamp geometry with or without sag angle. However, the dynamic strains relate to the bending amplitude adjacent to the clamp in equation (2.22) and also to the bending amplitude at antinode in equation (2.23).

2.2.4 Bending Strain-Energy Balance Method [26]

The simplest way to determine the stress produced under known circumstances is to measure the accompanying strain. The strain measurement is comparatively uniform over a considerable length of the analyzed part, but becomes difficult when the stress is localized or varies abruptly since its measurement is made over a short gauge length and needs great precision.

The general expression for bending strain of a conductor under varying loads as showed by Wolf et al. [26] is mathematically expressed by the bending diameter over the inverted radius of curvature which is given by the second derivative of the equation (2.15) function of the amplitude Y_B and the time t as $y''(y,t)$ is given as follows

$$\varepsilon(x,t) = \frac{d_s}{2} y''(y,t) \tag{2.24}$$

d_s is called the bending diameter which is not equal to the conductor diameter d and is given by :

$$d_s = k_s d \tag{2.25}$$

k_s is the slippage coefficient, determined empirically and depends on the localization (mid-span and at the suspension clamp of the conductor).

2.2.5 Static Strains - Ramey and Townsend [25]

The static strain measured on the conductor is a result of the tension and the force induced on the top of the clamp during installation of the clamp and gives an approximate longitudinal static strain of:

$$\epsilon_t = \frac{H}{(\lambda A_s + A_a)E_a} \tag{2.26}$$

where H is the tension in the conductor, A_s is the total area of steel A_a is the overall area of aluminum, λ is the ratio between the modulus of elasticity of steel and aluminum and E_a is the Young's modulus of the aluminum.

In general, the stress mechanism of the conductor at the suspension clamp is given by five components: (i) stringing tension, (ii) bending due to the conductor weight, (iii) bending due to the conductor vibration, (iv) bearing due to the conductor tension, and (v) bearing due to the radial clamping pressures. Equation (2.27) below shows a practical application for evaluate the static bending strains in the conductor at the mouth of a fixed clamp due by the weight of the conductor [26].

$$\epsilon_{sb} = \frac{w\left[\frac{Ls}{2}\sqrt{\frac{EI}{H}} - \frac{EI}{H}\right]c}{EI} \tag{2.27}$$

W is the weight per unit length of the conductor, *Ls is* the span length, *EI* is the flexural rigidity of the conductor, c is the distance from the neutral axis to the point in question (the strand radius is the value normally used) and *H* is the tension of the conductor. This equation (2.27) is indicated the occurrence of substantial plastic deformation [26].

2.3 Conductor stiffness

The bending stiffness or flexural rigidity *EI* of a conductor is defined as the algebraic product of Young's modulus (*E*) and the moment of inertia (*I*). For a conductor, the calculation of the bending stiffness becomes complex since the structure is constituted of twisted wires.

In the PS model (equation 2.20) connector or factor k_{p-s} (equation 2.20) is widely dependent on the bending stiffness parameter that is well highlighted by Papailiou [16]. Poffenberger and Swart [7] stated that there is a correlation between the bending amplitude and bending stress .This relationship is not dependent on the frequency and length but the factor k_{p-s} which is affected by the tension.

Many models on the bending stiffness of the conductor have been attempted in the past. In this session two models are presented.

2.3.1 Static stiffness *EI* -Scanlan and Swart [2]

In theory, the bending stiffness *EI* of the conductor during the bending motion is found between its minimum and maximum value. For its minimum EI_{min} the wires in the conductor are assumed to bend independently around their own axis and the conductor is considered behaving as a chain [2] ($EI \to 0$ And $EA \to \infty$) and given by the expression below:

$$EI_{min} = \frac{\pi}{64}(E_a {d_a}^4 n_a + E_s {d_s}^4 n_s) \tag{2.28}$$

Wherein, E_a and E_s are respectively the Young's modulus of the aluminum and steel, $d_a$and d_s are diameters of the aluminum and steel wire in the strand respectively, n_a and n_s are related to the number of aluminum and steel wires.

The second assumption postulated that during the bending motion the wires move together as homogenous body (welded) and this is defined as the maximum stiffness EI_{max} which is written as follows:

$$EI_{max} = E_a \sum I_{max,a} + E_s \sum I_{max,s} \tag{2.29}$$

This stiffness is related to the maximum moment of inertia I_{max} and is given by this expression:

$$I_{max} = \frac{n\,\pi\,d^2}{8}\left(\frac{d^2}{8} + R^2\right) \tag{2.30}$$

where, δ_a is diameter of the wire, n is the number of strand per layer and R is the layer radius

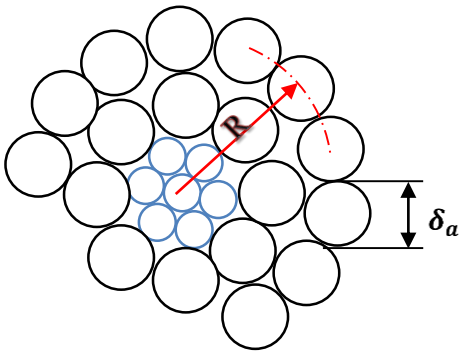

Figure 2-4 Generalized cross section used in the development of equation (2.30)

It was postulated by Scanlan and Swart [2] that the stiffness or the flexural rigidity of a conductor is expressed as the strain on the outer layer conductor, the bending stiffness is close to its minimum value ($EI \geq EI_{min}$) . The outer layer may behave independently as a chain and glide over the wires in the inner layer which may act together. However, Sturm [2] suggested using the stiffness EI equal to one- half of the maximum stiffness ($EI = \frac{EI_{max}}{2}$).

The above suggestions are based on assumption and experiments on the adequate stiffness model to be used in the Poffenberger-Swart formula. In the above no convincing scientifically explanations could be found until the model has been developed by Papailiou [16].

2.3.2 Dynamic stiffness EJ (k) -Papailiou [15]

Papailiou developed a realistic bending stiffness model which explained the "stick-slip state" of a conductor during bending. This model shows how the tension affects the strand friction between the wires and consequently the bending curvature.

Mathematically, to determine k_{p-s} as the k_{p-s} (*EI, H*) which is illustrated in the equation (2.20), is simple because the static stiffness is used which is constant. When the bending stiffness is replaced by the expression EJ (k), which is a function of the curvature k and consequently of the bending amplitudes Y_b, the number of layer, wires of the conductor and of the interlayer and interwire friction. The stiffness is easy to calculate for a homogeneous body with known Young's modulus. The conditions in a conductor are different, since in this case the individual wires are not permanently fixed in their position, but, depending on the load, may change position relative to each other. Thus, whilst the conductor is in motion, its bending $EJ(k)$ could be found between the minimum EJ_{min} and maximum EJ_{max}values according to the vibration amplitude and the applied tension. Then, the variable bending stiffness is given by

$$EJ_i(k) = EJ_{min} + \sum_{j=1}^{i-1} EJ_{stick,j} + \sum_{j=i}^{a} EJ_{slip,j} \tag{2.31}$$

Where , $EJ_{stick,j}$ is the bending stiffness when the wires are considered as a homogenous body, $EJ_{slip,j}$ is the maximum bending stiffness when the conductor are slipping and EJ_{min} is the stiffness of the individual wire around their own axis .

From equation (2.31), the actual stress EJ may be written more compactly as,

$$EJ = EJ_{min} + EJ_{slip} = function\ (k) \tag{2.32}$$

Where for each wire there is

$$EJ_{min}^{wire} = E\frac{\pi\delta^4}{64}cos\beta \tag{2.33}$$

$$EJ_{stick}^{wire} = \sigma_T A\left(e^{\mu sin\beta\,\varphi} - 1\right) r\, sin\varphi cos\beta \,/\, k_c \tag{2.34}$$

Where in, r, δ, β and φ are the factors of the conductor shown in figure 2-5 and σ_T is the tensile stress in the wire prior to bending and A is the area of the wire cross section. k_c is the critical curvature which is defined as the average curvature between the stick and the slip state of the conductor [15].

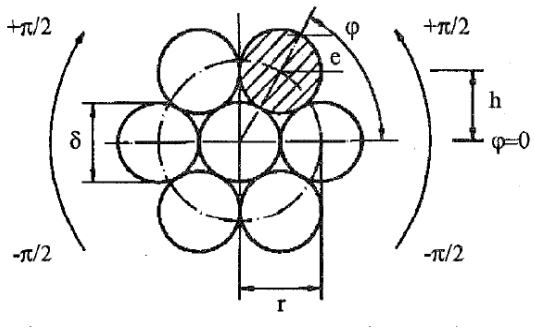

Figure 2-5 Cross-section of a single layer conductor used in development of the equations (2.33) and (2.34)

The lay angle is given by the following equation

$$\frac{rd\varphi}{\rho d\alpha} = sin\beta \tag{2.35}$$

The maximum bending can be calculated by:

$$EJ_{max} = EJ_{min} + EJ_{stick} = const \tag{2.36}$$

With

$$EJ_{stick}^{wire} = EA(r\, sin\varphi)^2 cos^3\beta \tag{2.37}$$

For this study as well as the study dealing with small amplitude relating to bending stiffness, the second assumption in the first chapter must not be taken into account, especially if the friction interlayers are present. The bending stiffness is localized between two extremities: the minimum and maximum as illustrated by the figure 2-6.

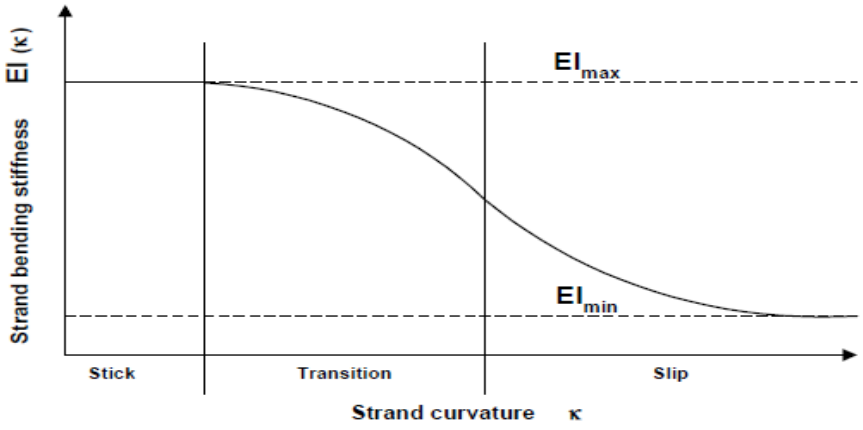

Figure 2-6 The conductor bending stiffness EJ (k) as function of the curvature during bending

It is important to know in which region the bending stiffness is localized for the purpose of possible evaluation. Although the bending stiffness of the conductor is small and does not significantly affect the resonant frequencies, it is necessary to know its value to determine the bending strain ε. Experimental work [26] shows that the value of the bending rigidity depends on the applied load, which implies that the radial pressure increases the friction between the strands and the stiffness of the conductor [26]. The actual stiffness values are closer to the minimum than the maximum value.

The bending stiffness of a conductor *EJ* can be determined empirically due to the complex structure of the conductor. However the above the basic of the analytical evaluation of the flexural rigidity of a conductor has been presented.

In addition, the curvature $k(x)$ is determined using a finite element analysis (FEA) package adapted to simulate the alternating motion of the conductor structure. The friction coefficient considered is reported to be $\mu = 0.55\ to\ 0.99$ [17].

2.4 Previous laboratory work

Various laboratory work around the world are performed in order to find out how well the crude effects of Aeolian vibration and its control on the overhead line conductors can be assessed. A great amount of data have been collected and analyzed from both outdoor and indoor tests. It is obvious that the PS method is a good approximation to determine the stress at the outer layer

wires of a conductor. However, certain reservations have been raised from the analysis of laboratory work completed by previous researchers [2].

Poffenberger and Swart recorded that at small amplitudes, the bending amplitude method presented significant uncertainties [11]. Claren and Diana recorded [14] after several experimental works, that the average difference between predicted and measured stress were in the range of 30% difference compared to the test performed on many ACSR conductors. Recently, Goudreau, Levesque, Cloutier and Cardou [18-20] concluded that the correlation between experimental strains and theoretical (PS) is weak.

Two previous experimental works have given particular attention as illustrated by figure 2-7 [2] and figure 2-8 [31]; these studies report on the comparison between predicted and measured strains at the mouth of the clamp. The measured and predicted strains showed considerable difference between them.

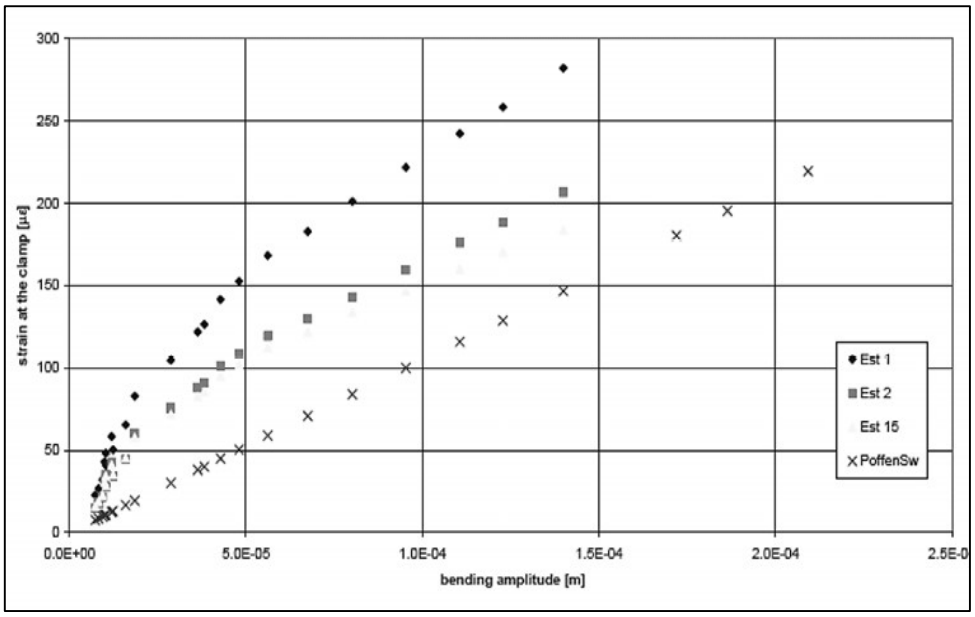

Figure 2-7 Bending strains vs. bending amplitude: comparison between measured and predicted using the PS formula on ACSR Drake

.

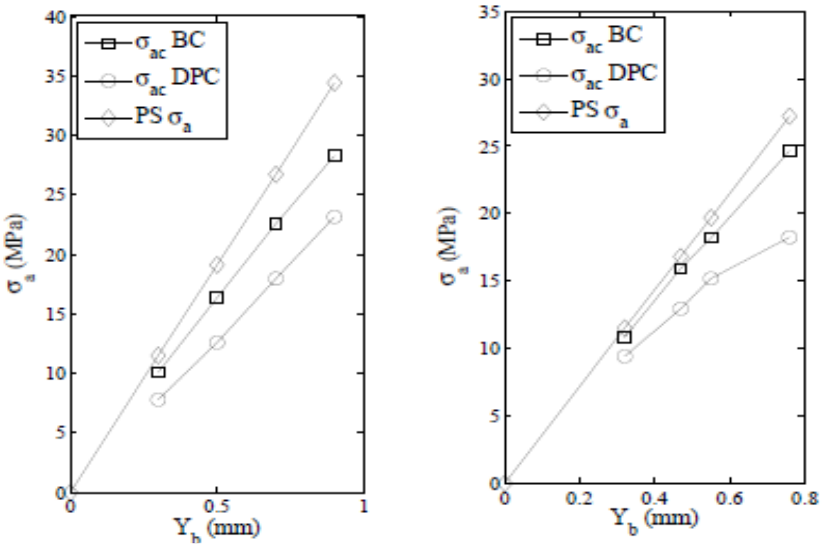

Figure 2-8 Bending Stain vs. bending Amplitude comparison between predicted and measured values on Bersfort (right) and on Drake at 25% UTS

The measured curves show non-linearity, while the predicted curves (PS) are linear curves [31]. The test arrangement was with the conductor Bersfort tensioned at 25 % UTS fitted by a commercial clamp. The average difference between the prediction and the measurement [18] was about 20 %.

The second example is the test performed [27] in Spain on ACSR Condor conductor as illustrated by figure 2-8, the scatter graph looks different to the first one, the amplitude had been measured at 76 mm distance to the clamp for the indoor test and tensioned at 46 % UTS. Concerning the outdoor test, the distance to clamp was 63 mm and tensioned at 11 % UTS. The average of the indoor result is 9 % UTS while the outdoor is about 39 % UTS. The results [27] showed that for a high tension the use of other model than PS correlated well enough between the prediction and the measurements performed indoor [27]. Hence, the theory can be explained in the bending stiffness theory [15]; the wires are very sticky to each other at high tension and the conductors behave like a homogenous body. This observation is valid for average and high amplitudes. However, at low tension with small amplitudes the result is satisfactory. Test performed on the Drake conductor [2] illustrated in figure 2-9 showed a large difference between the calculated and the measured stress.

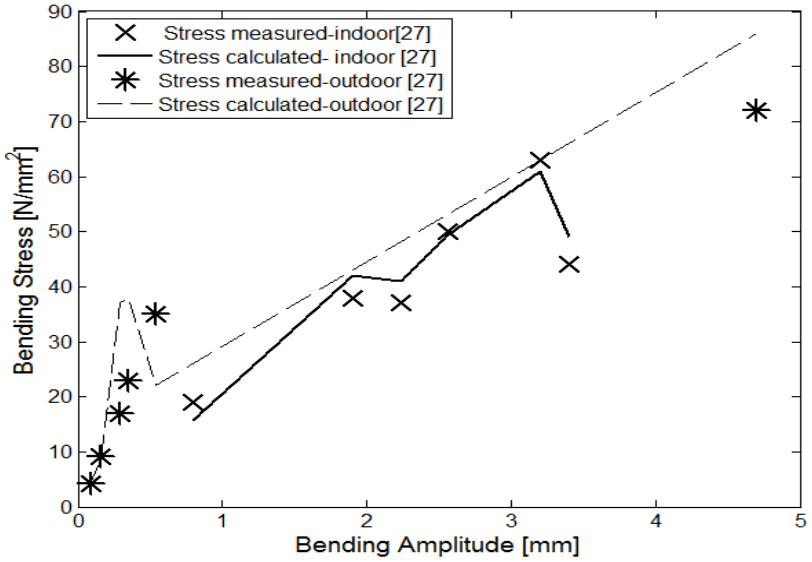

Figure 2-9 Bending Stress vs. bending Amplitude comparison between Predicted and measured on Condor conductor both indoor and outdoor at 45 % UTS and 11 % UTS, respectively

Papailiou [17] in his model on the ACSR Cardinal concluded that the results give a good agreement with his model but a considerable difference was observed using the PS prediction model. The figure 2-10 [16] shows the experimental results on the ACSR cardinal.

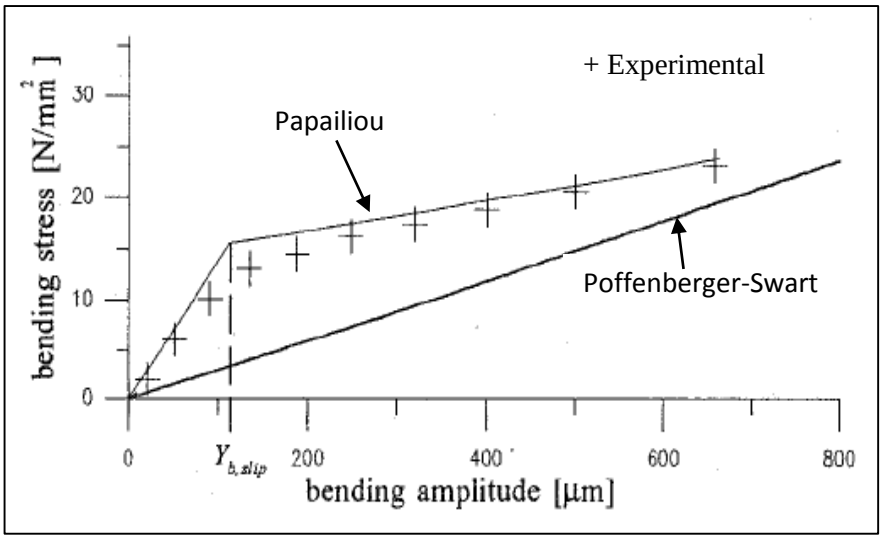

Figure 2-10 Bending Stain vs. bending Amplitude comparison between Predicted and measured results on Cardinal conductor

2.5 Use of statistical tools and techniques

Gillich et al [36] work identified the mechanical characteristics of materials with non-linear behaviour using statistical methods i.e. polynomial and logarithm regression. In their work static and dynamic stiffness were assessed from the collected elongation (strain) data.

In many scientific disciplines (exact, pure, humanities …etc.), statistical tools and techniques are commonly used for data collection and its analysis. The generalization of collected data in a prediction model is usually the main concern and the experimental data could be deterministically or probabilistically modeled when establishing the correlation of a relationship.

There are in general two methods of generalization of the experimental findings in statistics: the linear regression method and nonlinear regression method. The selection of one of these methods depends on how the shape of the plotted data is presented in order to obtain the best curve-fitting to a set of data.

The aims of use of the statistical tools and techniques are to obtain a curve prediction curve with zero deviation if possible.

2.5.1 Polynomial regression technique

The polynomial regression technique gives a simple model of the data set and is simple to use to compute application which may represent the bending amplitude and bending stress relationship using the polynomial regression model which is given as follows:

$$y_i = B_0 + B_1 x_i + B_2 {x_i}^2 + \cdots + B_m x^m + \in_i, (i = 1,2,3, \dots, n) \tag{2.38}$$

Where, $B_0,\ B_1,\ B_2, \dots, B_m$ are the coefficients of the general polynomial model, $\in_i$is the errors between the actual and the predicted model and is related to the residual sum of squares or standard deviation. This explains how good the prediction is and given by

$$SSE = \sum_{i=1}^{n} \left(y_{iexp} - y_{ifit}\right)^2 \tag{2.39}$$

Wherein y_{iexp} is the actual data function of x_i, $y_{i,fit}$ the predicted model (which matches with the curve-fitting). The expression (2.38) is the nth polynomial order equation which may characterize the bending stress with respect to the bending amplitude.

2.5.2 Non-linear regression technique

Non-linear regression modelling are often used and considered to have more scientific significance than the previous technique. The mathematical expression most commonly used is described by the power series as follows:

$$y_i = a{x_i}^{\alpha}\, Q(x_i) \tag{2.40}$$

Where a and α are the function parameter depends on the material characteristics. From a linearized form linearized, equation (2.40) initially represented the log-log scale where a is the antilog of the intercept resulting from intersection of the curve plot in log-log scale with y-axis illustrated in the equation (2.41), α is the slope and $Q(x_i)$ is the factor of correction. In the work done by Newman [39], this factor was reviewed and modelled according to the regression model transformation which is based on equation (2.41)

$$\log y_i = \alpha\, log x_i + \log a + \epsilon_i \tag{2.41}$$

Where ϵ_i is the random error which is a parameter in the correction factor $Q(x_i)$ equation (2.41) and after transformation when using the simple logarithm gives the following expression:

$$y_i = a{x_i}^{\alpha} 10^{\epsilon_i} \tag{2.42}$$

Considering here that the regression was based on the natural logarithm transformation curve, the equation (2.42) becomes:

$$y_i = a{x_i}^{\alpha} e^{\epsilon_i} \tag{2.43}$$

The correction factor by identification function is related to $Q(x_i) = 10^{\epsilon_i}$ and $Q(x_i) = e^{\epsilon_i}$. At this stage, the main concern is to find out among those two correction factors which is more suitable to use which will give a good approximation of the prediction that is close to the experimental data.

The random errors are given by the half of the mean of errors from the regression when using the simple logarithm which is described as follows:

$$10^{\epsilon} = 10^{\frac{MSE}{2}} \tag{2.44}$$

MSE is the mean square of the errors from the regressions. If the residual errors are normally distributed, then the MSE may be calculated indicated in equation:

$$MSE = \sum_{i=1}^{N} \frac{(y_{iexp} - y_{ifit})^2}{N-2} \tag{2.45}$$

Where N is the number of pairs and $y_{iexp} - y_{ifit}$ are the residual errors

On the other, when the residual errors are not normally distributed the equation (2.45) becomes:

$$MSE = \sum_{i=1}^{N} \frac{(y_{iexp} - y_{ifit})^2}{N} \tag{2.46}$$

Regardless of the type of correlation or the normality of the residuals, the estimation of the correction factor is obtained. The predicted stress values may then be obtained from the equation (2.41) or equation (2.42) by a using correction factor (estimates of 10^{ϵ}) from equation (2.44).

2.6 Summary

Many laboratory works are presented by various researchers who wanted to validate or verify the analytical and numerical models.

It is well known that laboratory apparatus and test arrangements can be quite different from each other. Some experiments are performed with the rigid clamp and other are using commercial clamp with different sag angles. The comparison between two different experimental works is usually not appropriate because many parameters must be taken into account.

From the analytical approach of PS formula to the experimental work, there are discrepancies because the calculated stress, which is an idealized stress, and the measured stress, which is the actual stress [20]. The analytical approach is based on many assumptions which can be the cause of deviation from the measured stress (strain).

Various approaches [21] were used to solve this problem using empirical bending stiffness but none of them achieved wide acceptance [2].

Many deeper works are currently in progress in order to quantify the real stress from experimental work. This will allow improving the results obtained using the analytical PS formula that depends

strongly on the bending stiffness [20] and evaluating the non-linearity at small amplitudes in this formula.

Based on the elaborated theories such as PS formula, the bending stiffness mechanism model of Papailiou, including the experimental approach which will be performed in this study, a model could be developed. The new model will give a real stress through a correspondent bending stiffness and will be used on the conductor with the same number of layers and at different range tension each.

In many disciplines, the experimental approach and statistical analysis have showed giving a good prediction of the event of mechanical characteristics with non-linear behaviors. Claren and Diana [14] noticed that the experimental curve is non-linear and this was observed in the most conductors tested. In these conditions, statistical technique may be the unique solution to accurately express the mechanical behavior of conductor under alternated motion.

CHAPTER 3

EXPERIMENTAL EQUIPMENT AND PROGRAMME

3.1 Background

The Vibration Research and Testing Centre (VRTC) research unit has been initiated in 2004 as the result of the partnership between ESKOM and University of KwaZulu-Natal. The purpose of the VRTC is to accompany ESKOM in its power line studies and research development.

The main objective of this work was to collect the stress/strain obtained in relation to the amplitude between 0.01 mm, and 1.2 mm of four different suspended overhead lines common used in ESKOM transmission lines and each conductor at three different levels of tension (as percentage to its Ultimate Tensile Strength (UTS)).

In this chapter, the material used, laboratory set up and equipment, as well as the experimental procedures and methodology are presented according to international recommendations and standards. In addition, an overview of the design of a new loading arm is given.

3.2 Laboratory configuration and equipment

In this section, the laboratory configuration and different equipment used for this research are described.

3.2.1 General

The VRTC's bench consists of an 84.5 m span length of conductor, supported by rigid clamps, which are fixed on two concrete blocks adequately designed to absorb the vibration during the test as presented in figure 3-1. An electrodynamic shaker was placed at 1.2m away from the tension end concrete block to simulate the wind input force on the conductor which is illustrated in figure 3-2. More details of the laboratory test arrangement are reported [30].

In accordance with the international and national standards, the VRTC lab has been designed to perform the experiments at the recommended temperatures between 19.5℃ and 21.5℃, for this reason six powerful air conditioners were disseminated along the laboratory and these are monitored by using the thermocouples surrounding the entire conductor bench. The test

arrangement of the VRTC laboratory is illustrated in figure 3-1

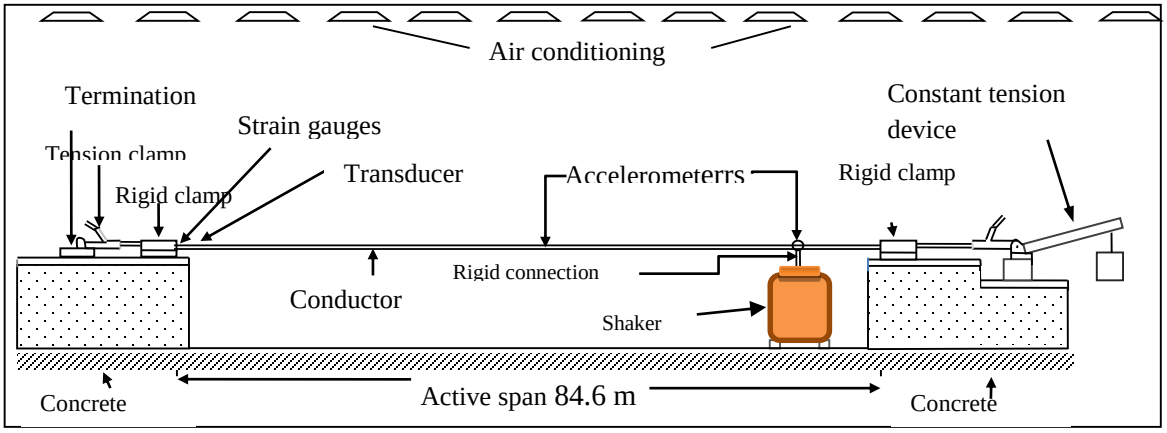

Figure 3-1 Test arrangement of conductor at VRTC

Two shaker control systems were used for the tests: The Vibration Interactive Program (VIP) and the PUMA control system. With the VIP control system the first system presents advantages since the output parameters i.e. amplitudes and velocities are manually controlled by adjusting the excitation voltage to shaker. The control is done by using a function generator (Agilent 33220A) that is connected to the amplifier of the shaker with measurements taken using the Lab View software (National Instrumentation). Figure 3-2 illustrated Electrodynamic vibration exciter: shaker and rigid connection:

Figure 3-2 Electrodynamic vibration exciter: shaker (left) and rigid connection (right)

In figure 3-3, the control and acquisition system used are illustrated:

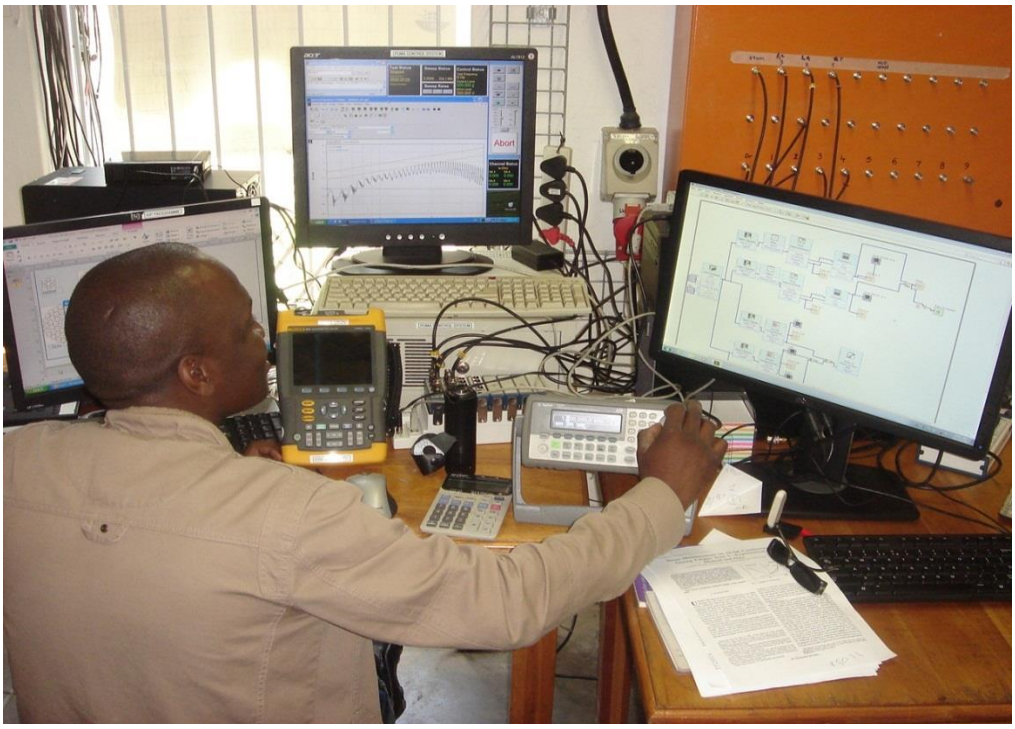

Figure 3-3 Control and acquisition system at VRTC

3.2.2 Design of new loading Arm

In the first stage of this project, an old unused loading arm was modified which could reach a tension of 200kN as opposed to a small loading arm that is limited to a maximum tension of 50kN. The new loading arm will be used to stretch heavier conductors i.e. ACSR Dinosaur, Bersfort and even some types of bundle conductors. Finite element analysis (FEA) was carried out using a special commercial package, MSc SimXpert, to assess the mechanical critical strength based on the drawing geometry, material, maximal loading, boundary conditions and welding operation.

3.3 . Materials

To have a better assessment of the experimental relationship between bending amplitude and bending stress of a conductor; four different types of ACSR (Aluminium Conductor Steel Reinforced) conductors were used: Rabbit (6Al. /1St.), Pelican (18 Al. /1 St.), Tern (45 Al. /7 St.) and Bersfort (48 Al. /7 St.). Their mechanical characteristics and cross section configurations are shown in table 3-2, table 3-3, table 3-4, and table 3-5. Each aluminium layer of the conductors was numbered in the anticlockwise direction as suggested by Rawlins [31] and the steel layer are

coloured in blue. ACSR conductor are composed of one or more layers of hard-drawn concentrically-stranded type *1350 H19* aluminium wire with a high-strength galvanized steel core. The core could contain one or many steel wires (1, 7, and 19). These conductors are actually among the most used by ESKOM in low voltage (LV), medium voltage (MV), high voltage (HV) and extra high voltage (EHV) and are manufactured in South Africa. Examples of commonly used conductor in HV and EHV in South Africa are shown in table 3-1 (ESKOM's transmission line map)

Table 3-1: example of the commonly used conductors in HV and EHV in South Africa

Conductor Type	**Distance km**	**Start Name**	**End Name**	**Design Volt**
4 Pelican	17.19	Grassridge	Poseidon	220kV
4 Pelican	115.13	Dedisa	Poseidon	400kV
6 Tern	429.48	Gamma	Perseus	765kV
3 Tern	406.80	Beta	Delphi	400kV
3 Tern	285.05	Arnot	Maputo	400kV
3 Tern	246.07	Droerivier	Hydra	400kV
2 Bersfort	173.04	Athene	Pegasus	400kV
3 Bersfort	119.17	Ariadne	Venus	400kV
3 Bersfort	112.47	Camden	Duvha	400kV
3 Bersfort	154.70	Majuba	Pegasus	400kV

In South Africa, Tern and Bersfort conductors are the most commonly used transmission line conductors and are used in different configuration i.e. single and bundle (twin, triple…). It is important to underline that Tern conductor are the most used in kilometres of conductor and in high voltage and Extra High Voltage(EHV) between 400 and 765 kV. Four conductors were chosen for this study: Two conductors Rabbit and Pelican having a single steel core and the other two Tern and Bersfort having a steel core with seven steel wires. It is indeed a good scenario to explore the effect of conductor sizes for those **categories** of conductors in order to assess the distribution of stress when the amplitude is varying on many steel wires (1, 7, and 19). It is

necessary to emphasise that ACSR Rabbit conductor is used in Mean Voltage (MV) and it is why it is not in listed table 3-1.

The minimum stiffness of different conductors are given in table 3-2, table 3-3, table 3-4, and table 3-5 was calculated using equation (2.28). All other parameters .i.e. diameter, number of wires, linear mass, and the rated tensile strength, have been given by the supplier (Aberdare cable) and by EPRI [2].

Table 3-2 Mechanical characteristic and cross section of ACSR Rabbit (18 Al. / 1 St.) conductor

Total area (mm^2)	8.81
Overall diameter (mm)	10.05
Number of strand per layer - Steel - Aluminium	 1 6
Ø of Aluminium wire (mm)	3.35
Ø of Steel wire (mm)	3.35
Linear Mass (kg/m)	0.214
Rated Tensile Strength (N)	18 500
Conductor Stiffness (Nm^2)	12.21

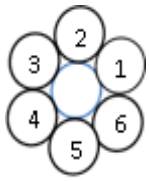

Table 3.3 Mechanical characteristic and cross section of ACSR Pelican (18 Al. /1 St.) conductor

Total area (mm^2)	255.77
Overall diameter (mm)	20.68
Number of strand per layer - Steel - Aluminium	 1 12 - 6
Ø of Aluminium wire (mm)	4.14
Ø of Steel wire (mm)	4.14
Linear Mass (kg/m)	0.771
Rated Tensile Strength (N)	52 490
Minimum Stiffness (Nm^2)	20.78

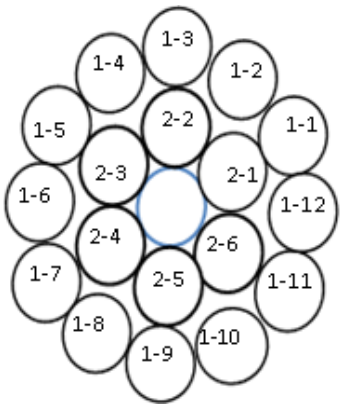

Table 3.3 Mechanical Characteristics and cross section of ACSR Tern (45 Al. /7 St.) conductor

Total area (mm^2)	430.71
Overall diameter (mm)	27
Number of strand per layer - Steel - Aluminium	 6 -1 21-15-9
Ø of Aluminium wire (mm)	3.38
Ø of Steel wire (mm)	2.25
Linear Mass (kg/m)	1.334
Rated Tensile Strength (N)	98 310
Minimum Stiffness (Nm^2)	21.60

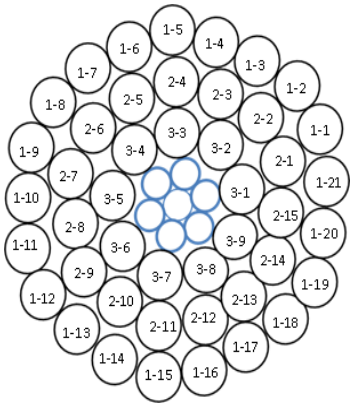

Table 3.4 Mechanical characteristics and cross section of ACSR Bersfort (48 Al. /7 St.) conductor

Total area (mm^2)	746.9
Overall diameter (mm)	35.56
Number of strand per layer - Steel - Aluminium	 6-1 22-16-10
Ø of Aluminium wire (mm)	4.27
Ø of Steel wire (mm)	3.32
Linear Mass (kg/m)	2.37
Rated Tensile Strength (N)	180 **1**00
Minimum Stiffness (Nm^2)	62.76

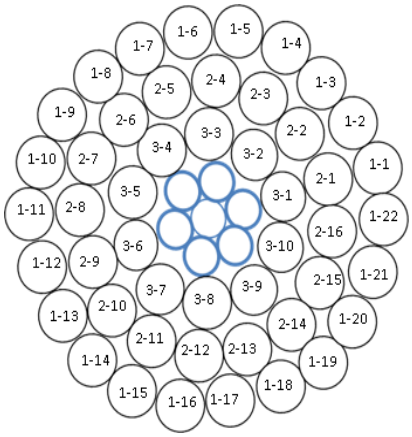

3.4 Experimental Methodology

Based on many assumptions the PS formula [2] gives the relationship between the bending amplitude and bending stress/strain on the uppermost wire of the conductor at the point where the conductor enters, or becomes restrained by, the clamp. This nominal stress determined by PS formula is an idealized stress because it relies on many assumptions .i.e. the cable is considered as a rod, but in reality it is constituted by the helical structure (constituted of twisted wires). Analysis of the dynamic stress at these supports is complicated because due to the stranded configuration of the conductors during bending the conductor cross section does not remain plane [16].

This work is mainly intended to collect data from different ACSR conductors at different levels of tensile loads (in relation to their ultimate tensile strength (UTS)) and then to provide a realistic model by statistically analysing those collected data (regression) in order to better assess the stress (strain) as a function of bending amplitude. Statistical analysis is commonly used in several research fields using various analysis models of regression i.e. linear, non-linear and polynomial. The choice of the listed regression is related to fitting the best curve to the data results [32]. It is well recognised that the polynomial regression is much easier to program even though often found difficult to interpret. Also the power series model regressions were carried out and showed a very good fit in many research disciplines.

IEEE standard [13] and CIGRE recommendations [28] suggest investigating the strains localized on top of the surface of the conductor at the edge of the rigid clamp (at the o-called last point of contact), where the fretting fatigue mostly happens (high stress part). The amplitude sensor for displacement measurement is suggested to be placed at 89 mm (x_b) from the clamp edge. This suggestion was initiated by Tebo [12] for the reason that at this distance, the shape of the conductor was governed only by the stiffness characteristic not by the inertial force induced by the acceleration in the loops.

The experimental analysis of the dynamic stresses measured on the uppermost wire of the outer strand layer is considered in the PS model. The experimental stresses thus collected, should provide a realistic model (analytical or deterministic model) after statistical analysis. This model was established for three different level of tension that can be determined by using strain gauge measurements associate with Hooke's Law which gives the correlation between strain and stress illustrated in the equation (3.1).

$$\sigma_b = E.\varepsilon_b \tag{3.1}$$

The stress results, that were initially collected as strains were explored by using equation (3.1), because the stress data gives an insight of the fatigue failure (nominal stress).

3.4.1 Measurements of elongations (strain)

The strains in question have very low values and must be recorded from the far ends of the laboratory and at the frequency of the vibration system. For this reason a strain measurement system was used which is constituted of:

- Strain gauges: Three strain gauges were glued according to the sketch of the conductor cross section as illustrated in above on three uppermost outer layer wires: Top or Center (1-X), Right (1-Y) and Left (1-Z). The strain-gauges used have a resistance of 350 ± 5 % Ω and a Gauge Factor of 2.07 ± 0.5 % a 24 °C.

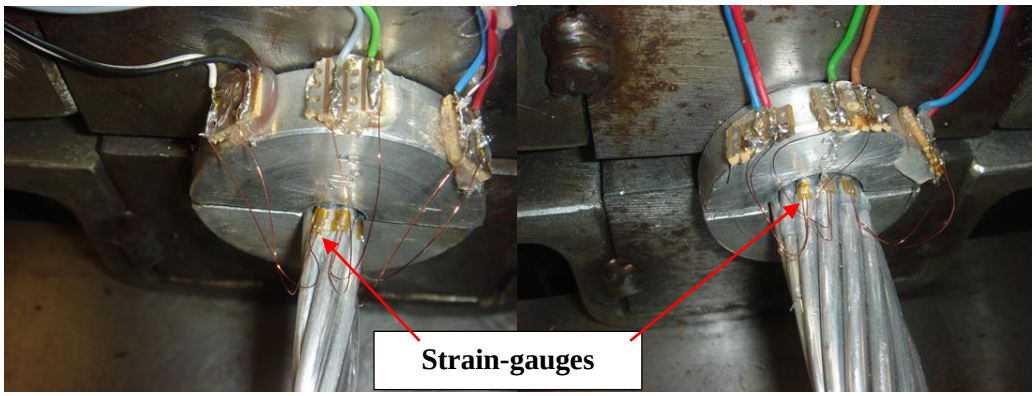

Figure3-4 Photo of strain gauges glued on the Rabbit (left) and Pelican (right) ACSR conductors

The position of the wire in the strand was numbered as wire i-j in anti-clockwise direction as suggested by Rawlins [31] where i is the layer in the strand and j is the wire in the layer. There is an exception to the wires in the ACSR Rabbit strand which has only one aluminium layer numbered as wire j (j=1,2,3...6). This way it is simple to localise the strain-gauges on the conductor as shown in table 3-5 below.

Table 3-5: Location of strain-gauges on different wire positions on the conductor

Position	Rabbit	Pelican	Tern	Bersfort
Left	wire 1	wire 1-2	wire 1-4	wire 1-5
Centre	wire 2	wire 1-3	wire 1-5	wire 1-6
Right	wire 3	wire 1-4	wire 1-6	wire 1-7

-Amplifiers: Three signal strain gauge amplifiers (MP55) illustrated in the figure 3-5 (HBM model voltage supply of 24 V DC and the amplification factor G: 5000) were used to condition the signal from the strain i.e. the signal amplified 2 mV are given 10 V. A 100 m length of cable was wired from the measurement to the computer to collect the strains and was connected to the strain gauges in the half bridge. The half-bridge was constituted of an active strain gauge, which

was glued on the wire and a dummy strain-gauge placed on a separate aluminum plate (with the same characteristic as the measuring wire) for temperature compensation. The MP55 amplifier is constituted of a filter module which is useful for filtering the overflow signal and interference (noise). A virtual filter from LabView was used associated to the physical filter incorporated in the MP55 (100 Hz) which also aims to prevent aliasing such as the shift of zero reading.

-Data acquisition (DAQ) device: The type of DAQ used is a brand of National Instruments (NI) that constituted of a chassis (card) for input data into the computer and two NI 9233 modules each having 4 differential analogue inputs (rate of sampling 52 kilo samples/sec and a resolution of 24 bits). One module was allocated for the strain measurements and the other for acceleration and displacements measurements as illustrated in figure 3-5.

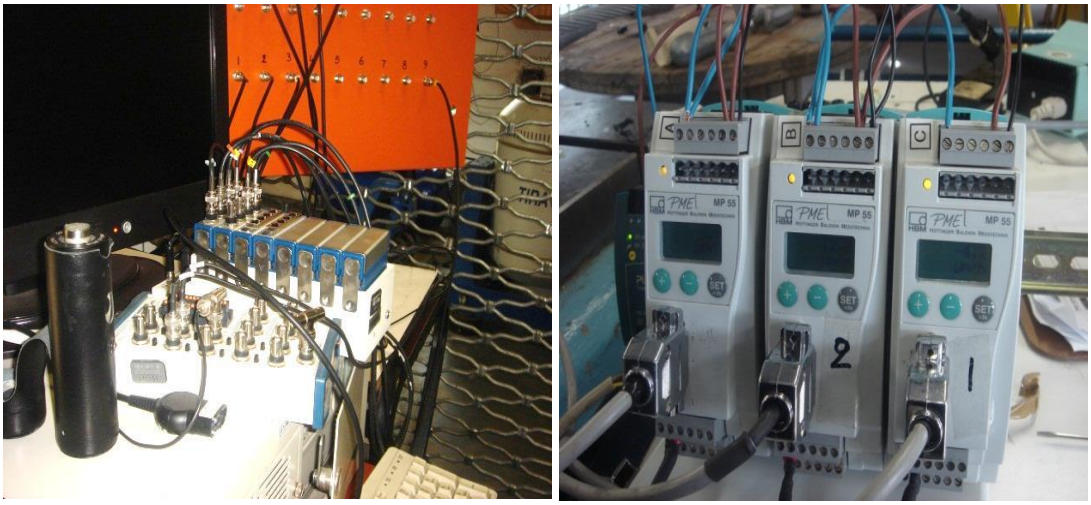

Figure 3-5 Data acquisition- NI 9233 modules (Left) and signal amplifier MP55 (right)

-Wirings: In order to prevent signal losses and interferences, a special kind of cable is used to transfer signals from different points of measurement (strain-gauges and accelerometer as displacement transducers) was used. From the strain-gauges to the amplifier, ordinary electrical cables could be used for the short distance. Due to the distance between the computer and the amplifier, the coaxial cables (MIL-C-17F-RG 058) were used for the displacement transducer and the strain-gauge MP55 meters which cable of low resistance since the cable is of 100 m length.

-Computer: The shaker controller and data acquisition was accomplished using a commercial package .i.e. NI LabView and Signal Express driver, allowing the real-time processing signal and

storing of data. Virtual digital filters were placed in the block diagram in order to clean up the noisy signals i.e. interference due to the electromagnetic field of equipment. These filters were used for accelerometer and strain-gauges since the value picked are at low amplitudes (low signal which is easy to be influenced by the interference). The principle of measurement using the strain-gauges illustrated by the schematic in figure 3-6:

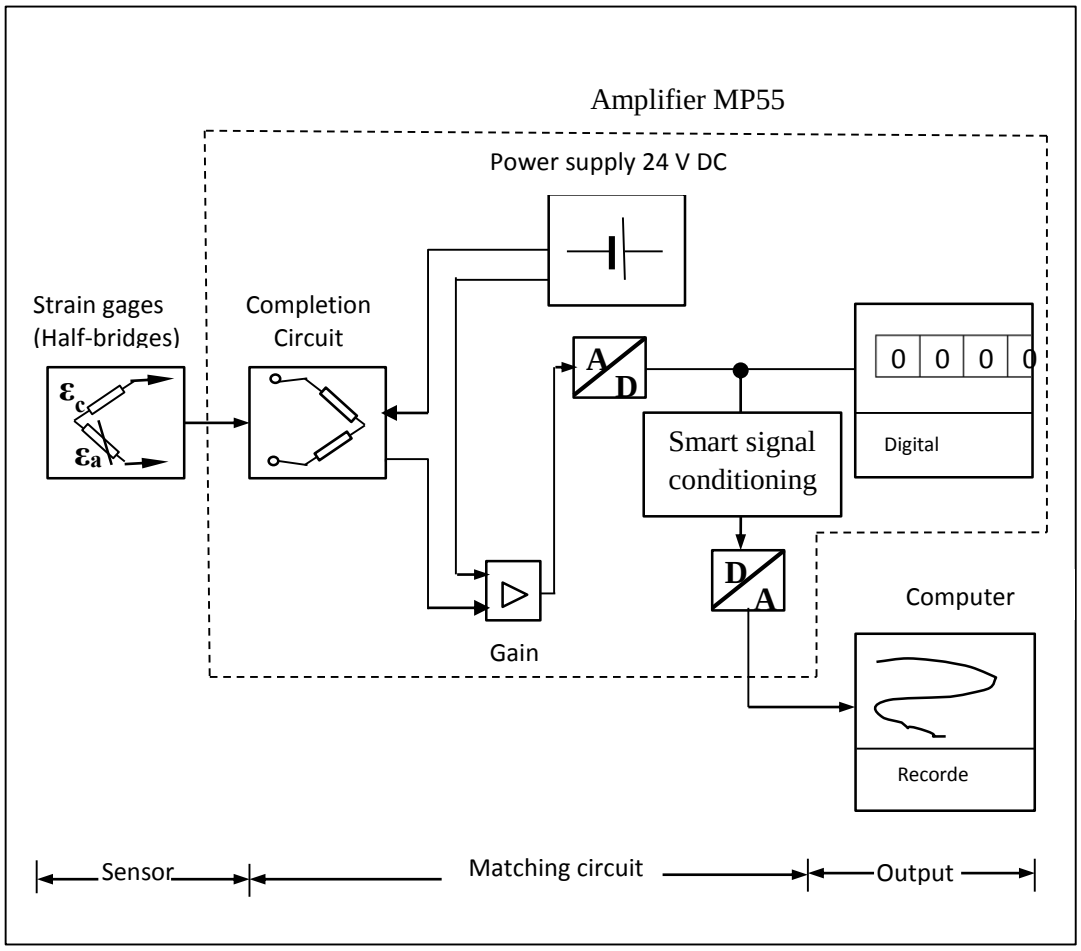

Figure 3-6 Block diagram of strain measurements showing: active ε_a and dummy ε_c strain-gauges, the amplifier, wirings and the computer

3.4.2 Experimental Procedures

In order to minimise possible errors due to the measurements, the experimental procedures were conducted according to International Standard (IEEE and IEC), and recommendations (CIGRE). It is thus important to underline that the VRTC Lab is designed to perform the testing with

constant temperature (between 19.5 ℃ and 21.5 ℃) since six powerful air conditioners are installed along the conductor bench and are controlled internally and measurements are done by eight suspended thermocouples disseminated on the length of the conductor.

3.4.2.1 Installation of the conductor on the bench

Conductors were donated by Aberdare cables and were brought on drums. The conductor was opened, then stretched and conditioned for 35 % UTS for more than one night since the conductor was rolled up for quite a long time on the drum. To attach the conductor on both sides, pistol grips were used for the Rabbit and Pelican which is illustrated by figure 3.3, and dead-ends used for Tern and Bersfort conductor.

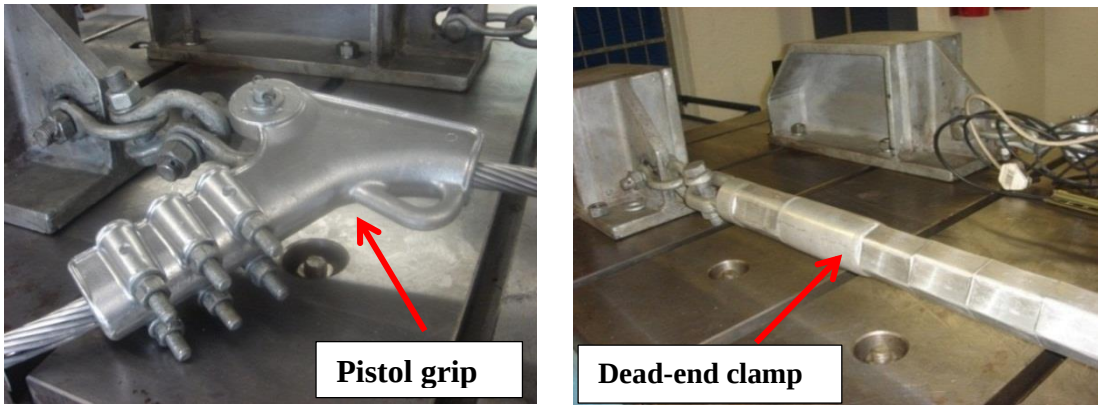

Figure 3-7 Photo of pistol grip; Pelican (left) and dead-end clamp: Bersfort (right)

For the two other bigger diameter size conductors, a dead-end clamp was used to grip the conductor using the relevant procedure underlined in the IEC standards [37]. The advantage of using the crimped dead-end in the laboratory work is to avoid the internal layers to slip during the loading procedure as opposed using the pistol grip especially for bigger diameter conductors. An automatic hydraulic crimping machine (IZUMI) was used for crimping the dead-end on the conductor, starting by the steel core layer itself and then both steel and aluminium layers were crimped together. Several dies were used in the crimping machine according to the type, diameter and size of the conductor).

Rigid clamps placed on the concrete blocks (figure 3-1) are designed to be tightened with four bolts at a torque of ± 52 Nm based on IEC recommendations [1] and rigidly fixes the conductor

by compression of the keeper on the base of the rigid clamp. An aluminium insert was used for each conductor diameter size in the rigid clamp.

3.4.2.2 Strain-gauges and accelerometers on the conductor

The objective is to glue the strain gauges at the location where the most significant strain occurs. The first position susceptible to get the highest strain is on the top of the last point of contact (LPC: the edge of the clamp) which is considered as the reference in the PS calculations. The strain gauges were inspected before and after they were glued on the conductor. The inspection was aimed at assuring that the gauges were not broken or to make sure that the resistance value of the extensometer used is 350 ± 1.5 Ohms.

Two accelerometers were placed on the conductor: one at 89 mm from the LPC and the other one at the shaker position with respectively sensitivities of 97.2 mV/g and 96.7 mV/g. It was observed in the all cases that the resonance frequencies were found during the experiments when the ratio on the amplitudes of the shaker Y_s and that on the 89 mm bending amplitude Y_b equal or smaller than six, i.e.:

$$y_s/y_b \leq 6 \tag{3.2}$$

3.4.3 Dynamic Measurements

.4.3.1 Choice of bending amplitude peak-to-peak(mm)

Based on the CIGRE safe line design it is recommended to investigate the amplitudes between 0.2 mm and 1.2 mm [28]. In addition, the amplitudes between 0.01 mm and 0.1 mm were investigated because of the uncertainty of the P-S formula at small amplitudes. From these amplitudes, a non-linearity curve of stress results were observed on the ACSR Drake conductor by Poffenberger-Swart [2] which stated that the small amplitudes were in the cloudy region because, it could not be adequately represented by their formula.

Some particular amplitudes were chosen in order to compare with some previous results with past research i.e. work on ACSR Ibis (done by Aida and co-worker), ACSR Bersfort by Levesque et al conductor which has the characteristic almost close to the ACSR Pelican and Papailiou on the ACSR Cardinal [17].

.4.3.2 Choice of the static loading (% UTS)

In this work, a proposal was made to examine a range of the ultimate tensile strengths which are used in South Africa especially on ESKOM's transmission lines. The criteria used to string up the conductor on the tower is based on the EDS (everyday stress) which is the allowable stress design (ASD) and is based on national and international recommendations [36] given by the following equation (3.3)

$$C = {}^{H}/_{w} \tag{3.3}$$

Where C the is parameter (m) referred to the catenary equation of the conductor, the everyday stress (EDS) value (MPa), H is the static loading (kN) and w is the linear mass (kg/m). ESKOM recommends [1] a C value of 1800 m, which means that tensions are in the range of 20% UTS and 30 % UTS. Three tensions therefore were chosen i.e. 20 % UTS, 25 % UTS, and 30 % UTS .The ESKOM C value corresponds to 20.8 % UTS for ACSR Rabbit, 26.5 % UTS for ACSR Pelican, 24.4 % UTS for ACSR Tern, and 23.70 % UTS for ACSR Bersfort.

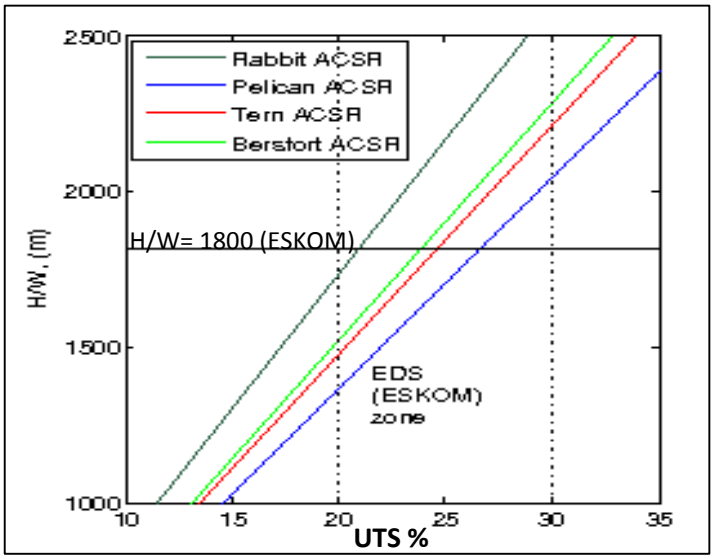

Figure 3-8 Recommended UTS for ACSR conductors (Rabbit, Pelican, Tern and Bersfort) as given by ESKOM

The scenario of the EDS limit proposed was presented in figure 3-8 where the points of intersection between the conductor's sag and the ESKOM's EDS correspond to the transmission lines in South Africa for the mentioned conductors. These points correspond to the above mentioned UTS.

The safe tension design has been investigated by the EDS panel which has been active since 1960 by CIGRE working group in order to develop a guide for the safe tension of conductor under Aeolian vibration [28]. It is important to remind, that the tension is the most important parameter in the bending amplitude-bending stress relationship [12] and also that the tensions are the controlling factor in an overhead line conductor: knowing that as higher the tension is in the strand the more severe and more damaging are the vibrations. Table 3-6 is given the different tensions in N in relation to the ultimate tensile strength of the conductors used:

Table 3-6: Different tensions (N) in relation to the Ultimate tensile strength of the conductor used

ACSR Conductor	**Tension used[N]**		
	20% UTS	**25%UTS**	**30%UTS**
Rabbit	3700	4625	5550
Pelican	10498	13122.5	15747
Tern	19662	24577.5	29493
Bersfort	36020	45025	54030

3.4.3.3 Choice of natural frequency

The experiments were performed at constant velocity (0.3 m/s). the frequencies which were chosen in the range of 8 Hz - 25 Hz (Aeolian Vibration), which is close to the resonance frequencies [30] or particular natural frequencies well-known as Eigen-frequencies. It is obtained:

i) analytically i.e. use of the VIP simulator (incorporated with a resonance calculator) by putting in the simulator all the conductor parameters i.e. weight per length, ultimate tensile strength, and overall diameter,

ii) experimentally by the sweep method the using the Puma control system. This method is recommended because it gives the actual resonance frequencies.

The resonance frequencies are very important because if not suitably chosen, the shaker can be damaged.

3.4.4 Static Measurements

The static measurements were performed with two objectives:

i) to check on how the stress varies from the low to high UTS,

ii) to assess the stress induced by the rigid clamp pressure imparted when tightening it.

It was thus tested firstly with the clamp tightened at 52 Nm following the recommendations and secondly with clamps loosened as performed in the previous work [30]. The conductor was tensioned at the lowest possible tension (when the sagging conductor soft touches the floor) and thereafter the strain-gauge meters were zeroed.

3.5 Experimental Analysis

The objective is to reduce possible errors which may occur during experimental measurement and which may due by the noisy signals (interferences). The choice of a reliable experimental analysis is necessary in order to minimize those possible errors for this project which depends on the experimental outputs.

3.5.1 Static strain analysis

The sensitivity for the strain-gauge is 2 mV/V with sensitivity at 400 με/V from the amplifier. This is considered in the strain amount read ε_{read} on the computer having in mind that the signal of the strain-gauges collected in voltage has been amplified and is given by the equation (3.4).

$$\varepsilon \approx \frac{4V_{out}}{V_{exc}G_f}\frac{10^6}{K_f} \tag{3.4}$$

where V_{out} is the voltage drop at the bridge sensor, V_{exc} is the voltage of excitation, G_f is the gauge factor which is equal to 2.07 and k_f is the amplifier factor which is equal 5000. The amount of 10^6 is multiplied in the equation in order to have the measurement in microstrains. To eliminate as possible errors due to the noise in the measurement, the average was determined after three measurements were performed using the equation (3.5).

$$\varepsilon_s = \frac{\sum_{i=1}^{N}\varepsilon_{s,i}}{N} \tag{3.5}$$

3.5.2 Dynamical strain analysis

The measurement of the strain due to bending is determined by the peak to peak amplitude which gives the maximum and the minimum strains defined by the plot "strain as a function of time" which is shown in seconds in the figure 3-9. This was respectively positive and negative according to the principle of traction and compression. The mean ε_{bi} was calculated for each period in time and is considered equal for every second and then the average over 60 seconds was determined and given by the equation (3.6)

$$\varepsilon_{bi} = \frac{\sum_{j=1}^{N}(\varepsilon_{bj,max} - \varepsilon_{bj,min})}{2} \tag{3.6}$$

Where $\varepsilon_{bn,max}$ and $\varepsilon_{bn,min}$ are respectively the maximum and the minimum strains collected corresponding to one amplitude peak-to-peak, and which are most closely equivalent $|\varepsilon_{bn,max}| \simeq |\varepsilon_{bn,min}|$ (traction and compression). The strain curve as a function of time is showed in the figure 3-9 and is defined by the shape of a sinusoidal function. For more accurate results, the experiment was conducted at each amplitude level and performed at least three times in order to minimize the errors due to the measurement. The bending strain ε_b thus present is the average strain of n measurements of strains collected ($\varepsilon_1, \varepsilon_2, \varepsilon_3, \dots, \varepsilon_n \; and \; n = 1,2,3, \dots$) at each amplitude level.

$$\varepsilon_b = \frac{\sum_{i=1}^{N} \varepsilon_i}{N} \tag{3.7}$$

Equation (3.3) is used to validate the experimental measurement and to verify the reliably of the instruments used which were calibrated before the experimental work.

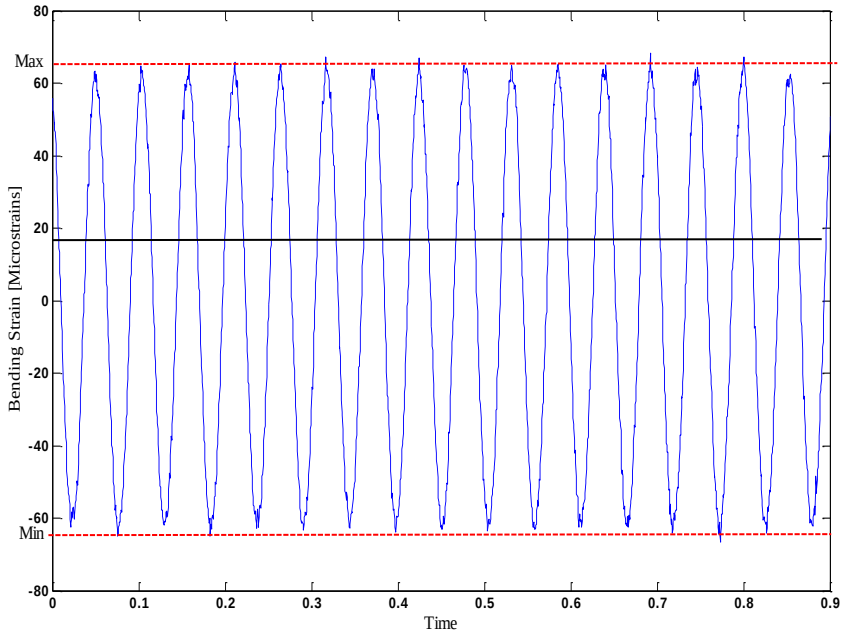

Figure 3-9 Figure strain vs. time curve during a bending strain measurement on ACSR Tern conductor at an amplitude of 0.1 mm peak-to-peak

During the dynamic measurement, the strain-gauges were read continuously whilst being loaded, and then it is evident that non-uniformities in the strain signal occurred. To overcome this, several measurements were performed for the reason to limit uncertainty and errors; the related bending stress σ_b is obtained using the expression (3.1).

The strain due to the temperature was not considered according to the assumption taken in the first chapter about the variation of temperatures. Although the ambient temperature along the conductor in the laboratory is maintained constant close to 21 ℃ ($\pm$ 1 ℃) as recommended by the measurement standard, a temperature compensated strain-gauge and also the preventive device was employed to eliminate the thermal effect, otherwise errors in the measurements may occur.

The frequencies from both the measurements and the conductor-shaker system should be synchronised whereby sinusoidal wave form is obtained. The manufacturer of the LabView package [35] suggested choosing a minimum sampling frequency which is the sampling rate f_s (number of samples per second) defined to be greater than ten times the frequency of the system to measure. Levesque's research [33] suggested that this frequency has to be equal to the spectral frequency ($\Delta f \approx 0.1$) multiplied by the number of points as described in the equation (3.8).

$$f_s = Number\ of\ points\ \times \Delta f \tag{3.8}$$

Indeed, as the strain recorded as function of the peak-to-peak amplitude 2500 samples have been recorded for each second at a rate of 5000 Hz.

3.5.3 Identification of appropriate statistical regression technique

To identify the appropriate statistical regression technique, the step should be followed:

- **Step 1:** the variables collected are plotted in a scatter-diagram Bending stress σ_a as function of bending amplitude y_b.The relationship between two variables is represented in the graph.
- **Step 2:** observing the scatter shape curve which is a form of existing relationship model shape, the type of regression technique is chosen among the several predefined in the package. Three factors have to be:
- i) the estimator or predictor factor R^2 which has to be $R^2 \cong 1$ (strength of the relationship),
- ii) the standard deviation SSE between the result and the prediction model and
- iii) the model of stress distribution on which the standard error depends.

There are several statistical analysis methods which are used for the prediction of the experimental result. The appropriate model should:

(i) give a good correlation with the results and

(ii) depend on decision of the researcher i.e. expected applications and analysis.

In most of the cases, it is a compromise between the above. Other concerns in statistical prediction are its limitation: the results can be valid for the values between the points tested.

In figure 3-10 the flowchart showing different step for prediction with statistical regression technique.

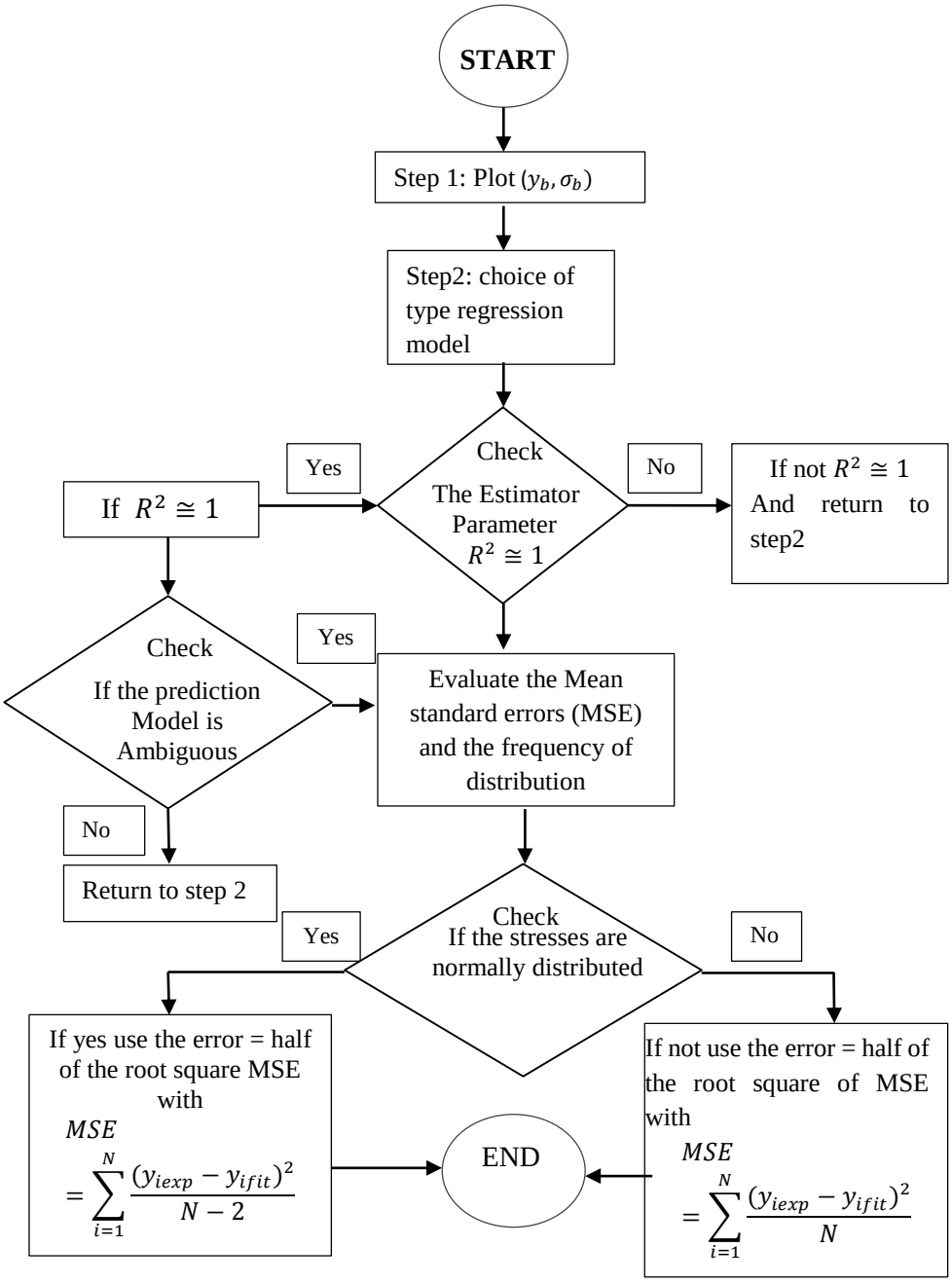

Figure 3-10 Flowchart showing step of model prediction using statistical regression technique

3.6 Summary

The procedures of dynamic measurement were performed as follows:

The conductor was well-prepared and was rigidly clamped on the bench at a preloaded tension. The required tension was then monitored by suitable instrumentation procedures. The strains were recorded using three different conductor tensions H1, H2 and H3 as a function of the amplitudes Yb, between 0.01 mm to 1.2 mm which is adjusted manually using the function generator. The measurement at each amplitude level was repeated at least three times (in order to minimize errors due to imperfection of signal during measurements). The measurement time was set for 60 seconds at the natural frequency which is close to the resonance frequency was determined by both the analytical and the sweep method [30]. The data collected were computed and stored for analysis. Finally the measured strain data have been converted to stress using the Hooke's law and plotted, i.e. bending stress as function of bending amplitude.

CHAPTER 4

EXPERIMENTAL RESULTS

Background

In this chapter, the strain data were collected and plotted as a function of the amplitude. After calculating the average of the strains there was no significant ($\pm$ 2 %) difference between the three measurements. The tests were performed at resonance frequency between 10 Hz and 25 Hz which were both predicted and measured values. The measurements were carried out according to the IEEE standard [13] and CIGRE guide [28]. Today, the accuracy of strain-gauges technology, iteration software, and data acquisition are much better than the ones used in the past. The strain measured was plotted as a function of the amplitude for each wire and was performed at different tension levels.

In addition, comparison was done between the results and some prediction models i.e. the Poffenberger-Swart model and the improved model using the bending stiffness model by Papailiou [15].

The retained static measurements were compared to the theoretical expression of Ramey and Townsend [25] that was earlier reported in chapter 2, which gives the axial tension in the strand and causes an approximate longitudinal static strain of

$$\varepsilon_t = \frac{H}{(nA_s + A_a)E_a} \tag{4.1}$$

With H = tension in the conductor; $A_s =$ total area of steel; $A_a =$ total area of aluminium; n = modulus of elasticity for steel/modulus of elasticity for aluminium; and Ea = modulus of elasticity for aluminium. Two equations are commonly used to estimate static bending strains in conductor strands at the tower support points located at the mouth of a fixed clamp.

4.2 ACSR Rabbit conductor

In this section, the static and dynamic measurements of the ACSR Rabbit are given:

4.2.1. Static measurement

The conductor was brought to the lowest possible tension of about 2 kN. From this level, the tension was gradually increased in a step of 0.4 kN until 4.4 kN. A remarkable difference was observed in wire 1 with the clamp tightened (CT) and the clamp loosened (CL). One explanation may be given, because of the static pressure due to the clamping. A torque of 52 kN was used to clamp the conductor on the bench. On the other two wires, 2 and 3, there was no significant difference between CT and CL shown in figure 4-1 about $\pm$ 15 %.

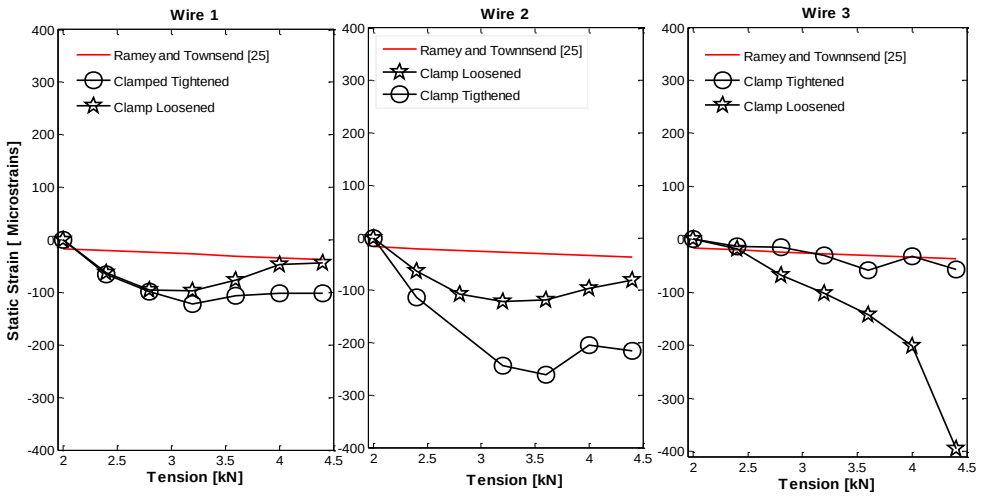

Figure 4-1 Static strain vs. tension on the three different wires (1, 2, and 3) in the **ACSR Rabbit** strand according the sketch in table 3-2

4.2.2. Dynamic measurement

The dynamic strains as illustrated by figure 4-2 presents a general scenario of Rabbit conductor at three tension levels. from 0.01 mm to 0.2 mm. It was thus noticed that the top wire (wire 2) provided a smooth growth of data . The exception is observed at 20 % UTS for the amplitude 0.5 mm and 1.2 mm. A simple explanation may be given, is that there is no interference of the top wire according to the configuration (constituted of two underneath wires: the steel core and the aluminum wire). Wire 1 presents irregularity of the strain data in general with exception for the amplitudes lower than 0.5 mm. As the weight of this conductor is not significant, many ranges of frequency may be used to perform the bending strain measurement. The resonance frequency between 10 Hz and 15 Hz were used to get the strain at the fixed amplitude.

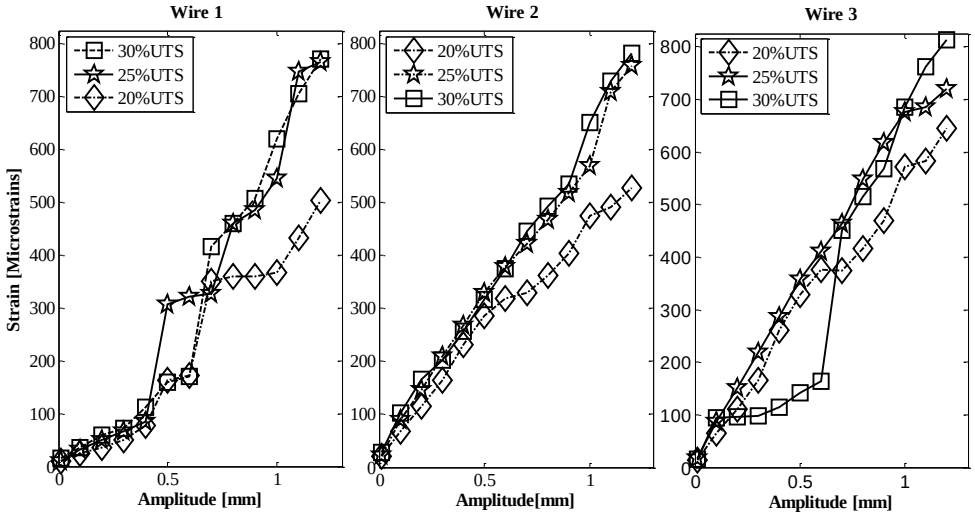

Figure 4-2 Dynamic strain vs. Amplitude at 20 % UTS, 25 % UTS and 30 % UTS on the three different wires (1, 2, and3) in the ACSR **Rabbit** strand according the sketch in table 3-2

4.3 ACSR Pelican conductor

In this section, static and dynamic measurements on the ACSR Pelican are given:

4.3.1. Static measurements

The static measurement on the ACSR Pelican conductor are almost similar to the results obtained on the Rabbit conductor. However, there are diffrence in their magnitude and the steps used. Figure 4-3 shows the static result on the ACSR Pelican conductor.

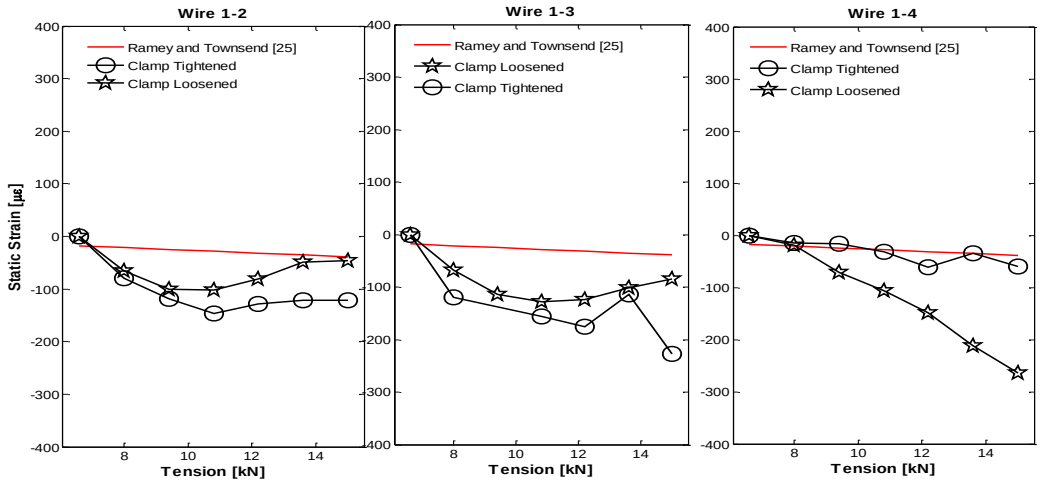

Figure 4-3 Static strain vs. tension on the three different wires (1, 2, and 3) in the **ACSR Pelican** strand according the sketch in table 3-3

4.3.2. Dynamic measurements

In figure 4-4 different plots are given in which the strain as a function of amplitude shown for the three uppermost wires (wire 1-2, wire 1-3 and wire 1-4) of the Pelican conductor. In general the result at 20% UTS and 25 % UTS are the same as show by their curve shape in all the wires. The slip-stick state can be observed in the plots represented in the figure i.e. the strain at 30% UTS is smaller as compared to the stress at 20% UTS and 25 % UTS. This phenomena is significant in the wire 1-2 and wire 1-4, while the wire 1-3 the results observed are almost similar for these different tensions. A simple explanation based on this, is that the stiffness of the ACSR Pelican is not much affected by the tension

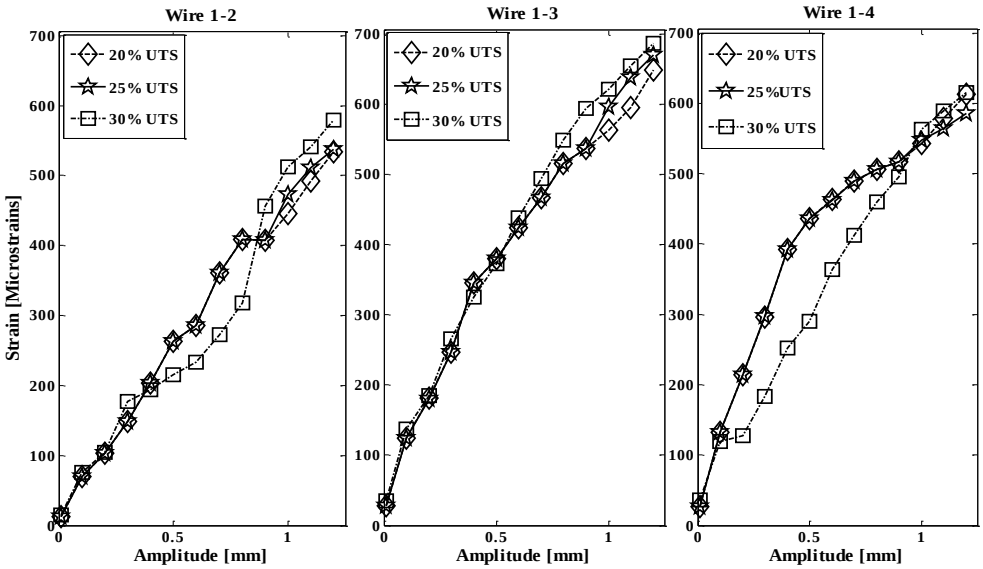

Figure 4-4 Dynamic strain vs. Amplitude at 20 % UTS, 25 % UTS and 30 % UTS on the three different wires (1-2, 1-3, and 1-4) in the **ACSR Pelican** strand according the sketch in table 3-3

4.4 ACSR Tern Conductor

In this section, static and dynamic measurements on the ACSR Tern conductor are given:

4.4.1. Static measurements

The pressure of the clamp on the conductor affected the wire 1-5 and wire 1-6 when the tension varies from 10 kN to 24.1 kN. These variations are observed between the strain collected when the clamp is tightened and loosened i.e. at 20.1 kN, which are in magnitude equal to - 67.1 $\mu\varepsilon$ and 64.7 $\mu\varepsilon$ for the clamp tightened and the clamp loosened, respectively. The strain observed on the wire 1-4 indicated no difference for the clamp tightened and the clamp loosened.

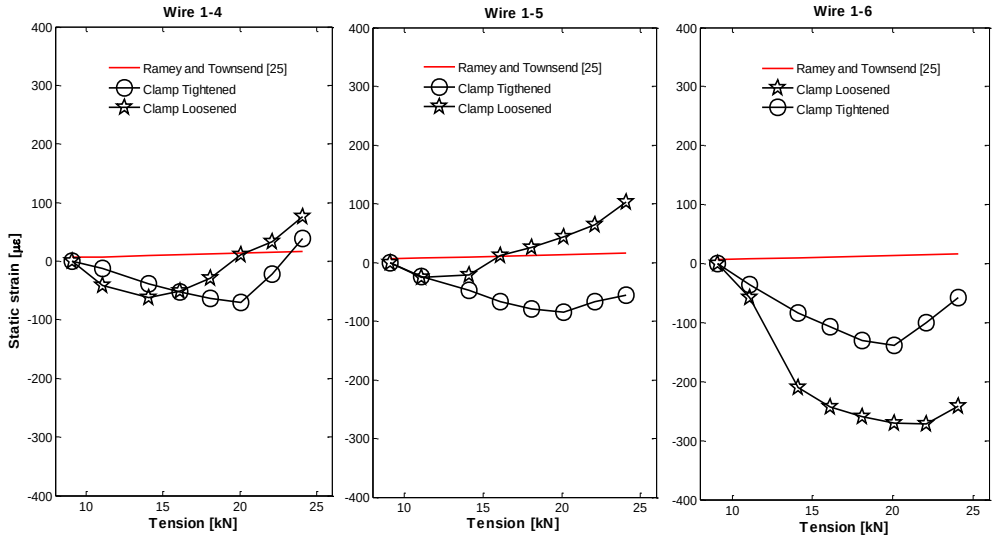

Figure 4-5 Static strain vs. tension on the three uppermost wires (1-4, 1-5, and 1-6) in the **ACSR Tern** strand according the sketch in table 3-4

4.4.2. Dynamic measurements

Comparatively with the two previous conductors, the dynamic strain collected on the Tern conductor can be clearly observed in figure 4-6. The strains were measured for the amplitudes less than and equal to 1 mm due to the weight of the conductor and limitations of the shaker.

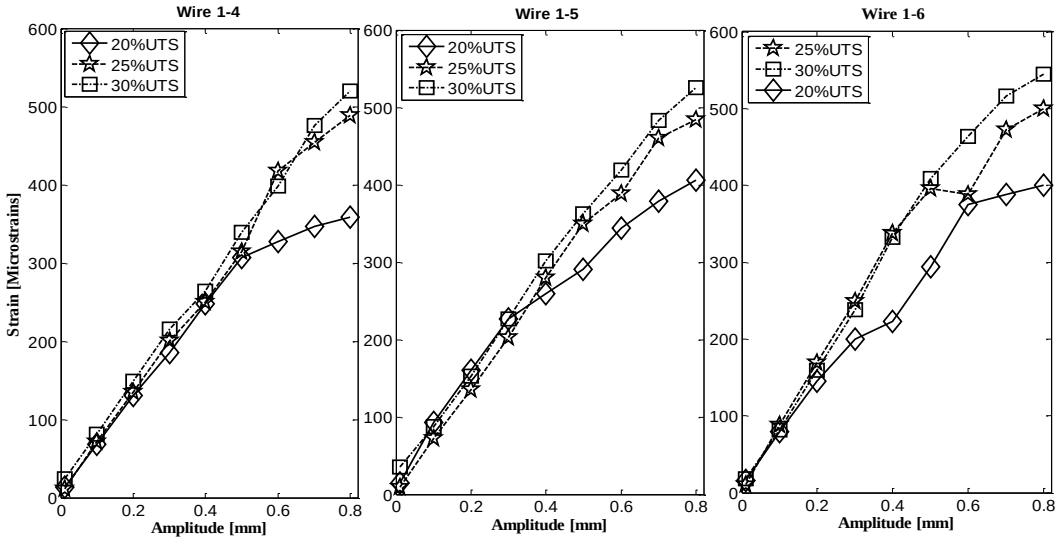

Figure 4-6 Dynamic strain vs. Amplitude at 20 % UTS, 25 % UTS, and 30 % UTS on the three different wires (1-4, 1-5, and 1-6) in the **ACSR Tern** strand according the sketch in table 3-4

4.5 ACSR Bersfort

In This section, static and dynamic measurements on the ACSR Bersfort conductor are given:

4.5.1. Static Measurement

The static measurements with the clamp tightened and with the clamp loosened are similar in Bersfort conductor, with the exception noticed on the strain result of the wire 1- 4 and on the wire 1-6. On the wire 1-4, there is big difference between the results for the clamp tightened and clamp loosened with an average deviation of 20 %. A small deviation of about 10% is observed in the results on the wire 1-6 the tension above 40 kN.

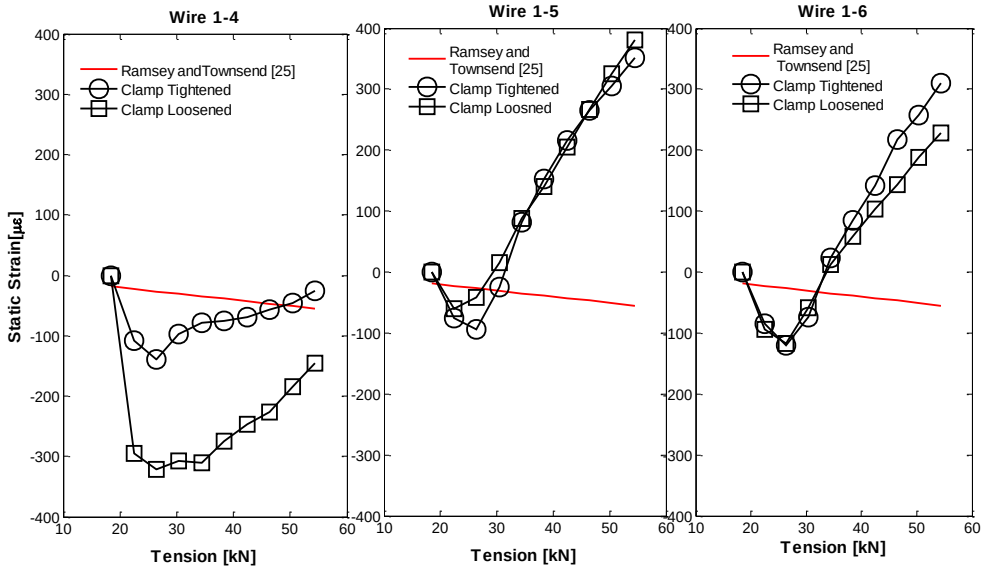

Figure 4-7 Static strain vs. tension on the three uppermost wires (1-4, 1-5, and 1-6) on the **ACSR Bersfort** strand according the sketch in table 3-5

4.5.2. Dynamic Measurement

During the dynamic measurements on the ACSR Bersfort conductor, the strain-gauges sinusoidal signals were clearer than the other conductors that were tested. Due to the weight of the Bersfort conductor (2.37 kg/m) it was not easy to maintain constant amplitude above 0.8 mm and the limitation of the shaker since the rigid connection was used. In figure 4-8 the bending strain vs. bending amplitude is given for different wires 1-4, 1-5 and 1-6. The input resonant frequencies from the shaker was used for obtaining the amplitude at 89 mm were greater compared to the previous conductor i.e. at 20 % UTS. The amplitude at the resonance frequency was found at 21 .78 Hz for Bersfort and 19.5 Hz for the Tern conductor.

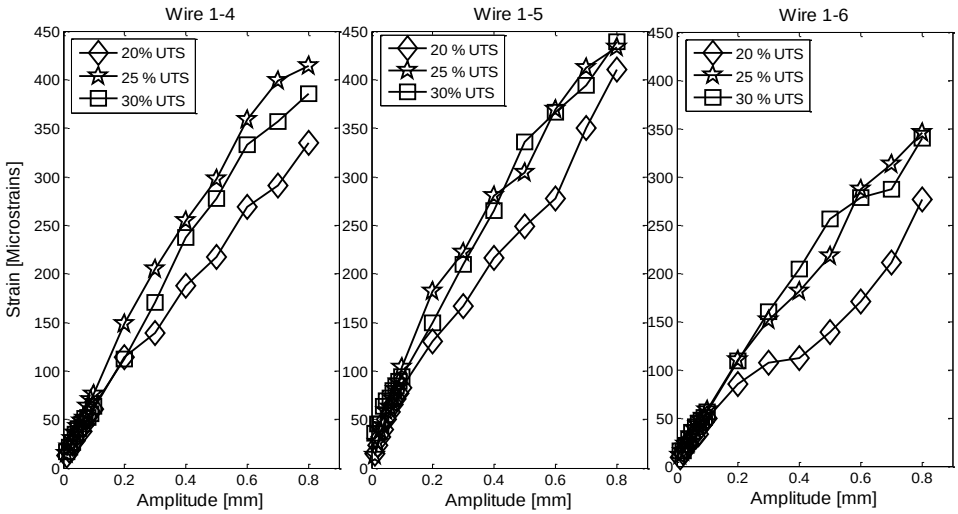

Figure 4-8 Dynamic strain vs. Amplitude at 20 % UTS, 25 % UTS, and 30 % UTS on the three different wires (1-4, 1-5, and 1-6) in the **ACSR Bersfort** strand according the sketch in table 3-5

Comparison to previous experimental work

There is limited data available in literature regarding the stress measurement on the conductor used in this research. Levesque et al. [33] performed static and dynamic measurements on ACSR Bersfort at the univesity of Laval. The conductor was mounted on a bench of 11 m length and was fastened using a short commercial clamp with an exit angle of 62°. In table 4-1, the comparison between previous research and this work is shown:

Table 4-1: Comparison between (i)Levesque et al[41], (ii) Ouaki et al [40] and the present study on Bersfort conductor.

Levesque et al [41]		Ouaki et al [43]		present work	
amplitudes	strains-LPC	amplitude	strains LPC	amplitudes	strain CE
0.32	157	-	-	0.3	223
0.47	231	0.43	200	0.5	304
0.55	264	0.55	300	0.6	370
0.76	357	0.65	330	0.8	439

The LPC is the last point of contact , where the strain-gauge has been glued. The comparison shows, that the short commercial clamp with the exit angle of 62° reduces the bending strain between 20%-30% with the variation of the amplitude, even the results seem to be in the same range level. This can be explained that the radius of curvature of the short commercial clamp reduces the shear force compared to the squared faced rigid clamp (exit angle equal to 0) used in

this research . Similar conclusions were made by Dalpe [48] in the experimental work for ACSR Drake and Zebra conductors. which compared two types of clamp with an exit angle of 5° and 10°. McGill et al [10] compared the fatigue performance results between ACSR Drake conductor attached with four different types of clamp i.e.

(i) short radius and deep groove,
(ii) medium radius and shallow groove,
(iii) medium radius and deep groove, and
(iv) long radius and deep groove.

They concluded that the conductor fatigue performance is reduced when the radius of the clamp decreases. The figure 4-9 illustrated the different clamps used in [25].

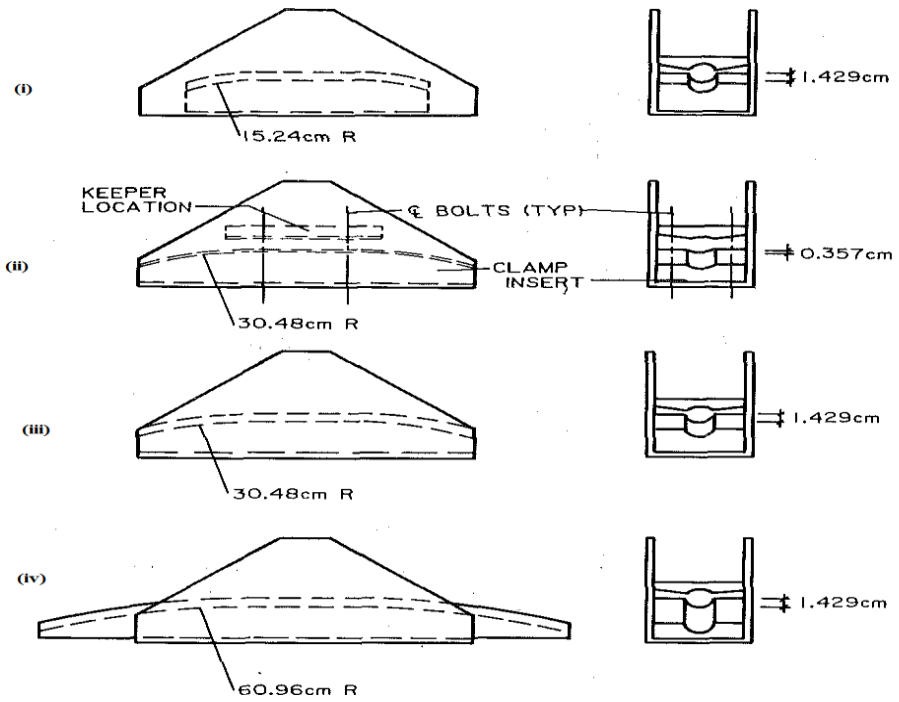

Figure 4-9 Examples of clamps used to compare the performance fatigue of a Drake conductor

Comparison between experimental, P-S and Papailiou Model

The most disseminated and practical model used for design and maintenance purposes (assessment of life expectancy) is the Poffenberger-Swart formula as noticed in chapter 2 and given as follows:

$$\sigma_a = \frac{E_a\,\delta\,p^2}{4(e^{-px}-1+px)} Y_b \text{ (where } p = \sqrt{\frac{H}{EJ}}\text{)} \tag{4.1}$$

wherein E_a is the Young modulus of aluminium (70 GPa which is not applied to stranded wires), δ is the diameter of the outer layer wire (mm), H is the static tension in the conductor (N), EJ is the bending stiffness ($N.mm^2$) and x (89 mm) is the distance from where the amplitude is measured.

The crucial element in equation (4.1) is the bending stiffness EJ that is normally taken as the minimum bending stiffness EI_{min} (constant) as initially developed in the PS model. In the model developed by Papailiou the bending stiffness is given as a function of the curvature $EJ(k)$ and the tension in the strand (slip-stick state). The calculation of the varying stiffness is not so easy to use and it is required to determine the curvature k as a function of the amplitude of the conductor attached at the clamp. The software SEIL has been developed at PFISTERER for the use in the Vibrec 400 (vibration recorder) which is not public domain used software. This provides the total stress as function of the amplitude peak-to-peak with as the scenario where the bending stiffness model of Papailiou is used in the P-S model. Equation (4.2) is also discussed in chapter 2.

$$EJ(k) = EJ_{min} + \sum_{j=1}^{i-1} EJ_{stick,j} + (2)\sum_{j=1}^{a} EJ_{slip,j} \tag{4.2}$$

4.7.1 ACSR Rabbit conductor

The results obtained on different conductors shows that there is a good correlation between the predicted (Papailiou model) and the experimental results. On the ACSR Rabbit conductor, the Papailiou model gives an excellent prediction for this conductor stretched at 20 and 25% UTS at the level range of 0.1 mm to 1.2 mm. At 30 % UTS, and from 0.9 mm to 1.2 mm through the gap between prediction and experiments becomes significant with the amplitude greater than 0.9 mm. The deviation between the results and the PS prediction was $\pm$45 % as shown in figure 4-10.

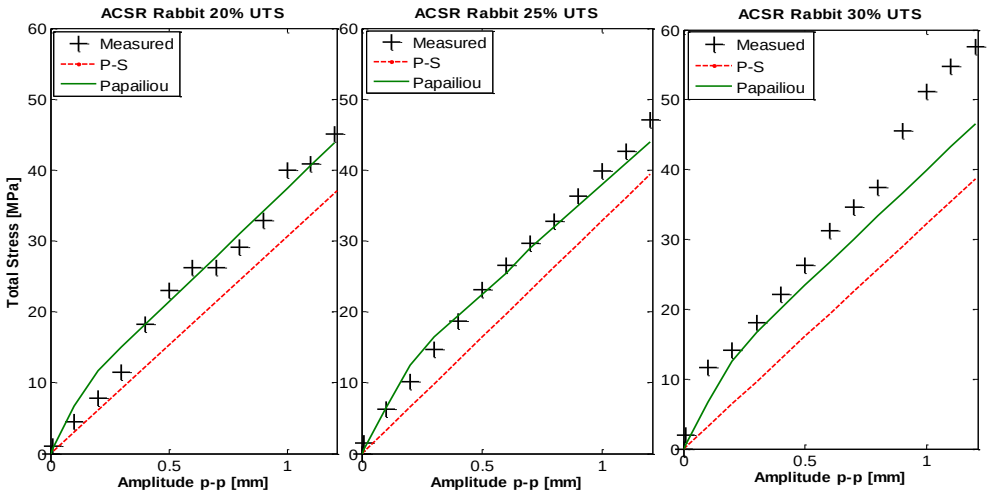

Figure 4-10 Measured and Predicted (PS Formula and Papailiou Model) of The **ACSR Rabbit** conductor at 20 % UTS, 25 % UTS and 30 % UTS

4.7.2 ACSR Pelican conductor

In the ACSR Pelican conductor which is illustrated in figure 4-11, it was observed that there is good correlations with the Papailiou model with the variation of the tension in the strand and the correlation was better with the measurements from 0 mm to 0.6 mm at 20% UTS, until 0.8 mm at 25% UTS and 1 mm for 30% UTS. The shape of the data looks similar with the one developed by Papailiou on the Cardinal conductor [17].

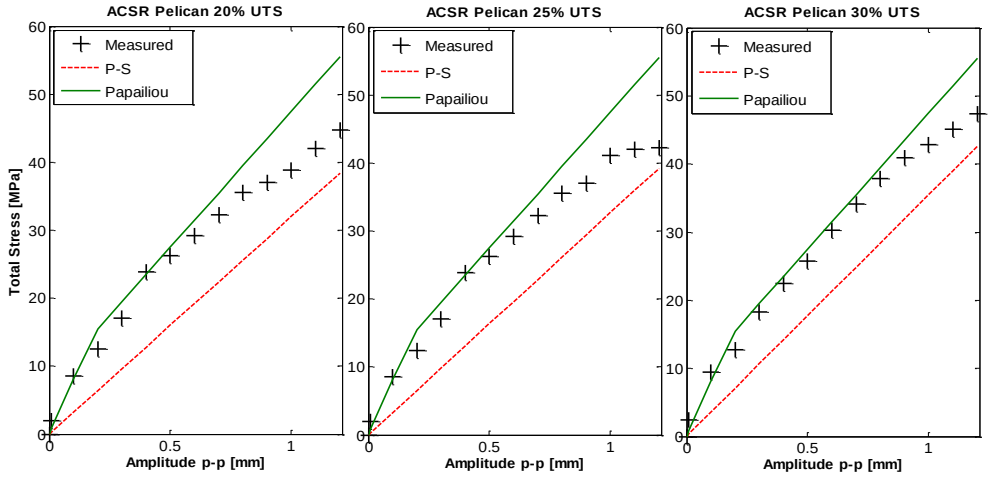

Figure 4-11 Measured and Predicted (PS Formula and Papailiou Model) of The **ACSR Pelican** conductor at 20 % UTS, 25 % UTS and 30 % UTS

4.7.3 ACSR Tern conductor

In figure 4-12, the stresses collected on the top wire of ACSR Tern conductor correlates well at 20 % UTS from 0.01 mm to 0.7 mm and toward the Poffenberger-Swart prediction model for the amplitudes greater than 0.7mm. At 25 % UTS, the small amplitudes can be represented by Papailiou model i.e. from 0.01 mm to 0.2 mm. in contrast to the previous tension, at 30 % UTS the stresses correlate well enough from 0.04 mm to 1 mm.

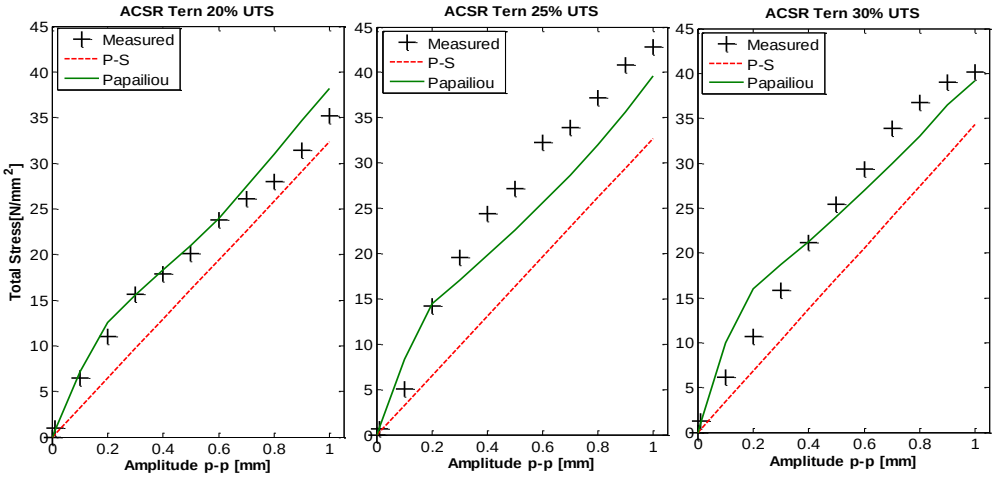

Figure 4-12 Measured and predicted (PS Formula and Papailiou Model) of The **ACSR Tern** conductor at 20, 25 and 30 % UTS

4.7.4 ACSR Bersfort conductor

The measured results correlate well enough with the PS formula except at small amplitude especially from 0.01 mm to 0.1 mm where the results match with the Papailiou's model. The predictions of the stress using the PS model show a deviation of ± 10% (figure 4-13)

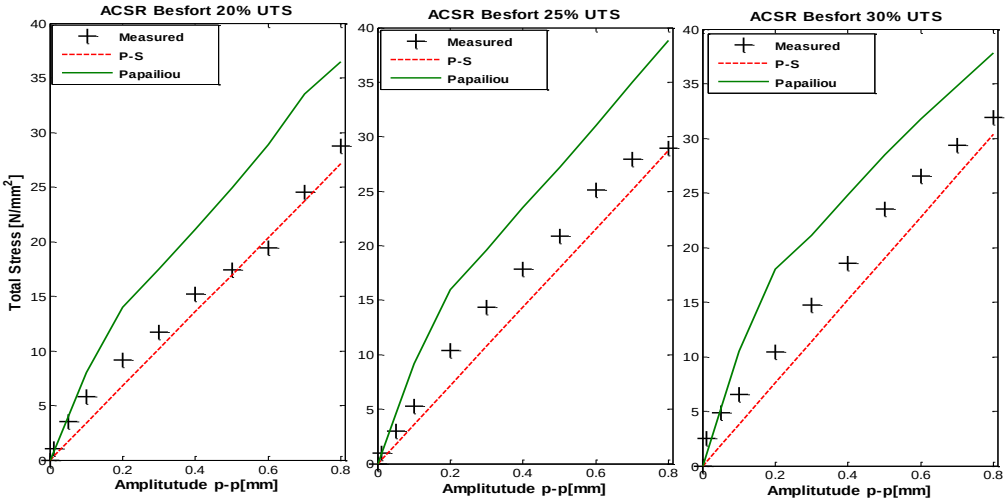

Figure 4-13 Measured and Predicted (PS Formula and Papailiou Model) of The **ACSR Bersfort** conductor at 20, 25 and 30 % Ultimate Tensile Strength (UTS)

Summary

In general, a considerable discrepectancy was observed between the actual and the predicted stress measurement when using the PS formula and there was a better correlation with the model developped by Papailiou [15]. The comparison was made between the theory and the stress collected at the uppermost wires where the first sign of fatigue damage happenes and is summarized in the table (Appendixes). The model developed by Papailiou requires many calculations and a special package in order to determine the curvature as a function of the bending amplitude. The table 4-2 below shows the comparison between the measurements and (i) the prediction model using the PS model [9] and (ii) the prediction model using the Papailiou theory [17]. Δ and Δ^* represent the average deviation between the measurements (i), and (ii), above respectively.

Table 4-2: Comparison between measurement and prediction models: P-S [9] and Papailiou [17]

Tension	Rabbit		Pelican		Tern		Bersfort	
UTS (%)	Δ (%)	Δ*(%)	Δ(%)	Δ*(%)	Δ(%)	Δ*(%)	Δ(%)	Δ*(%)
20	45.2	2.1	36.7	1.1	27.2	2.8	21.1	27.9
25	29.9	3.39	36.1	2.1	39.1	2.9	27.8	25.2
30	44.8	20.4	34.7	9.3	36	7.1	30.3	32.1

For the ACSR Rabbit, Pelican and Tern conductors, the model of Papailiou can be used to predict the relationship between the bending amplitude and bending stress at the clamp fitting. However, the PS model seems to be better suitable for the ACSR Bersfort conductor.

The focus is on the stress collected on the uppermost wire on which numerous expressions of the bending stress as function bending amplitude were proposed by several researchers. it is for the reason that in most the observations, the first sign of fatigue damage start on the top wire of the conductor where the stress during bending is the highest.

CHAPTER 5

STATISTICAL EVALUATION OF TEST RESULTS

5.1. Background

Poffenberger and Swart [11] have presented a practical and analytical model for characterisation of the bending stress on the uppermost wire where the first sign of fracture may be observed. This PS model depends on the diameter of the outer layer wire d_a, minimum stiffness EI_{min} and the tension in the strand (% UTS). Later, Papailiou improved the PS model in giving the varying bending stiffness model $EJ(k)$ which is a function of the curvature k and explained by the slip-stick state.

As observed in the previous chapter in general, there is no good relationship between the measurements and the prediction when using the stiffness EI_{min} in the PS model. However good correlation with (k) , i.e. the Papailiou model, was observed for a certain range of bending amplitude levels under tension. But the model by Papailiou requires the use of special software for the curvature and stress calculations.

5.2. Prediction models of bending stress

In this chapter, two main realistic models were developed for each ACSR conductor used i.e. Rabbit, Pelican, Tern and Bersfort. The data were collected at different ranges of their ultimate tensile strengths (UTS) i.e. 20 % UTS, 25 % UTS, and 30% UTS. The choice of the tension is used by Eskom to describe the stress distribution.

Various techniques, methods and software i.e. Microsoft Excel, MatLab, GraphPad…, etc. have been developed in order to obtain a more accurate simulation or prediction function. This is done by using a deterministic or statistical approach algorithm for the analysis of the experimental results (data).

Several types of curve fitting i.e. bilinear, exponential, and polynomial, etc. were attempted on the bending amplitude-bending stress results: two curve fittings were found interesting in the analysis of the outcome data:

- Curve fitting with a polynomial function of the third order in terms of four parameters using the multi linear regression technique the so called polynomial regression

- Curve fitting with exponential function using a non-linear model: the logarithm regression model.

Statistical analysis of the collected data was performed using a commercial package i.e. Excel GraphPad and MatLab package. In this research, the data was analysed using a comprehensive program called GraphPad Prism, which is a powerful three-in-one commercial package consisting of biostatistics; curve fitting and scientific one graphing.

The software mentioned indicated a simple click to all-important statistical parameters that are calculated and the data is computed in the data sheet model where the x-axis is the amplitude peak-to-peak and bending stress is the y-axis. A simple click on the analyse function and then on the types of regression models i.e. linear, quadratic, log-log etc., allowed many possibilities to be explored. The programmer has to use judgement when chooses the regression technique that will be suitable and this must be based on the observation of the data distribution and the expectation of its use.

5.3. Stress function parameters

The stress function parameters for the different conductors be found in the plots (figure 5-1):

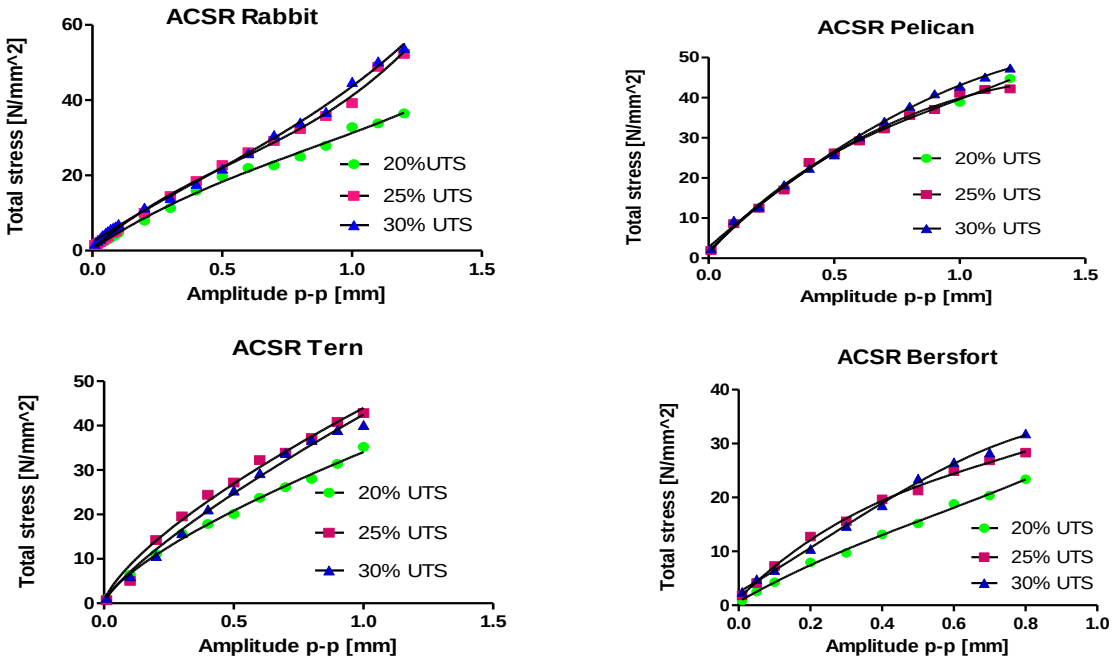

Figure 5-1 The data points represent the stresses measured and the lines shows a curve fitting equation that can be used to approximate the data point at 20 % UTS, 25 % UTS and 30% UTS for different conductor tested i.e. Rabbit, Pelican, Tern and Bersfort

In chapter 3, a flow chart was presented showing the basic steps used on how to undertake the regression technique and how scientifically to examine the models developed from these regressions.

Based on the shape of the plots (stress as function of the amplitude), two statistical techniques were suitable to be applied in this research polynomial regression and non-linear regression:

5.3.1. Polynomial regression technique

The bending stress σ_b was plotted as a function of the bending amplitude y_b in the range of 0.01-1.2 mm which is used to obtain the predicted bending stress function. A polynomial regression technique was executed on the result data in order to obtain small variations between experimental measurements $\sigma_{b,expt}\,(y_b)$ and predicted values $\sigma_{b,model}(y_b)$. The polynomial regression was implemented and a curve-fitting with polynomial function of the third order in amplitude terms of four coefficients as illustrated by the equation (4.1):

$$\sigma_{bi} = B_0 + B_1 y_{bi} + B_2 {y_{bi}}^2 + B_3 {y_{bi}}^3 + \in_i , \qquad i = 1,2,\dots,n \tag{5.1}$$

wherein B_0, B_1, B_2, and B_3 are the curve-fitting coefficients which obviously depend on the conductor characteristics (d_a , H, and EJ) and $\in_i$ is the random error on the bending stress. As underlined above the aim of the prediction model is related to minimize the standard error given as follows:

$$SSE = \sum_{n=1}^{N} \left[\sigma_{b,expt}\,(y_b) - \sigma_{b,model}(y_b)\right]^2 \tag{5.2}$$

where N is the number of tested amplitudes, from 0.01 mm-0.1mm with a step of 0.01 mm and 0.1 mm-1.2 mm with a step of 0.1 consecutively, N = 21for Rabbit and Pelican. The amplitudes attempted for Tern and Bersfort were 1.0 mm and 0.8 mm, respectively which give N = 19 for Tern and N =17 for Bersfort.

$\sigma_{b,expt}\,(y_b)$ is the experimental stress obtained on the uppermost wire at the amplitude y_b

$\sigma_{b,model}(y_b)$ is the stress from the predicted model.

It was noticed that the precedent model is the simplest polynomial to be employed for the characterization of stress on the uppermost wire for all tested conductors. The function parameters of different tested conductors are given in table 5-1

Table 5-1: function parameters of ACSR Rabbit, Pelican, Tern and Bersfort according to equation (5.1)

	ACSR Rabbit			**ACSR Pelican**		
Coefficient	20% UTS	25%UTS	30%UTS	20%UTS	25%UTS	30%UTS
B0	-0.364	0.9309	3.703	1.302	1.794	2.732
B1	52.29	52.7	52.04	69	61.08	54.68
B2	-25.44	-23.17	-16.36	-46.39	-26.03	-13.27
B3	11.18	9.237	9.574	15.73	3.035	-1.082
	ACSR Tern			**ACSR Bersfort**		
Coefficient	20% UTS	25%UTS	30%UTS	20%UTS	25%UTS	30%UTS
B0	0.3913	-0.9799	0.9462	0.6686	1.222	2.422
B1	66.5	84.92	47.22	37.87	65.58	39.17
B2	-70.58	-66.95	15.58	-23.08	-61.72	14.04
B3	38.9	26.01	-23.48	14.01	28.07	-21.85

Since the distributions of the stresses are not normal with respect to the bending amplitudes, the random errors can be given by

$$\in = \frac{1}{2}\sqrt{\frac{SSE}{N-k-1}} \tag{5.3}$$

With N the number of the amplitude analysed, k is the degrees of freedom (DOF), and SSE is the standard errors

However, it was found that the accuracy of the fit is not improved by the inclusion of higher order terms. Therefore, only four-parameters (for all cases high order polynomials higher than 3 are ambiguous, in spite of the regression parameter or predictor were $R^2 \geq 0.998$ but standard errors were large for higher than 3rd order).

5.3.2. Significance of the results (interpretation)

The scenario in this experimental work is that the ACSR Rabbit and Pelican conductors are constituted of one steel core where the diameters of the aluminum δ_a and core wire δ_s are the same. On the other hand ACSR Tern and Bersfort have the multi steel core conductors (7-steel wires) with different diameters of aluminum and steel. The stress function is given by the

expression in equation (5.1) where the function parameters or coefficients i.e. B_0, B_1, B_2, and B_3 are particular (unique) for each conductor and each tension H i.e. 20 % UTS, 25 % UTS, and 30 % UTS. It is therefore important to find out the physical interpretation of different parameters in the mentioned expression. Although, the polynomial model is not simple to interpret [36], the variation of the different coefficients with respect to tension gives an overview on the factor which affects the stress behavior.

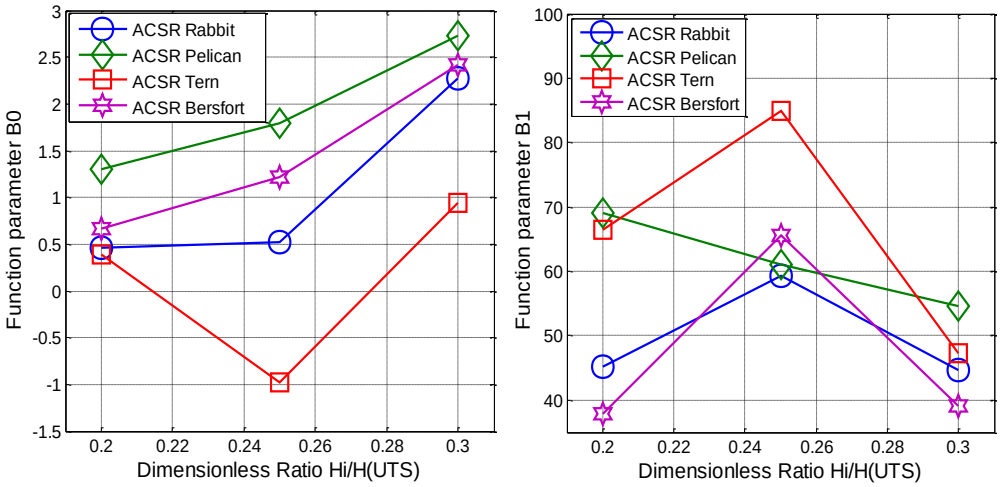

Figure 5-2 Variation of function parameter B_0 (left) and Function parameter B_1 (right) with respect to the tension which is given by the ratio between the tension and the ultimate tension

In general, for all conductors it was noticed that the coefficient B_0 is too small and the dimensional analysis is the same as the bending stress (N/mm^2). The physical interpretation of the parameter B_0 may be considered as a residual stress in the wire due to interference of wires within the layer and not as a static stress caused by the tension of the strand. In these conditions, it is because the strain gauge-meters are zeroed before the measurements. Furthermore, it means that there is not only elasticity in the material and there is plasticity as well [40].The first order parameter B_1 is expressed in stress per unit length [MPa/mm] like the PS coefficient [11]. For the Rabbit conductor the coefficients B_1 remained constant for the range of the UTS used and are 52.3 MPa/mm, 52.7 MPa/mm, and 52.1 MPa/mm respectively. In the Pelican conductor B_1 decreases as the tensile load increases. Finally for the Tern and Bersfort conductor B1 jumps from 20% to 25 % UTS and then decreases at 30 % UTS as illustrated in table 5-2.

The coefficient B_2 is expressed in the stress per unit surface (MPa/mm^{-2}) and this parameter is negative for the single core conductors i.e. Rabbit and Pelican but changes to positive for Tern

and Bersfort at 30 % of their UTS. This parameter could be related to the stress by the elliptic surface of contact [40]. B_2 increases in magnitude with the tension. The stress per cubic unit is characterized by the coefficient B_3 ($MPa.mm^{-3}$) and remains positive in the Rabbit and Pelican while it becomes negative at 30 % of the UTS.

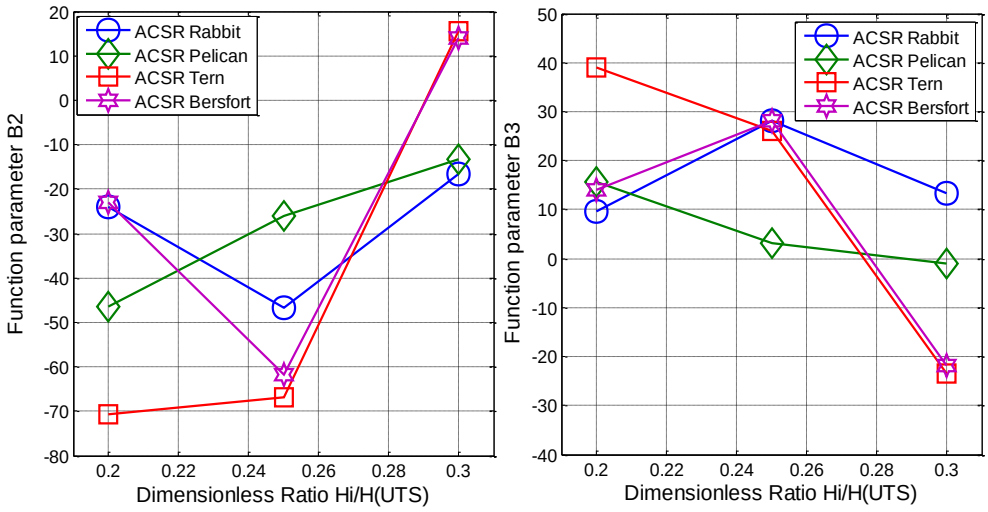

Figure 5-3 Variation of function parameter B_2 (left) and Function parameter B_3 (right) with respect to the tension which is given by the ratio between the tension and the ultimate tension

It is not so easy to give physical meanings of the function parameters B_0, B_1, B_2, and B_3 that were developed, but the dimensional analysis described above highlight the importance of the tension level in the distribution of the stress. A second technique was explored and presented in the following section. The main objective of the physical interpretation was to match the function parameter with important characteristics of the conductor such as diameter, stiffness, coefficient of friction and tension.

5.3.3. Non-linear regression technique

Based on the above and the theory in Chapter 2, log-log line transformation performed in the experimental results of stress can be expressed as follows:

$$\sigma_{bi} = a{y_{bi}}^{\alpha} Q(y_{bi}) \tag{5.4}$$

Where a is the stress σ_b-axis intercept in the log-log scale, α is the slope of the trend line in log-log scale and $Q(y_{bi})$ is the correction factor which is equal to $10^{\in}$ or $e^{\in}$ if the natural logarithm is considered in the scale transformation. The accuracy of the stress function is based on the correction factor $Q(y_{bi})$ which statistically defines how confident the stress parameter is. Therefore both results presented in table 5-2 have to be observed in a scientific way. The second form function of characterisation is more scientific and simple for identifying the parameters a and α corresponding to the properties of the conductor such as the diameter of the wire and overall diameter, friction and static strain induced by the tension in the strand. Also the correction factor also depends on the cable cross section which does not remain in the same plane during bending.

Table 5-2 Function parameters of ACSR Rabbit, Pelican, Tern and Bersfort according to equation (5.4)

	ACSR Rabbit			**ACSR Pelican**		
Coefficient	20% UTS	25%UTS	30%UTS	20%UTS	25%UTS	30%UTS
a	37.45	42	43.88	40.07	39.9	42.75
α	0.90	0.91	0.90	0.67	0.67	0.69
	ACSR Tern			**ACSR Bersfort**		
Coefficient	20% UTS	25%UTS	30%UTS	20%UTS	25%UTS	30%UTS
a	34.22	44.8	44.07	31.8	36.66	36.08
α	0.73	0.77	0.7508	0.78	0.72	0.71

5.3.2.1. Significance of the results (interpretation)

The power model resulted from non-linear regression techniques by log-log scale transformations are illustrated by the equation (5.4). In this equation two function parameters were deduced: the stress axis-intercept a and the slope α.To highlight the physical interpretation, these parameters have to be evaluated according to the conductor characteristic i.e. diameter, stiffness and tension for the power model which is more scientifically explicit than the polynomial model.

The slope α can be given in the tangential expression (5.5):

$$\alpha = \frac{\Delta \log \sigma_b}{\Delta \log y_b} \tag{5.5}$$

By using the realistic model has to be represented firstly by the statistical model and referred to equation (5.2):

$$\sum_{n=1}^{N}\left[\sigma_{b,expt}\,(y_b) - \sigma_{b,stat}(y_b)\right]^2 = SSE_{stat} \tag{5.6}$$

With $\sigma_{b,stat}(y_b)$ as the stress model that resulted from the statistical model and SSE_{stat} is the standard deviation between the experiments and the statistic model.
Secondly if using the PS model to predict the stress function the equation (5.2) becomes:

$$\sum_{n=1}^{N}\left[\sigma_{b,expt}\,(y_b) - \sigma_{b,P-S}(y_b)\right]^2 = SSE_{P-S} \tag{5.7}$$

Wherein $\sigma_{b,P-S}(y_b)\ is$ the PS model of stress prediction and SSE_{P-S} is the standard devition between the actual and the prediction using PS. As the PS model is simple and constituted basic characteristics of the conductor.

By transforming and substituting the experimental $\sigma_{b,expt}\,(y_b)$ in the equation (5.6) and equation (5.7), the following expression can be written:

$$\sigma_{b,stat}(y_b) - \sigma_{b,P-S}(y_b) = \frac{\left(\sqrt{SSE_{P-S}} - \sqrt{SSE_{stat}}\right)}{N} \tag{5.8}$$

Where k_{P-S} is the constant of Poffenberger and Swart characterised by the stiffness, diameter of the outer layer wire and the tension in the conductor

By transforming and substituting the experimental $\sigma_{b,expt}\,(y_b)$ in the equation (5.6) and equation (5.7), the following expression can be written:

$$\sigma_{a,stat}(y_b) - \sigma_{a,P-S}(y_b) = \frac{\left(\sqrt{SSE_{P-S}} - \sqrt{SSE_{stat}}\right)}{N} \tag{5.9}$$

And by substituting $\sigma_{a,stat}(y_b)$ and $\sigma_{a,P-S}(y_b)$ respectively by equation (5.4) and equation (4.1)

$$a{y_{bi}}^{\alpha}Q(y_{bi}) - k_{P-S}y_{bi} = \in^{*}(y_{bi}) \tag{5.10}$$

Here $\in^{*}(y_{bi})$ is the error between the PS and the statistical models comparatively to the measurements.

The objectives behind this approach are to express the function parameters a and α as function of the dynamic characteristics of the conductor. Therefore, from the equation (5.10) and equation (5.5) arise:

$$\alpha = \frac{\log\frac{\sigma_{aj}}{\sigma_{ai}}}{\log\frac{y_{bj}}{y_{bi}}}, \qquad i < j \; and \; i = 1,2,\dots,n \tag{5.11}$$

With σ_{bi} and σ_{bj} are stresses related to the amplitudes y_{bi} and y_{bj} for the conductor stretched at the same tension. This equation defines the slope of the line which is given in the log-log scale by the non-linear regression technique and necessitates at least two amplitude levels. Equation (5.11) then gives:

$$\alpha = \frac{1}{\log\frac{y_{bj}}{y_{bi}}}.\frac{\log\left[y_{bj}k_{p-s} + \epsilon^{*}(y_{bj})\right]}{\log\left[y_{bi}k_{p-s} + \epsilon^{*}(y_{bi})\right]} \tag{5.12}$$

The coefficient α is a dimensionless parameter and the intercept a given by the expression below:

$$a = \frac{\left[y_{bi}k_{p-s} + \epsilon^{*}(y_{bi})\right]}{{y_{bi}}^{\alpha}Q(y_{bi})} \tag{5.13}$$

Equation (5.12) and equation (5.13) give the function parameter as a function of PS factor and consequently related to the conductor i.e. diameter, stiffness and tension. The PS model associated with the dynamic stiffness $EJ(k)$ in which the parameters such as friction coefficient and contact stress are taken into account. Knowing that the PS factor is given by:

$$k_{p-s} = \frac{E_a\, d_a\, p^2}{4(e^{-px} - 1 + px)} \tag{5.14}$$

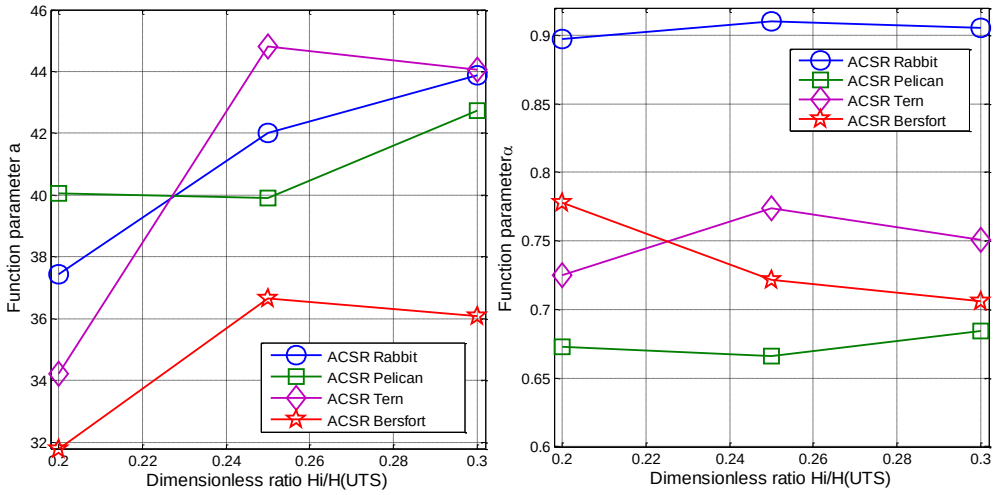

Figure 5-4 Variation of function parameter a (left) and Function parameter α (right) with respect to the tension which is given by the ratio between the tension and the ultimate tension

An alternative way to evaluate the function parameters is to check how they are affected by the varying tension in the strand. The shape of the curve is illustrated in the above figures and show that the shapes are different for each conductor according to the tension that is used. In the ideal case the PS formula may be modified as follows:

$$\sigma_{bi} = b\, k_{PS} {y_{bi}}^{\alpha} \tag{5.15}$$

With b the factor is the ratio between a and k_{PS} is factor of PS

5.3.4. Bending strain and bending curvature

Other expression mentioned in the chapter 2, equation (2.24) can also be exploited to developed the bending amplitude method such the expression with the radius of curvature and overall of the conductor

$$\varepsilon(x,t) = \frac{d_s}{2} y''(x,t) \tag{5.16}$$

Where in d_s is the variable diameter and $y''(x,t)$ given as function of the radius of curvature If assumed that the diameter vertical axis remains constant during the bending and the equation (5.16) become as the expression (5.17) with the constant diameter given by Goudreau et al. [19]:

$$\varepsilon_a = \frac{d}{2\rho_i} \tag{5.17}$$

With ρ_i the radius of curvature and d is the overall diameter, here the coefficient of deformation k_s is close to 1 for small amplitudes.

Figure 5-5, figure 5-6, figure 5-7, and figure 5-8 are illustrated the graph of the conductors tested as bending curvature vs. the bending amplitude according to the equation (5-17) for different conductors tested conductor showing the bending curvature as function of bending amplitude. Using the power regression model, a general equation of curvature arose from equation (5.17)

$$\sigma_{ai} = \frac{d}{2} E_a {\rho_0}^{-1} {y_b}^{\theta} \tag{5.18}$$

Wherein, d is the overall diameter of the conductor , E_a is the Young's modulus of the aluminum. θ and ${\rho_0}^{-1}$ are the function parameters given in table 5-3. The curvature depends on the bending amplitude, the bending stiffness and the diameter of the conductor.

Table 5-3: Function parameter θ and ${\rho_0}^{-1}$ related to equation (5.18) for different conductor tested

function parameter	**Rabbit**			**Pelican**		
	20% UTS	25 % UTS	30% UTS	20% UTS	25 % UTS	30% UTS
${\rho_0}^{-1}[10^{-6}]$	102.04	109.9	111.11	57.8	58.5	57.8
θ	0.87	0.79	0.71	0.68	0.7	0.66
function coefficient	**Tern**			**Bersfort**		
	20% UTS	25 % UTS	30% UTS	20% UTS	25 % UTS	30% UTS
${\rho_0}^{-1}\ [10^{-6}]$	37.31	52.08	47.16	24.63	32.05	25.05
θ	0.76	0.9	0.8	0.74	0.79	0.62

.

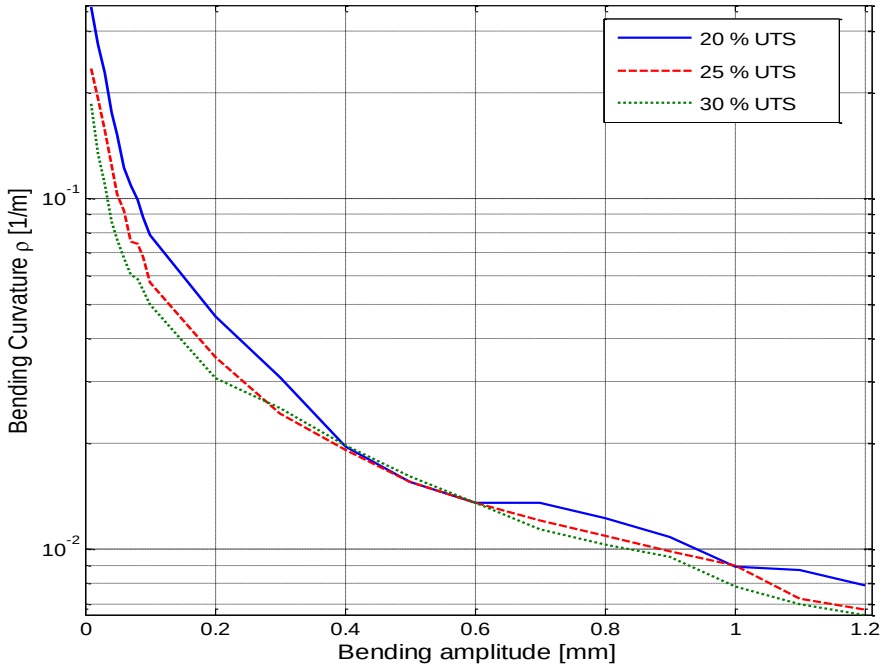

Figure 5-5 Bending curvature vs. bending amplitude for **ACSR Rabbit** conductor

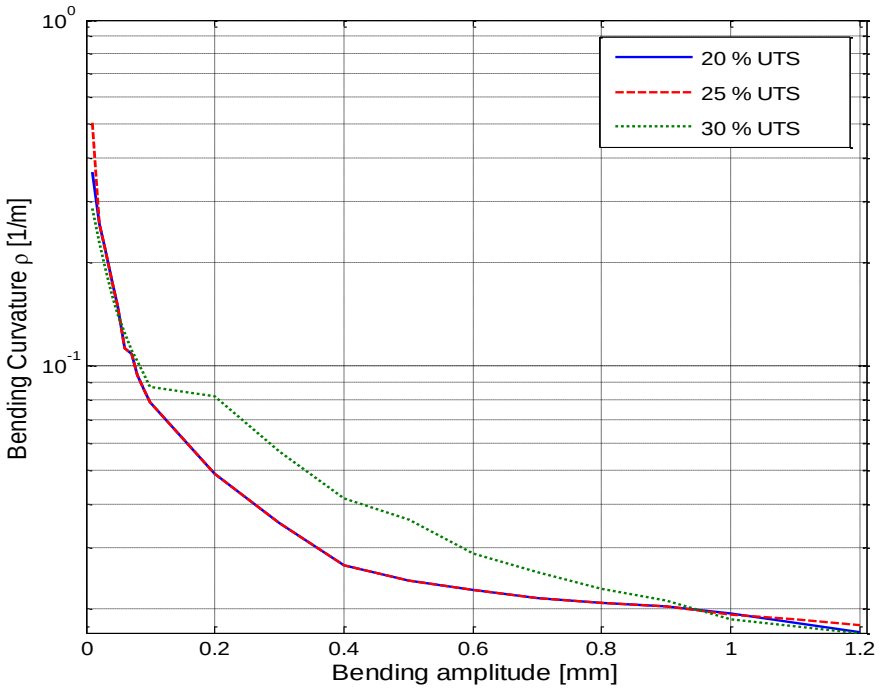

Figure 5-6 Bending curvature vs. bending amplitude for **ACSR Pelican** conductor

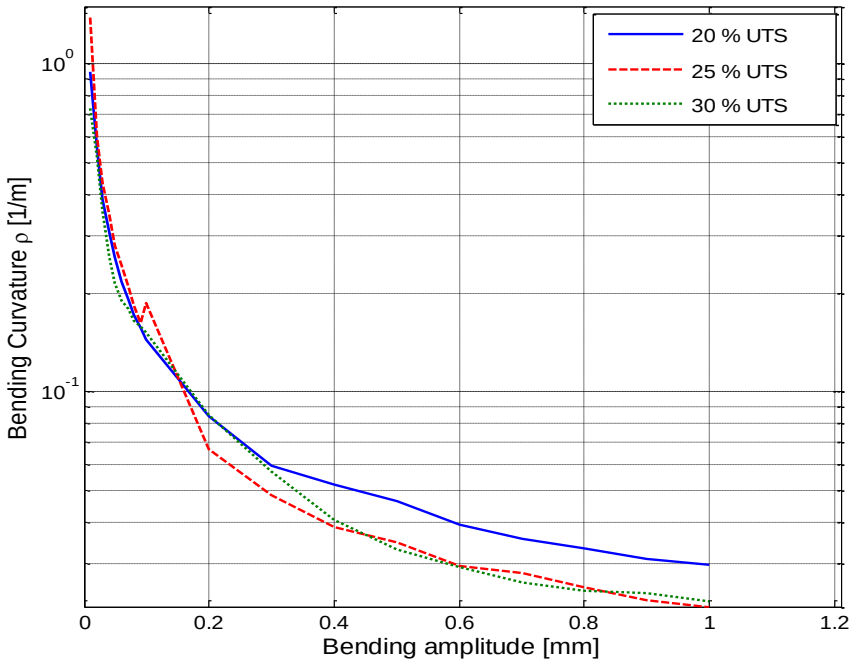

Figure 5-7 Bending curvature vs. bending amplitude **for ACSR Tern** conductor

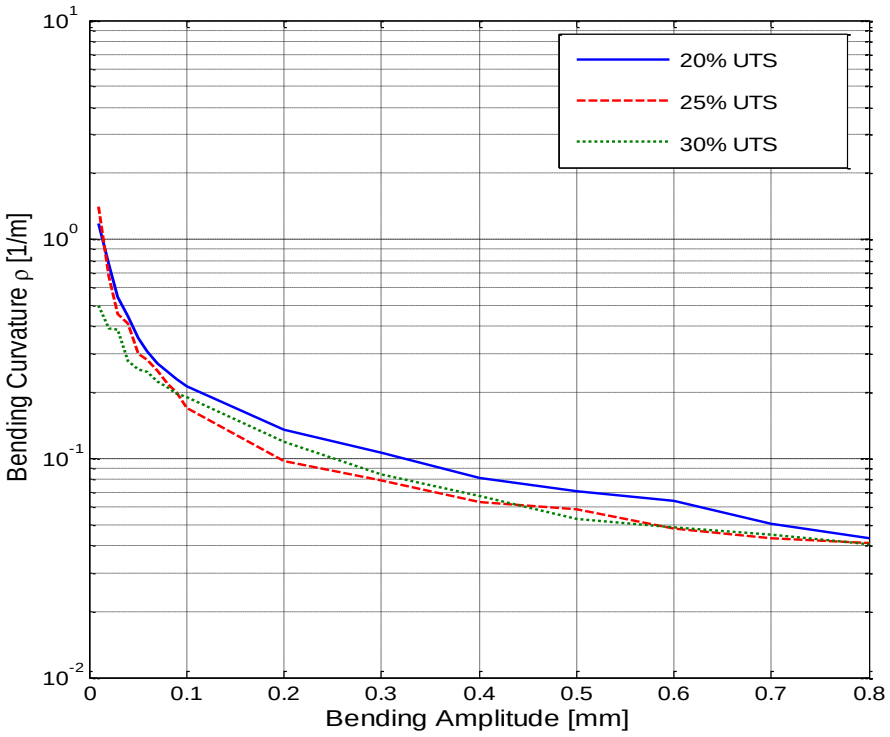

Figure 5-8 Bending curvature vs. bending amplitude for **ACSR Bersfort** conductor

5.4. Effect of tension level in stress distribution (size effect)

The criteria of effective sizes used in this work were based on Cohen's theories [45]. It was assumed that each tension level of the conductor constitute a group therefore, three groups are found for each conductor according to the tension used 20 % UTS, 25 % UTS and 30% UTS. The one-way ANOVA (analyse of variances) technique was explored to evaluate the effect sizes using the GraphPad package. The effect size is characterized by the Eta square value η^2 value based on Cohen Criteria which is found that if η^2 value is equal to (i) 0.01 as small effect, (ii) 0.06 as a medium effect and (iii) 0.14 as a large effect. There were not a statistically significance difference (NS) were found for the p-value $>$ 0.05 in the all three conductor.

Table 5-4: The Eta square value of each conductor summarised the effect of the tension in difference conductor

ANOVA parameter	Rabbit	Pelican	Tern	Bersfort
p-value	0.923	0.9572	0.7751	0.7669
η^2	0.003	0.002	0.011	0.013
Effect tension	very small	very small	small	small

The data was collected at three different tensions i.e. 20 %, 25 %, and 30 % of their UTS for each conductor. This allowed the possibility of expressing the different coefficient factors in polynomial and power law form developed for other tensions used during the experiments. The distributions within the strands are different and based on the slip-stick state which is affected by the variation of the tension. The tension of the conductor is given as a ratio between a given tension H_i and the ultimate tensile strength and considered as the maximum H_0. Contrary to what one might have thought at the beginning the variation of bending stress due tension in the strand is not linear. In figures 5-2, figure 5-3 and figure 5-4 there is a variation of the different coefficient with the tension. These function parameters may be determined by using the Lagrange quadratic interpolation (basic function).

5.5. Summary

In this summary a numerical application is given in order to compare which is the most accurate method of prediction among the method developed in the section above. Comparing the results on the ACSR Tern conductor i.e. amplitude peak to peak: 0.3 mm, 0.5 mm and 0.7 mm, overall diameter: 27 mm, tension 25 % UTS. The comparison was taken on the experimental results and the prediction model developed i.e. polynomial model, power model, and from the curvature model given in equation (5.1), equation (5.4) and equation (5.18), respectively.

Table 5-4: Comparison of the experiments and prediction method given in equations (5.1), (5.4) and (5.18)

Amplitude	**Experiments**	**Prediction Model**		
[mm]	[MPa]	Eq.(5.1)	Eq.(5.4)	Eq.(5.18)
0.3	15.6	14.9	14.03	16.7
0.5	24.2	22.6	22.4	26.4
0.7	33.9	29.7	30.4	35.7

It was noticed that equations (5.1) and equation (5.4) are most suitable for the smaller amplitude than 0.5 mm with an average deviation of $\pm$ 6 % and the equation (5.18) for the amplitude above 0.5 mm. the experimental results are between the prediction value of the two equations (5.1) and equation (5.18) or the equation (5.4) and equation (5.18)

CHAPTER 6

CONCLUSION AND FUTURE WORK

In this last chapter, the conclusion of this work is presented on what has been achieved and the suggested proposals for future work based on observations, literature and practical experience acquired.

Measurements of Stress vs. amplitude were collected on three ACSR conductor (Rabbit Pelican, Tern and Bersfort), common used in South Africa. These measurements were compared to theoretical models such as the Poffenberger-Swart Formula and Papailiou's model. In general, discrepancies were observed between the measurements and the predicted model. Exception was noticed with Papailiou's model for Rabbit, Pelican and Tern conductors.

Tern and Bersfort conductors having triple layer of wires, from this exception a question can arise: why does the stress not correlated with the Papailiou's model on the Bersfort conductor measurements? The simple answer to this case it is because their configurations are quite different in the conductor. The stresses measured on the Bersfort conductor are varying less than the ones observed on the Tern conductor for the same conditions (amplitude and tension)

Three simple and accurate models for the characterisation of the bending stress of the conductor outer layer wires were examined. This makes it possible to have a better assessment of one of the fundamental parameters of the fretting fatigue phenomenon which takes place in overhead line at the suspension clamp. It was possible to establish a model which characterises the outer layer behaviour of overhead lines conductors based on both experimental data and statistical theory. The models thus developed could be also extended to contact metal-non-metal between conductors–clamp systems which are limited for the Poffenberger-Swart (PS) model.

A practical application of the new models consequently developed, can be used in the vibration recorder measurements. This research can be taken as the first step in the life expectancy and vibration severity evaluation of the transmission line conductor. The second step will be to analyse the data from the vibration recorder which collected the amplitude at 89 mm from the last point of contact between conductor and the commercial clamp.

ESKOM has disseminated many vibration recorders on the various type of overhead line

conductors in order to measure amplitudes which have to be correlated with the stress (strain) using the model developed in this research according to CIGRE's method [46] (appendices F). For other kind of conductors which were not part of this research, there is possibility to establish the stress vs. amplitude signature of conductors using VRTC lab's facilities.

6.1 Future work

From the outcome of this research, the proposals of future work are suggested:

- Prospectively the realistic model thus developed may be improved using the same approach on several conductors with the same configuration and number of layers but different in the wire diameter. This intends to assess the dependence of different coefficients of the above model i.e. B_0, B_1, B_2, B_3, a and α. A generalized model on the bending amplitude might even be established.

- In chapter 4, the results on the Bersfort conductor were compared with the data found in literature obtained especially by Levesque et al [41] and Ouaki et al [40]. It was found that the strain is reduced when the radius angle of the short commercial clamp is increased compared to the actual results using the rigid clamp. An interesting investigation could be made where the shear force can be quantified for different short commercial clamps.

List of references

[1] ESKOM "The Planning, Design and Construction of Overhead Power Lines", *Eskom, Power Series* Vol. 1, pp. 324-371, JHB, February 2005.

[2] EPRI (2006), Transmission Line Reference Book: Wind-induced Conductor Motion, *EPRI, Palo Alto*, CA 2006, 1012317.

[3] CIGRE, Fatigue Endurance Capability of Conductor/Clamp System Update of Present Knowledge, *Cigre*, Technical Brochure, Helsinki, July 2007.

[4] T.Varney, "Notes on the Vibration of Transmission Line Conductors", Trans. AIEE, p.791, 1926.

[5] T.Varney, "The Vibration of Transmission Line Conductors", Trans. AIEE., p.799, 1928.

[6] RA. Monroe and R.Templin, "Vibration of Overhead Transmission Lines", Trans .AIEE, p.105, 1932.

[7] G. Stickley, "Stress-Strain Studies of Transmission Line Conductors", Trans. AIEE. 51, p. 1052. 1932

[8] RF. Steidel, "strain induced in Transmission Line cables by Aeolian Vibration" meeting of Experimental stress analysis, Ohio, May, 1958.

[9] M B. Elton, AR. Hard, and AN. Shealy, "Transmission Conductor Vibration Tests", Trans AIEE, Vol.14, 1958.

[10] A.T. Edwards and M. Boyd, "Ontario Hydro Live-Line Vibration Recorder for Transmission Conductors", IEEE Transactions on Power Apparatus and Systems, Vol. PAS-82, 1963, pp. 269-273

[11] JC. Poffenberger and RL. Swart, "Differential displacement and dynamic conductor strain". *IEEE, Trans*.; Vol. 84, pp.281–9. 1965.

[12] G.B. Tebo, 'Measurement and Control of Conductor Vibration', AIEE Trans. , vol.60, pp.1188, 1941.

[13] IEEE" Standardization of conductor vibration measurements," IEEE Trans. Power App. Syst., vol. PAS-85, no. 1, pp. 10–22, Jan. 1966.

[14] R. Claren and G. Diana, "Dynamic strain distribution on loaded stranded cables," *IEEE Trans. Power App. Syst.*, vol. PAS-89, no. 11, pp. 1678–1686, Nov. 1969.

[15] K.O Papailiou 1994, Bending of helically twisted cables under variable bending stiffness due to internal friction, tensile force and cable curvature, Dr. Sc. thesis Eidgenössische Technische Hochschule Zurich.

[16] KO. Papailiou, "On the Bending Stiffness of Transmission Line Conductors," *IEEE Trans. Power App*. Vol. 12, No. 4, pp. 1576-1588, Oct. 1997.

[17] KO. Papailiou, "On the Bending Stiffness of Transmission Line Conductors-Discussions," *IEEE Trans. Power Del.*, Vol. 12, No. 4, pp. 1576-1588, Oct.1997.

[18] F. Lévesque, S. Goudreau, A. Cardou, and L. Cloutier, "Strain measurements on ACSR conductors during fatigue tests I—Experimental method and data," IEEE Trans. Power Del., vol. 25, No. 4, pp. 2825–2834, Oct. 2010.

[19] F. Lévesque, S. Goudreau, A. Cardou, and L. Cloutier, "Strain measurements on ACSR conductors during fatigue tests I—Experimental method and data," IEEE Trans. Power Del., vol. 25, No. 4, pp. 2825–2834, Oct. 2010.

[20] S. Goudreau, F. Lévesque, A. Cardou, and L. Cloutier, "Strain measurements on ACSR conductors during fatigue tests II—Stress fatigue indicators," *IEEE Trans. Power Del.*, vol. 25, No. 4, pp. 2997–3006,Oct. 2010.

[21] S. Goudreau, F. Lévesque, A. Cardou, and L. Cloutier, "Strain Measurements on ACSR Conductors during Fatigue Tests III—Strains Related to Support Geometry" *IEEE Trans. Power Del., Vol. 25, No. 4, October 2010*

[22] Dalpé, C. 1999. "Interaction mécanique entre conducteur électrique aérien et pince de suspension: étude sur la fatigue, la rigidité et la FIP", mémoire de 2ème cycle, Université Laval, Avril.

[23] J. Lanteigne and A. Akhtar, "Evaluation of Tensile Strength of Multi-Strand Conductors – Part II: Experimental results," ASME J. Eng. Mater. Technol., vol. 120, No. 1, pp. 39–47, 1998.

[24] Hardy, C. and Leblond, A. 2003, "On the Dynamic Flexural Rigidity of Taut Stranded Cables", Proc. 5th International Symposium on Cable Dynamics, Santa Margarita Liguria (Italy), Sept.15-18, pp. 45-52.

[25] PB. McGill and E. Ramey Effect Of Suspension Clamp Geometry On Transmission Line Fatigue, The Journal of Energy Engineering, Vol. 112,No. 3 A. M. ASCE, , December, 1986

[26] H. Wolf, B. Adum, D. Semenski and D. Pustaic, Using the Energy Method in Estimation of Overhead Transmission Line Aeolian Vibrations, *Strojarstvo,* Vol.50 (5), pp.269-276 2008.

[27] CIGRE SC22 WG 04, Studies Carried out in Spain on Aeolian vibration Of Overhead Conductors, International Conference on large voltage Electric Systems, *Cigre*, Paris,1976.

[28] CIGRE SC22-WG04, "Guide for endurance tests of conductors inside Clamps," Electra, No.100, .p.77-86; May 1986

[29] CIGRE SCB2-08 WG30 TF7 2007,''Fatigue endurance capability of conductor Conductor/Clamp Systems-update of Present Knowledge,'' TB 332, Paris; 2007

[30] YD. Kubelwa, KO. Papailiou, R. Loubser and P. Moodley, "How Well Does the Poffenberger-Swart Formula Apply to Homogeneous Compact Overhead Line Conductors? Experimental Analysis On the Aero-Z® 455-2z Conductor", 18th WCNDT, ISBN: 978-0-620-52872-6, Durban, 4000 pp118-128, April 2012

[31] C.B. Rawlins, "Analytical Elements of Overhead Conductor Fabrication", ISBN 1- 59682-072, pp. 6-9, USA, 2005.

[32] AA. Fadel, D. Rosa, LB. Murca, JLA. Fereira, and JA. Araujo, 'Effect of high mean tensile Stress on the fretting fatigue of an Ibis steel reinforced aluminium conductor', Int J Fatigue, 2011

[33] F. Levesque, "Analyse de la Fatigue par Petits d´Ebattements (« Fretting Fatigue ») de Fils d'un Conducteur ´Electrique", Ph.D Thesis,Universite Laval, 2009.

[34] C.B. Rawlins," Flexure of a Single-Layer Tensioned Cable at a Rigid Support, Sixth International Symposium on Dynamics, pp. 363-370, Charleston SC, September 19-22, 2005.

[35] NI, "Lab View user's manual", National Instruments, Texas 78759-3504 USA, 2011

[36] G. R. Gillich, et all, "Identifying Mechanical Characteristics of Materials with Non-linear Behaviour using Statistical Methods", *Proceedings of the 4th WSEAS International Conference on Computer Engineering and Applications*, WSEAS Press, 2010, p. 96-103.

[37] IEC 60652, "Loading test on the overhead lines structures", 2002

[38] Vibrec 400 User's Manual, Pfisterer SEFAG AG, Switzerland, 2003

[39] MC. Newman, "Regression analysis of log-transformed data: Statistical bias and its correction", Volume 12, Issue 6, Pages 955–1133, june1993

[40] Ouaki B. Analyse experimentale et theorique de l'endommagement par fatigue `apetits d´ebattements des fils de conducteurs ´electriques au voisinage d'une pince desuspension. Th`ese (Ph. D.)–Universit´e Laval, 1998.

[41] F. Levesque, S. Goudreau, and L. Cloutier, "Elastic-plastic microcontact model for elliptical contact areas and its application to a trellis point in overhead electrical conductors ", Journal of Tribology, vol. 133. 2011

[42] CIGRE Report #273, "Overhead Conductor Safe Design Tension with Respect to Aeolian Vibrations", Task Force B2.11.04, June 2005

[43] WF. Bruckner, R. Holms and KO. Papailiou, " Determination of the Lifetime of Transmission Line Conductor on the Basis of Vibration Measurements and Fatigue Test, cigre1985

[44] U. Cosmai (Cigre TF B2.11). Assessment of vibration severity on actual lines. Technical report, Cigre, 2005

[45] K. Kelley, "Confidence Intervals for Standardized Effect Sizes: Theory, Application, and Implementation", Journal of Statistic Software, Issue 8, Vol. 20, Indiana, May 2007

[46] U. Cosmai, " Assessment of Aeolian Vibration Severity", CIGRE, WG B2.25, Bangkok, February 2009

[47] A. Cardou, A. Leblond, and L. Cloutier, " Suspension and Electrical Conductor Contact Conditions", Journal of Energy Engineering, Vol. 119, No. 1, ISSN 0733-9402 April 1993

[48] WF. Bruckner and KO. Papailiou, " On the Accuracy of the Determination of the Endurance Capability of Transmission Line Conductors by CIGRE Method CSC22-WG04", Cigre September 2005

[49] IEEE, "Guide for Aeolian Vibration Field Measurements of Overhead Conductor", IEEE Std. 1368 WG, New York, 6 June 2006

Appendices

A	Characteristics of different types of conductor motion
B	ACSR conductors used in South Africa
C	Methods used to determine the resonance frequency
D	Results on Static strain measurement
E	Results on dynamic stress
F	Evaluation Lifetime and Vibration severity (CIGRE)
G	Copy of Conference Publication

Appendix A: **Characteristics of different types of conductor motion**

The Following is a summary and comparison of Aeolian, Gallop, and Wake-Induced Oscillation, reproduced from EPRI Transmission Line Reference Book, "Wind-Induced Conductor Motion", based on EPRI Research Project 792.

COMPARISON OF TYPES OF CYCLIC CONDUCTOR MOTION

	Aeolian Vibration	*Conductor Gallop*	*Wake-Induced Oscillation*
Types of Overhead Lines Affected	All	All	Limited to lines with bundled conductors
Approx. Frequency Range (Hz)	3 to 150	0.08 to 3	0.15 to 10
Approx. Range of Vibration Amplitudes (Peak-to-Peak) (Expressed in conductor diameters)	0.01 to 1	5 to 300	Rigid-Body Mode: 0.5 to 80 Subspan Mode: 0.5 to 20
Weather Conditions Favoring Conductor Motion			
Wind Character	Steady	Steady	Steady
Wind Velocity	1 to 7 m/s (2 to 15 mph)	7 to 18 m/s (15 to 40 mph)	4 to 18 m/s (10 to 40 mph)
Conductor Surface	Bare or uniformly iced (i.e. hoarfrost)	Asymmetrical ice deposit on conductor	Bare, dry
Design Conditions Affecting Conductor Motion	Line tension, conductor self-damping, use of dampers, armor rods	Ratio of vertical natural frequency to torsional natural frequency; sag ratio and support conditions	Subconductor separation, tilt of bundle, subconductor arrangement, subspan staggering
Damage			
Approx. time required for severe damage to develop	3 mos to 20 + years	1 to 48 hours	1 mo to 8 + years
Direct causes of damage	Metal fatigue due to cyclic bending	High dynamic loads	Conductor clashing, accelerated wear in hardware
Line components most affected by damage	Conductor and shield wire strands	Conductor, all hardware, insulators, structures	Suspension hardware, spacers, dampers, conductor strands

Appendix B: ACSR conductors used in South Africa

Table B.1 Pelican, Tern and Bersfort conductors used in South Africa

Conductor Type	Distance	Start Name	End Name	Design Volt	Line No
3 BERSFORD	1.87km	MAJUBA	VENUS	400kV	Line 1
3 BERSFORD	154.70km	MAJUBA	PEGASUS	400kV	Line 1
2 BERSFORT	0.20km	HECTOR	ILLOVO	275kV	Line 1
2 BERSFORT	10.19km	GEORGEDALE	KLAARWATER	275kV	Line 2
2 BERSFORT	4.79km	HECTOR	MERSEY	275kV	Line 1
2 BERSFORT	1.27km	HENDRINA	VULCAN	400kV	Line 1
2 BERSFORT	0.12km	HECTOR	KLAARWATER	275kV	Line 1
2 BERSFORT	173.04km	ATHENE	PEGASUS	400kV	Line 1
2 BERSFORT	13.92km	HECTOR	KLAARWATER	275kV	Line 2
2 BERSFORT	4.48km	HECTOR	ILLOVO	400kV	Line 2
2 BERSFORT	6.64km	IMPALA	BAYSIDE	275kV	Line 2
2 BERSFORT	6.62km	IMPALA	BAYSIDE	275kV	Line 1
2 BERSFORT	1.87km	ARNOT	VULCAN	400kV	Line 1
3 BERSFORT	7.81km	LULAMISA	MINERVA	400kV	Line 1
3 BERSFORT	119.17km	ARIADNE	VENUS	400kV	Line 1
3 BERSFORT	112.47km	CAMDEN	DUVHA	400kV	Line 1
3 BERSFORT	8.10km	LULAMISA	PLUTO	400kV	Line 1
3 BERSFORT	110.81km	APOLLO	DINALEDI	400kV	Line 1
3 BERSFORT	6.02km	DEDISA	GRASSRIDGE	400kV	Line 1
4 PELICAN	17.19km	GRASSRIDGE	POSEIDON	220kV	Line 2
4 PELICAN	115.13km	DEDISA	POSEIDON	400kV	Line 1
1 TERN	93.80km	AGGENEIS	PAULPUTS	220kV	Line 1
2 TERN	1.02km	BRENNER	SNOWDON	275kV	Line 1
2 TERN	19.51km	DURBAN SOUTH	KLAARWATER	275kV	Line 1
2 TERN	0.75km	LETHABO	SNOWDON	275kV	Line 1
3 TERN	32.35km	ARIADNE	HECTOR	400kV	Line 2
3 TERN	53.62km	MARANG	MIDAS	400kV	Line 1
3 TERN	171.66km	MATIMBA	WITKOP	400kV	Line 1
3 TERN	32.35km	ARIADNE	HECTOR	400kV	Line 1
3 TERN	87.32km	BIGHORN	SPITSKOP	400kV	Line 1
3 TERN	246.07km	DROERIVIER	HYDRA	400kV	Line 3
3 TERN	201.47km	MATIMBA	PHOKOJE	400kV	Line 1
3 TERN	285.05km	ARNOT	MAPUTO	400kV	Line 1
3 TERN	133.04km	CAMDEN	EDWALENI	400kV	Line 1
3 TERN	49.40km	PHOKOJE	INSUKAMINI	400kV	Line 1
3 TERN	143.52km	EDWALENI	MAPUTO	400kV	Line 1
3 TERN	53.42km	BIGHORN	DINALEDI	400kV	Line 1
3 TERN	406.80km	BETA	DELPHI	400kV	Line 1
3 TERN	193.22km	ATHENE	PEGASUS	400kV	Line 2
3 TERN	6.85km	DEDISA	POSEIDON	400kV	Line 1
3 TERN	28.14km	MATIMBA	WITKOP	400kV	Line 2
3 TERN	205.30km	DUVHA	LESEDING	400kV	Line 1
3 TERN	53.37km	MATIMBA	MARANG	400kV	Line 1
3 TERN	22.37km	BIGHORN	MARANG	400kV	Line 1
3 TERN	166.95km	EROS	VUYANI	400kV	Line 1
3 TERN	10.15km	ANKERLIG	KOEBERG	400kV	Line 1
3 TERN	80.03km	ARIES	NIEWEHOOP	400kV	Line 1
3 TERN	198.70km	FERRUM	MOOKODI	400kV	Line 1
3 TERN	81.35km	ANKERLIG	AURORA	400kV	Line 1
3 TERN	183.66km	NEPTUNE	VUYANI	400kV	Line 1
3 TERN	228.88km	MERCURY	MOOKODI	400kV	Line 1
3 TERN	1.36km	DROERIVIER	HYDRA	400kV	Line 1
6 TERN	234.77km	MERCURY	PERSEUS	765kV	Line 1
6 TERN	125.71km	GAMMA	HYDRA	765kV	Line 1
6 TERN	267.23km	MERCURY	ZEUS	765kV	Line 1
6 TERN	12.78km	BETA	PERSEUS	765kV	Line 1
6 TERN	429.48km	GAMMA	PERSEUS	765kV	Line 1
6 TERN	214.89km	MAJUBA	UMFOLOZI	765kV	Line 1

Appendix C: **Methods used to determine the resonance frequency**

Three methods were used to determine the resonance frequency of the conductor

(i) Analytical method which is based on the Strouhal theory
(ii) Using VIP software(in which a simulator is incorporated)
(iii) Experimental method by using a sweep Method(Puma control system)

In this part an example performed on the tern conductor is illustrated

C1 analytical method

This method is based on the Strouhal theory. The natural frequency (at its resonance frequency) is given by the equation (C.1)

$$f = \frac{n}{2l}\sqrt{\frac{H}{m_l}} \qquad \text{(C.1)}$$

Where n is the mode or the number of loops, l is the span length, H is the tension (Newton) and m_l is the mass per unit length.

The Strouhal formula is given as follows:

$$f = S\frac{V}{d} \qquad \text{(C.2)}$$

Where, S is the Strouhal Number (between 0.185 and 0.2), V is the wind velocity (Aeolian Vibration: from 1 to 7 m/sec) and d is the conductor diameter (mm).

The modes of vibration chosen are usually above 15 according to the span length and 2n+1. The annual average wind velocity in South Africa is between 3 and 4m/sec.

C.2 VIP (Vibration Interactive Programme)

In this method, the VIP Programme is used to evaluate the resonance frequency of the conductor by changing the mode of vibration in the simulator of the power method display. The procedure used to determine the resonance frequency with the VIP is as follows

Step 1: the conductor parameters are step up i.e. l is the span length, H is the tension (Newton) and m_l is the mass per unit length.

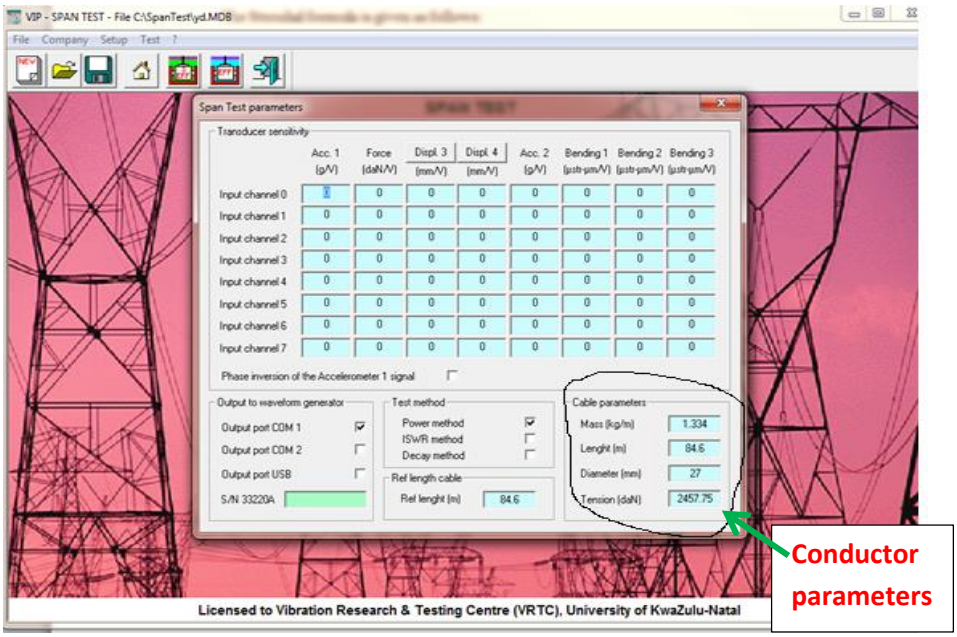

Figure C.1: VIP span test parameter display

- Step 2: determine different resonance frequencies by changing the mode of vibration .

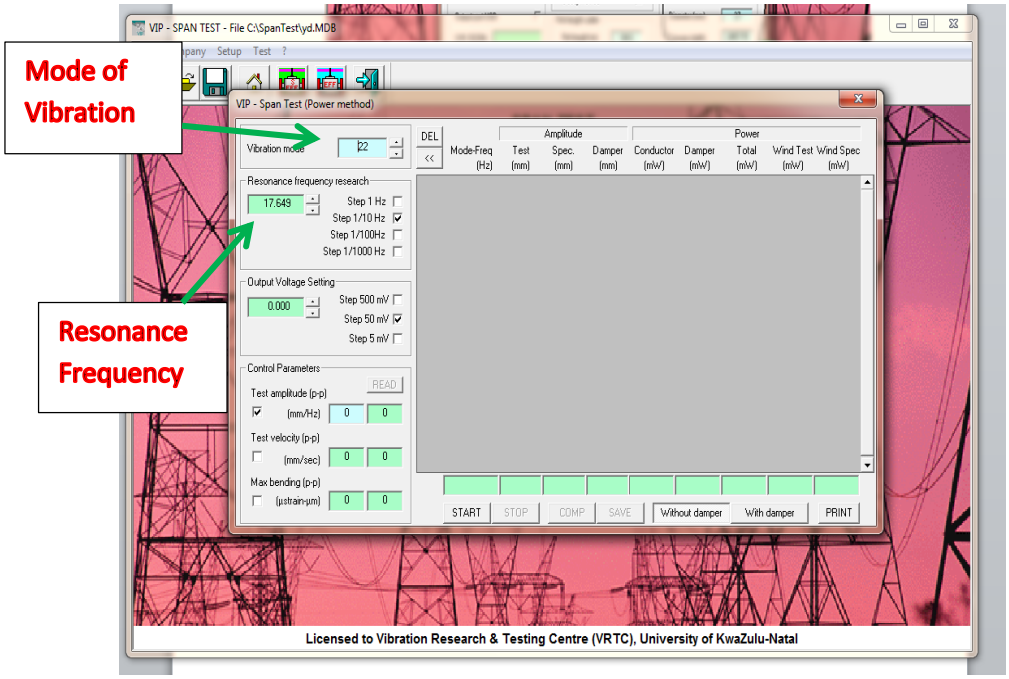

Figure C.2: VIP Power method display

C.3: Sweep or experimental Method

This is the most recommended method because the conductor parameters may change with the environment of the lab. The sweep frequency method is performed at constant velocity (0.2-0.3 m/sec) and at constant amplitude (0.5-1 mm).

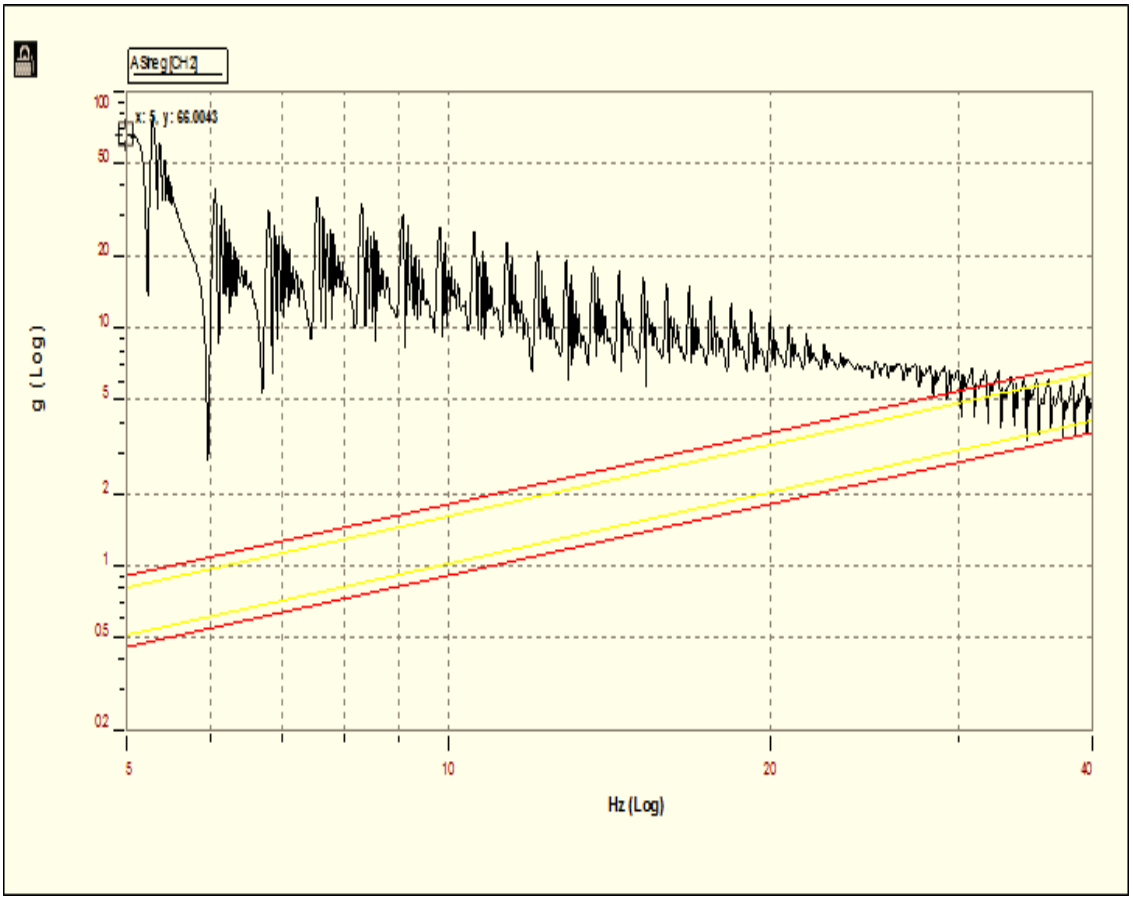

Figure C.3: Frequency sweep Graph for Tern conductor at 20 % UTS

Appendix D: Results on Static strain measurement

In this section, the static strain is presented from table D.1 to table CD.4

Table D.1 Static Stress measurements for ACSR Rabbit conductor

Tension	ε_t theory[25]	$\varepsilon_t$wire 1		$\varepsilon_t$wire 2		$\varepsilon_t$wire 3	
[kN]	Microstrains	CT	CL	CT	CL	CT	CL
2	-17.07	zeroed	zeroed	zeroed	zeroed	zeroed	zeroed
2.4	-20.48	-65.9	-62.3	-114.2	-64.3	-13.7	-18.2
2.8	-23.90	-99.3	-95.6	188.7	-107.9	-15.7	-67.3
3.2	-27.31	-121.7	-97.6	-243.2	-121.4	-30.6	-101.5
3.6	-30.72	-106.6	-77.1	-261.9	-118.3	-58.7	-142.1
4	-34.14	-101.8	-47.2	-204.3	-97	-32.6	-202
4.4	-37.55	-101	-44.3	-216	-80.7	-57.5	-394.5

Table D.2 Static strain measurements on The ACSR Pelican

Tension	ε_t theory[25]	$\varepsilon_t$wire 1		$\varepsilon_t$wire 2		$\varepsilon_t$wire 3	
[kN]	Microstrains	CT	CL	CT	CL	CT	CL
6.6	-17.5	0	0	0	0	0	0
8	-21.0	-79.1	-65.4	-119.9	-67.5	-14.4	-19.1
9.4	-24.5	-119.2	-100.4	198.1	-113.3	-16.5	-70.7
10.8	-28.0	-146.1	-102.5	-155.4	-127.5	-32.1	-106.6
12.2	-31.5	-127.9	-80.9	-174.9	-124.2	-61.6	-149.2
13.6	-35.0	-122.2	-49.5	-114.5	-101.9	-34.2	-212.1
15	-38.5	-121.2	-46.5	-226.8	-84.7	-60.4	-264.2

Table D.3: Static stress measurements on The ACSR **Tern** conductor

Tension	ε_{theory} **[25]**	ε_t **wire 1-4**		ε_t **wire 1-5**		ε_t **wire 1-6**	
[kN]		CT	CL	CT	CL	CT	CL
9.1	-6.22	zeroed	zeroed	zeroed	zeroed	zeroed	zeroed
11.1	-7.59	-12.7	-42.1	-24.5	-25.7	-35.5	-57.6
14.1	-9.64	-38.4	-62.7	-46.9	-21.4	-83.5	-209.4
16.1	-11.01	-52.3	-51.5	-67.2	11.5	-107.6	-243.4
18.1	-12.38	-64.1	-29.4	-79.3	25.1	-130.3	-259.3
20.1	-13.75	-70.7	11.6	-84.7	44.1	-138	-270.5
22.1	-15.11	-22.3	33.6	-67.2	64.4	-100.6	-272
24.1	-16.48	39	76	-55.4	103.2	-58.3	-241.5

Table D.4: Static Stress measurements on The ACSR **Rabbit** conductor

Tension	ε_{theory} **[25]**	ε_{st} **wire 1-4**		ε_{st} **wire 1-5**		ε_{st} **wire 1-6**	
[kN]	microstrains	CT	CL	CT	CL	CT	CL
18.42	-18.65	zeroed	zeroed	zeroed	zeroed	zeroed	zeroed
22.42	-22.70	75.4	59.8	84.3	93.6	-108.9	-295.1
26.42	-26.75	93.7	42.3	120.3	117.4	-138.6	-321.1
30.42	-30.80	24.6	-15.3	73.5	58.7	-97.2	-307.7
34.42	-34.85	-82.3	-87.6	-22.4	-12.8	-78.3	-309.9
38.42	-38.90	-152.9	-140.3	-84.7	-58.3	-75.3	-274.2
42.42	-42.95	-215.6	-205.4	-142.3	-103.6	-69.3	-246.4
46.42	-47.0	-264.6	-267.2	-217.6	-142.7	-56.3	-226.3
50.42	-51.05	-305	-324.6	-256.7	-187.7	-46.3	-184.6
54.42	-55.11	-351.7	-380.5	-309.3	-228.4	-26.3	-145.2

Appendix E: Results on dynamic stress

In this section, the results of dynamic stress collected on the three uppermost wires are presented for different conductors. They refer to the conductor tensioned at 20% UTS, 25% UTS, and 30 % UTS. Also, the frequency of excitation (resonance frequency) and the Poffenberger-Swart are given. The Young's modulus 70 GPa was used as the Young's modulus for the outer layer aluminum wire.

E 1.1 ACSR Rabbit conductor

Table E 1 Bending amplitude vs. Bending stress for ACSR **Rabbit** at 20%UTS

Amplitude	Frequency	Bending stress			
mm	Hz	wire1	wire 2	wire3	P-S
0.01	19.675	0.68	1.50	1.00	0.23
0.02		0.71	1.61	1.28	0.46
0.03		0.73	1.82	1.55	0.69
0.04		0.90	2.23	2.01	0.92
0.05		0.98	2.55	2.32	1.15
0.06		1.07	2.99	2.87	1.38
0.07		1.19	3.37	3.23	1.61
0.08		1.26	3.85	3.56	1.84
0.09		1.50	4.21	3.99	2.1
0.1		1.65	4.71	4.47	2.30
0.2	18.345	2.45	7.95	7.65	4.59
0.3		3.48	11.31	11.35	6.89
0.4		5.39	15.96	17.93	9.19
0.5		11.23	19.68	19.65	11.49
0.6		11.92	23.99	21.86	13.79
0.7		24.19	22.69	25.83	16.08
0.8		24.76	25.01	28.66	18.38
0.9		24.79	27.86	32.37	20.68
1	17.887	25.33	32.80	39.39	22.97
1.1		29.78	33.85	40.20	25.27
1.2		34.68	36.45	44.41	27.57

Table E.2: Bending amplitude vs. Bending stress for ACSR **Rabbit** 25%UTS

Amplitude	**Frequency**	**Bending Stress (MPa)**			
mm	**Hz**	**wire 1**	**wire2**	**wire3**	**P-S**
0.01	20.4	0.68	1.51	1.20	0.24
0.02		0.78	1.83	1.52	0.48
0.03		0.86	2.27	2.07	0.72
0.04		1.09	2.85	2.66	0.96
0.05		1.16	3.44	3.32	1.20
0.06		1.33	3.83	3.62	1.44
0.07	19.907	1.78	4.71	4.65	1.69
0.08		1.68	4.78	4.67	1.92
0.09		1.99	5.19	4.97	2.17
0.1	18.036	2.19	6.14	5.95	2.41
0.2		3.51	10.02	10.38	4.81
0.3		4.64	14.46	15.08	7.22
0.4		5.82	18.460	19.80	9.63
0.5		21.12	22.74	24.70	12.03
0.6		22.13	26.12	28.36	14.44
0.7		22.57	29.17	32.02	16.84
0.8		31.77	32.31	37.73	19.25
0.9		33.56	35.76	42.62	21.66
1		37.58	39.23	46.59	24.06
1.1		51.51	48.88	47.19	26.47
1.2		52.80	52.30	49.66	28.87

Table E.3. Bending amplitude vs. Bending stress for ACSR **Rabbit** at 30%UTS

Amplitude	**Frequency**	**Bending Stress (MPa)**			
mm	**Hz**	**wire 1**	**wire2**	**wire3**	**P-S**
0.01	20.798	1.01	1.89	1.07	0.25
0.02		1.26	2.61	1.74	0.50
0.03		1.40	3.20	2.35	0.75
0.04		1.71	4.11	3.20	1.00
0.05		1.84	4.61	3.81	1.25
0.06		1.98	5.20	4.56	1.50
0.07		2.1	5.79	5.22	1.75
0.08		2.11	5.98	5.49	2.01
0.09		2.27	6.43	5.92	2.26
0.1		2.51	7.07	6.49	2.51
0.2	20.05	4.11	11.44	6.65	5.01
0.3		5.01	13.95	6.81	7.52
0.4		7.71	17.77	7.84	10.02
0.5		10.95	21.84	9.76	12.53
0.6		11.70	25.92	11.24	15.04
0.7		28.64	30.75	31.05	17.54
0.8	19.543	31.75	34.073	35.52	20.05
0.9		34.98	36.89	39.18	22.55
1		42.78	44.86	47.23	25.06
1.1		48.69	50.35	52.48	27.57
1.2		53.16	53.93	56.01	30.07

E.1.2 ACSR Pelican Conductor

Table E.4. Bending amplitude vs. Bending stress for ACSR **Pelican** at 20%UTS

	Frequency	**Bending stress (MPa)**			
mm	**Hz**	**wire1-2**	**wire 1-3**	**Wire1-4**	**P-S**
0.01	19.24	1.42	1.98	1.01	0.32
0.02		2.68	2.79	1.42	0.64
0.03		3.32	3.29	1.81	0.95
0.04		4.26	4.11	2.21	1.27
0.05		4.56	4.83	2.58	1.59
0.06		5.63	6.4	3.45	1.91
0.07		5.97	6.63	3.66	2.22
0.08		6.84	7.68	4.08	2.54
0.09		7.88	8.48	4.64	2.86
0.1	13.76	8.6	9.14	4.83	3.18
0.2		12.49	14.75	7.14	6.35
0.3		17.04	20.45	10.27	9.53
0.4		23.86	27.04	14.06	12.7
0.5		26.22	30.07	18.16	15.88
0.6		29.24	31.94	19.68	19.05
0.7		32.23	33.78	24.9	22.23
0.8		35.59	34.9	28.19	25.4
0.9	10.75	37.06	35.67	28.08	28.58
1		38.84	37.47	30.76	31.75
1.1		42.07	39.9	33.99	34.93
1.2		44.75	42.27	36.85	38.1

Table E.5. Bending amplitude vs. Bending stress for ACSR **Pelican** at 25%UTS

Amplitude	Frequency	Bending stress (MPa)			
mm	Hz	wire1-2	wire 1-3	Wire1-4	P-S
0.01	19.7	1.41	1.43	0.94	0.335
0.02		2.68	2.79	1.42	0.67
0.03		3.32	3.29	1.81	1.01
0.04		4.26	4.11	2.21	1.34
0.05		4.56	4.83	2.58	1.68
0.06		5.63	6.4	3.45	2.01
0.07		5.97	6.63	3.66	2.35
0.08		6.84	7.66	4.08	2.69
0.09		7.87	8.48	4.64	3.02
0.1	13.894	8.6	9.14	4.83	3.36
0.2		12.46	14.75	7.14	6.71
0.3		17.04	20.49	10.27	10.07
0.4		23.86	27.04	14.06	13.42
0.5		26.22	30.07	18.16	16.77
0.6		29.24	31.93	19.68	20.13
0.7		32.23	33.78	24.9	23.49
0.8	10.564	35.59	34.9	28.19	26.84
0.9		37.06	35.67	28.08	30.2
1		41.16	37.76	32.67	33.55
1.1		42.04	38.97	35.25	36.91
1.2		42.2	40.38	37.1	40.26

Table E.6. Bending amplitude vs. Bending stress for ACSR **Pelican** at 30%UTS

Amplitude	Frequency	Bending stress (MPa)			
mm	Hz	wire1	wire 2	wire3	P-S
0.01	16.5	2.41	2.53	1.03	0.35
0.02		3.08	3.16	1.52	0.71
0.03		3.88	3.73	2.01	1.06
0.04		4.58	4.51	2.58	1.41
0.05		5.39	5.09	3.013	1.76
0.06		6.31	5.77	3.47	2.11
0.07		7.21	6.49	3.97	2.47
0.08		7.52	6.97	4.19	2.82
0.09	14.543	8.74	7.66	4.73	3.168
0.1		9.45	8.25	5.26	3.52
0.2		12.75	8.84	7.18	7.04
0.3		18.33	12.69	12.22	10.56
0.4		22.45	17.39	13.37	14.08
0.5		25.75	20.05	14.83	17.6
0.6		30.23	25.14	16.08	21.12
0.7	11.235	34.11	28.44	18.8	24.64
0.8		37.86	31.77	21.96	28.16
0.9		40.97	34.19	31.47	31.68
1		42.88	38.85	35.34	35.2
1.1		45.16	40.68	37.35	38.72
1.2		47.38	42.49	39.98	42.24

E.1.3. ACSR Tern conductor

Table E.7. Bending Amplitude vs. Bending stress for ACSR **Tern** 20%UTS

Amplitude	Frequency	Bending stress (MPa)			
mm	Hz	wire1-2	wire 1-3	Wire1-4	P-S
0.01	19.373	0.908747	0.981094	1.083206	0.3232
0.02		1.314018	1.668125	1.571976	0.6464
0.03		1.781696	2.415237	2.130345	0.9696
0.04		2.259378	3.043027	2.620454	1.2928
0.05		2.58167	3.615601	3.060627	1.616
0.06		3.07695	4.298454	3.586485	1.9392
0.07		3.476662	4.857544	4.091761	2.2624
0.08		3.892341	5.434468	4.561642	2.5856
0.09		4.271398	5.951305	4.983875	2.9088
0.1	17.938	4.703175	6.435319	5.484302	3.232
0.2		8.998269	11.056	9.998605	6.464
0.3		12.81294	15.64571	13.82461	9.696
0.4		17.10406	17.8697	15.38976	12.928
0.5		21.20427	20.09504	20.25043	16.16
0.6		22.55762	23.76453	25.87853	19.392
0.7		23.91851	26.1303	26.74751	22.624
0.8	13.633	24.75582	28.01391	27.58344	25.856
0.9		26.3254	31.41104	29.78935	29.088
1		29.654	35.2285	32.765	32.32

Table E.8. Bending Amplitude vs. Bending stress for ACSR **Tern** at 25%UTS

Amplitude	Frequency	Bending stress (MPa)			
mm	Hz	wire1-4	wire 1-5	Wire1-6	P-S
0.01	19.019	0.981094	0.684309	1.254012	0.3272
0.02		1.686687	1.568467	1.633403	0.6544
0.03		2.324868	2.172575	2.382268	0.9816
0.04		3.0317	2.721605	2.963955	1.3088
0.05		3.689297	3.371256	3.404013	1.636
0.06		4.060153	3.873368	3.829683	1.9632
0.07		4.921906	4.516635	4.448335	2.2904
0.08		5.504103	5.16441	4.980745	2.6176
0.09		6.122636	5.807723	5.253766	2.9448
0.1	17.342	6.435319	5.07609	6.119529	3.272
0.2		11.056	11.21362	10.66461	6.544
0.3		15.64571	15.55626	15.82723	9.816
0.4		17.8697	19.43104	21.12866	13.088
0.5		20.09504	24.1832	25.3997	16.36
0.6		23.76453	29.2297	29.32599	19.632
0.7		26.1303	33.88063	33.84447	22.904
0.8	13.876	28.01391	37.27659	36.79731	26.176
0.9		31.41104	40.8545	39.01651	29.448
1		35.2285	42.83232	40.1586	32.72

Table E.9. Bending amplitude vs. Bending stress For ACSR **Tern** at 30%UTS

Amplitude	Frequency	Bending stress (MPa)			
mm	Hz	wire1-4	wire 1-5	Wire1-6	P-S
0.01	19.253	1.686182	1.292363	2.508025	0.343
0.1		5.693985	5.72691	6.119529	3.43
0.02		2.071255	2.656151	1.633403	0.686
0.03		2.75662	3.653501	2.382268	1.029
0.04		3.590345	4.403012	2.963955	1.372
0.05		4.191897	4.995076	3.404013	1.715
0.06		4.331525	5.274014	3.829683	2.058
0.07		4.812239	5.744612	4.448335	2.401
0.08		5.104185	5.964056	4.980745	2.744
0.09	17.938	5.311789	6.235452	5.253766	3.087
0.2		10.43021	11.12648	10.66461	6.86
0.3		15.09076	16.63439	15.82723	10.29
0.4		18.50116	23.27032	21.12866	13.72
0.5		23.78427	28.59327	25.3997	17.15
0.6		27.85864	32.42979	29.32599	20.58
0.7		33.27398	36.15652	33.84447	24.01
0.8	15.242	36.41502	38.14903	36.79731	27.44
0.9		38.765	39.01651	38.8999	30.87
1		40.1235	41.1586	40.2336	34.3

E1.4 ACSR Bersfort conductor

Table E.10: Bending amplitude vs. Bending stress for **Bersfort** 20 %UTS

Amplitude	Frequency	Bending stress (MPa)			
mm	Hz	wire1-4	wire 1-5	wire 1-6	P-S
0.01	22.582	0.892591	1.047984	0.630622	0.343
0.02		1.245433	1.623694	0.974568	0.686
0.03		1.741145	2.270633	1.362426	1.029
0.04		1.989651	2.79779	1.652828	1.372
0.05		2.563813	3.500517	2.060616	1.715
0.06		2.633127	4.042436	2.136198	2.058
0.07		3.175368	4.58307	2.294606	2.401
0.08		3.713037	5.00654	2.916923	2.744
0.09		4.066397	5.410348	3.192504	3.087
0.1		4.267024	5.784436	3.460512	3.43
0.2	19.668	7.958936	9.144328	5.974969	6.86
0.3		9.717359	11.68051	7.485904	10.29
0.4		13.15374	15.18074	7.85207	13.72
0.5		15.18811	17.42129	9.716097	17.15
0.6	17.43	18.81815	19.45157	11.93372	20.58
0.7		20.34222	24.51679	14.77861	24.01
0.8		23.42746	28.7539	19.3658	27.44

Table E. 11: Bending amplitude vs. Bending stress for ACSR **Bersfort** 25 %UTS

Amplitude	Frequency	Bending stress (MPa)			
mm	Hz	wire1-4	wire 1-5	wire 1-6	P-S
0.01	23.619	1.007272	0.881305	0.796175	0.361
0.02		1.485323	1.828154	1.015107	0.722
0.03		2.118971	2.705148	1.572424	1.083
0.04		2.505617	3.026193	1.710355	1.444
0.05		2.980746	4.113223	2.283887	1.805
0.06	21.990	3.388813	4.388551	2.642048	2.166
0.07		3.560299	4.960062	2.964875	2.527
0.08		4.474748	5.644342	3.3185	2.888
0.09		4.884755	6.212722	3.61839	3.249
0.1	19.547	5.295049	7.274132	4.092582	3.61
0.2		10.40566	12.75579	7.68607	7.22
0.3		14.33998	15.57262	10.57847	10.83
0.4		17.84844	19.64262	12.67019	14.44
0.5	17.918	20.84281	21.28854	15.22485	18.05
0.6		25.12727	25.87841	20.05976	21.66
0.7		27.909	28.8715	21.8855	25.27
0.8		28.9716	30.303	24.206	28.88

Table E 12: Bending amplitude vs. Bending stress for ACSR **Bersfort** at 30 %UTS

Amplitude	Frequency	Bending stress (MPa)			
mm	Hz	wire1-4	wire 1-5	wire 1-6	P-S
0.01	23.197	1.159793	2.492723	1.083954	0.381
0.02		1.524289	3.165234	1.108132	0.762
0.03		1.865556	3.209415	1.51771	1.143
0.04		2.470392	4.471789	1.971379	1.524
0.05		2.831859	4.861946	2.46738	1.905
0.06		3.151338	5.019016	2.84089	2.286
0.07	21.412	3.584823	5.565041	3.137443	2.667
0.08		3.658642	5.901427	3.337074	3.048
0.09		3.881815	6.252484	3.514938	3.429
0.1		4.450131	6.559146	3.934529	3.81
0.2		7.846358	10.43627	7.6615	7.62
0.3		11.92515	14.71207	11.23815	11.43
0.4		16.58701	18.55242	14.3185	15.24
0.5	19.628	19.44689	23.51716	17.95627	19.05
0.6		23.28642	25.66559	19.45909	22.86
0.7		24.94707	27.55418	20.08909	26.67
0.8		27.00233	30.73978	23.7889	30.48

Appendix F: Evaluation Lifetime and Vibration severity (CIGRE)

The flow chart below gives an overview of different steps in the evaluation of the conductor lifetime and vibration severity.

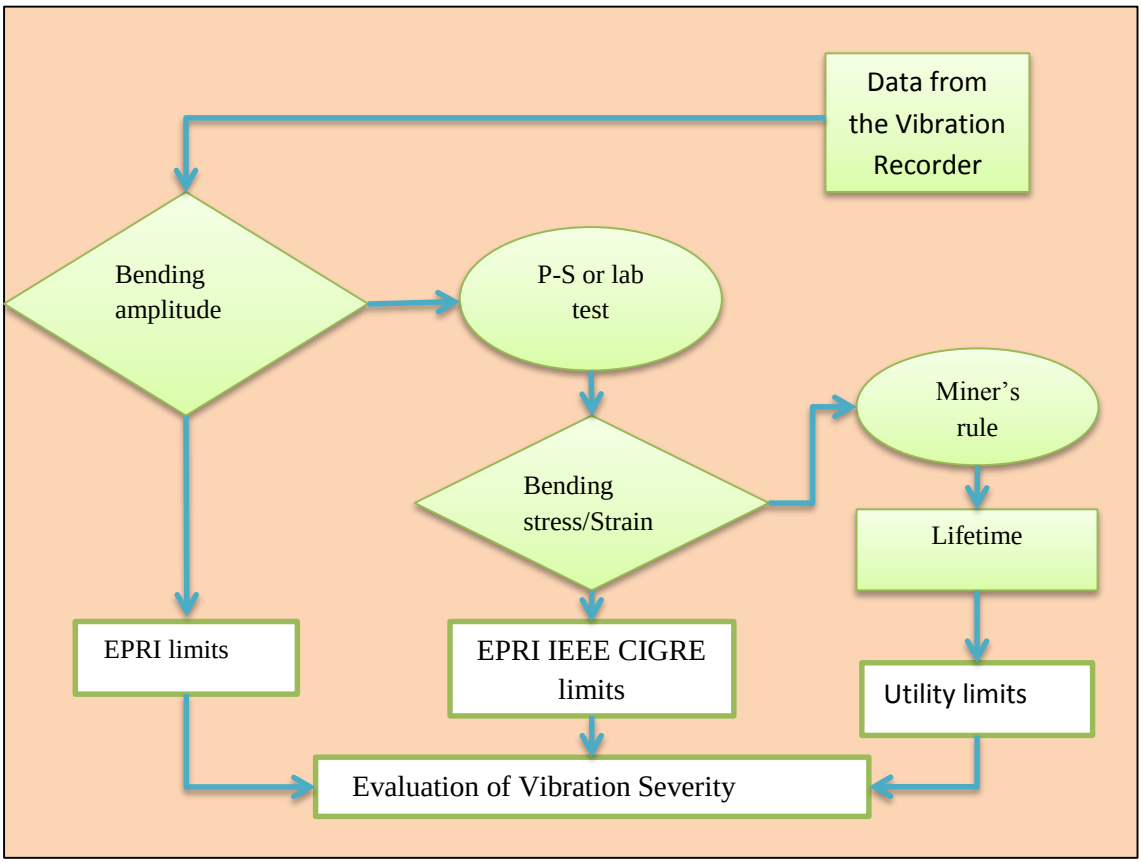

Figure F.1. Flow chart giving the step in the evaluation of the vibration severity (CIGRE)

Appendix G: Copy of Conference Publication

http://www.ndt.net/article/wcndt2012/papers/118_Kubelwa.pdf